REDUCTION OF INITIAL CONVERGENCE PERIOD

IN GPS PPP DATA PROCESSING

GARRETT SEEPERSAD

A THESIS SUBMITTED TO THE FACULTY OF GRADUATE STUDIES

IN PARTIAL FULFILLMENT OF THE REQUIREMENTS FOR THE DEGREE OF

MASTER OF SCIENCE

GRADUATE PROGRAMME IN EARTH AND SPACE SCIENCE

YORK UNIVERSITY

TORONTO, ONTARIO

AUGUST, 2012

REDUCTION OF INITIAL CONVERGENCE PERIOD

IN GPS PPP DATA PROCESSING

by **Garrett Seepersad**

A thesis submitted to the Faculty of Graduate Studies of York University in partial fulfilment of the requirements for the degree of

MASTER OF SCIENCE

REDUCTION OF INITIAL CONVERGENCE PERIOD

IN GPS PPP DATA PROCESSING

by **Garrett Seepersad**

By virtue of submitting this document electronically, the author certifies that this is a true electronic equivalent of the copy of the thesis approved by York University for the award of the degree. No alteration of the content has occurred and if there are any minor variations in formatting, they are as a result of the conversion to Adobe Acrobat format (or similar software application).

Supervisor: Sunil Bisnath

Examination Committee Members:

1. Jian-Guo Wang (Chair)
2. Regina Lee (Member)
3. Spiros Pagiatakis (Outside member)

Abstract

Precise Point Positioning (PPP) has become a popular technique to process data from GPS receivers by applying precise satellite orbit and clock information, along with other minor corrections to produce cm to dm-level positioning. Although PPP presents definite advantages such as operational flexibility and cost effectiveness for users, it requires 15-25 minutes initialization period as carrier-phase ambiguities converge to constant values and the solution reaches its optimal precision.

Pseudorange multipath and noise are the largest remaining unmanaged errors source in PPP. It is proposed that by reducing these effects carrier-phase ambiguities will reach the correct steady state at an earlier time, thus reducing the convergence period of PPP. Given this problem, this study seeks to improve management of these pseudorange errors.

The well-known multipath linear combination was used in two distinct ways: 1) to directly correct the raw pseudorange observables, and 2) to stochastically de-weight the pseudorange observables. Corrections to the observables were made in real-time using data from the day before, and post-processed using data from the same day. Post-processing has shown 47% improvement in the rate of convergence, as the pseudorange multipath and noise were effectively mitigated. A 36% improvement in the rate of convergence was noted when the pseudorange measurements were stochastically de-weighting using the multipath observable. The strength of this model is that it allows for real-time compensation of the effects of the pseudorange multipath and noise in the stochastic model.

Acknowledgements

I extend sincere gratitude to my supervisor Professor Sunil Bisnath, for the dedication, support and encouragement offered to me throughout this research. Not only has he enhanced my opportunity to expand my knowledge in the field of satellite positioning and navigation, but taught me general life skills that will serve me well. Further appreciation is extended to NSERC for the financial support necessary to make this research possible. I also acknowledge CDDIS for providing data necessary for executing the experiments and and NRCan for providing the base PPP code and PPP expertise. Finally, I dedicate this thesis to my grandmother and parents, thanking them for their endless support.

Table of Contents

List of Tables

List of Figures

List of Acronyms

AC	Analysis Centers
ANTEX	Antenna Exchange Format
ASPRS	American Society for Photogrammetry and Remote sensing
C/A code	Coarse/Acquisition code
CDMA	Code Division Multiple Access
COMPASS	China's satellite system, officially called BeiDou Navigation System
CSRS-PPP	Canadian Spatial Reference System-Precise Point Positioning
DCB	Differential Code Bias
ECEF	Earth Centred Earth Fixed
FCB	Fractional Code Bias
FDMA	Frequency Division Multiple Access
Galileo	European satellite navigation system
GLONASS	Russian satellite navigation system
GNSS	Global Navigation Satellite System
GPS	Global Positioning System
GPST	GPS Time
HPL	Horizontal Protection Level
IGS	International GNSS Service
IHO	International Hydrographic Organization
INS	Inertial Navigation System
IRC	Integer Recovery Clocks
ITRF	International Terrestrial Reference System
MEDLL	Multipath Estimation Delay Lock Loop
NRCan	Natural Resources of Canada
NRTK	Network RTK
ppm	parts per million
PPP	Precise Point Positioning
PPP-RTK	PPP and Real-Time Kinematic Integration
RAIM	Receiver Autonomous Integrity Monitoring
RF	Radio frequency
RHCP	Right Hand Circularly Polarized
RINEX	Receiver INdependent EXchange
rms	root mean square
RTK	Real-Time Kinematic
S/N	Signal-to-noise Ratio
ZPD	Zenith path delay

List of Symbols

A	design matrix
b_*^*	hardware biases (m)
c	speed of light (ms^{-1})
$\Delta\delta_j^i(t)$	clock offsets of the receiver and the satellite clock
dt	receiver clock error (s)
dT	satellite clock error (s)
d_{orb}	satellite orbit error (m)
$d_{multi}(P_{L_j})$	pseudorange multipath effect on L1 or L2 (m)
$d_{multi}(\Phi_{L_j})$	carrier-phase multipath on L1 or L2 (m)
d_{iono}	delay caused by the ionosphere
d_{tropo}	delay caused by the troposphere
$\epsilon(*)$	measurement noise (m)
L_{IF}	carrier-phase ionospheric linear combinations
P_x	priori weighted constraints
P	measurement weights
P_{IF}	pseudorange ionospheric linear combinations
P_{L_j}	measured pseudorange on L1 or L2 (m)
λ_{L_j}	wavelength on L1 or L2
$MP_{1\|2}$	multipath linear combination for P1 and P2 observables
N_j	non-integer phase ambiguity on L1 or L2 (cycle)
ρ	true geometric range (m)
$\rho_j^i(t)$	modelled range
$R_j^i(t)$	measured pseudorange
w	misclosure
X^i, Y^i, Z^i	components of the geocentric position vector of the satellite
$X_j. Y_j, Z_j$	unknown ECEF receiver coordinates
$\hat{X}$	state estimate
x_0	A priori estimate

1.0 Introduction to PPP Research

Navigation is the art and science of determining position, speed and orientation of an object on or above the surface of the Earth (Kaplan, 2006). Navigation has been evolving since the beginning of human history and has always been a critical aspect in our development. Navigation systems have taken many forms, varying from simple ones such as those making use of landmarks, compasses and stars to more modern techniques such as utilizing artificial satellites.

Satellite-based navigation technology was introduced in the early 1960s. The first such system was the U.S. Navy Navigation Satellite System (NNSS), known as TRANSIT, in which the receiver measured Doppler shifts of the signal as the satellite transited with a navigational accuracy of 25-500 m (National Space Science Data Center, 2011). In 1978, the Global Positioning System (GPS) was introduced. GPS is a satellite-based radio-positioning and time transfer system designed to provide all-weather, 24-hour coverage

for military users and reduced accuracy for civilian users. Since then, it has become the backbone of a whole body of navigation and positioning technologies.

Currently, the U.S., Russia, the European Union (E.U.), and China are each operating or in the case of the latter two, developing individual Global Navigation Satellite Systems (GNSS's): GPS, GLONASS, Galileo and Compass/Beidou, respectively. Evolving GNSSs can provide the worldwide community with several benefits, which include: the ability to work under environments with limited visibility of satellites; higher accuracy; more robust detection and exclusion of anomalies and improved estimation of tropospheric and ionospheric parameters and time (Zinoviev, 2005).

1.1 Overview of GPS

At the time of writing, GPS constellation consists of 32 satellites in 6 orbital planes, orbiting the Earth at an altitude of approximately 20,200 km (National Coordination Office for Space-Based Positioning, Navigation, and Timing, 2012). GPS uses the GPST timescale and the WGS-84 datum. The satellites are distributed in six equally spaced orbit planes inclined at 55° with respect to the Equator. Each satellite orbits the Earth with a period of 12 sidereal hours.

Each satellite transmits timing signals at two L-band frequencies, 1575.42 and 1227.60 MHz, referred to as L1 and L2. As part of the GPS modernization, new satellites will also transmit the L5 signal at a frequency of 1176.45 MHz (Montenbruck *et al.*, 2010) and it is

estimated that in 2014 a new civilian pseudorange L1C will be available (Ipatov and Shebshaveich, 2010). The Code Division Multiple Access (CDMA) signals contain codes that identify each satellite, time of the emitted signal, position, satellite clock corrections of the satellite, and other data related to the ionosphere and the satellite. Each satellite transmits a short code known as the Coarse/Acquisition (C/A)-code, which broadcasts at a rate of 1 Mbps (repeats after 1 ms) and Precision-code (known as P-code), which broadcasts at a rate of 10 Mbps (repeats after 266 days but resets weekly) (Kaplan, 2006). The P-code is encrypted with a military code; however, high-quality receivers use several techniques such as squaring and cross correlation to acquire the P-code on L1 and L2, but with noisier characteristics compared with the original codes. The receiver utilizes these time-tagged signals to determine the range to each GPS satellite in view by measuring signal travel time, which is then scaled by the speed of light to estimate range. Since the GPS satellite clocks and the receiver clocks are not synchronized, the term pseudorange is used to refer to the code-based range measurements (Hofmann-Wellenhof *et al.,* 2001).

There also exists the carrier-phase signal, which carries the modulations that are capable of more precisely measuring range. A carrier-phase measurement is a count of the number of transmitted carrier wave cycles of the signal since its acquisition, and does not contain the time-of-transmission information as is the case with the pseudorange observable, therefore giving the carrier-phase observable its ambiguous nature. Carrier-phase measurements also suffer from cycle-slips, which are discontinuities in the

measurements caused by loss of lock between the satellite and the receiver. There are many different algorithms that have been developed to resolve ambiguities and adjust for cycle-slips without causing relatively large degradation to positioning accuracy.

Relative GPS, Real-Time Kinematic (RTK) and Network RTK (NRTK) solutions are widely accepted methods for accurate positioning and navigation with two or more receivers. NRTK is based on regional or local reference station networks which are reliant on locking onto a minimum of four GPS satellites at any time period to solve for the four basic unknowns: x,y,z and receiver clock bias (Hofmann-Wellenhof *et al.*, 2001), which are discussed in more detail in Section 2.1.

1.2 Overview of PPP

PPP has become a popular technique to process data from GPS receivers by introducing precise satellite orbit and clock information. Typically, a dual-frequency GPS receiver is utilized with dual-frequency pseudorange and carrier-phase measurements linearly combined to remove the first-order effect of the ionospheric refraction and the real-valued carrier-phase ambiguity terms are estimated from the measurement model. The tropospheric refraction is also estimated, along with the position and ambiguity parameters from the measurements (Héroux *et al.*, 2004; Kouba and Héroux, 2001; Zumberge *et al.*, 1997).

PPP is considered a cost effective technique as it enables sub-centimetre horizontal and few centimetre vertical positioning with a single GPS receiver; in contrast to the methods such as relative GPS, RTK and Network RTK that require more than one receiver. PPP can be used for the processing of static and kinematic data, both in real-time and post-processing (Gao and Chen, 2005; Héroux *et al.*, 2004).

PPP's application has been extended to the commercial sector, as well in areas such as agricultural industry for precision farming, marine applications (for sensor positioning in support of seafloor mapping and marine construction) and airborne mapping (Bisnath and Gao 2009). In rural and remote areas where precise positioning and navigation is required and no reference stations are available, PPP proves to be an asset. Collins *et al.* (2008) are currently researching PPP ambiguity resolution to determine how plausible real-time PPP is for seismic monitoring. Based on PPP's performance, it may be extended to other scientific applications such as ionospheric delay estimation, pseudorange multipath estimation, satellite pseudorange bias and satellite clock error estimation (Leandro *et al.*, 2010).

In PPP, when the number of tracked satellites is less than the minimum number of satellites required, filter re-initialization occurs and can result in tens of minutes of greater than decimetre resolution positioning, until filter re-convergence and similarity for the initial convergence (Bisnath and Gao 2009). The solution convergence depends on several factors including: the number and geometry of visible satellites, observation

quality, user environment and dynamics, and sampling rate. As these different factors interplay, the period of time (from session start) required for the solution to reach a pre-defined precision level will vary (Héroux *et al.,* 2004).

One of the remaining unmodelled residual terms in PPP is (1) the pseudorange multipath and (2) noise, which, if efficiently accounted for, may provide improvement in the rate of convergence. Multipath occurs when signals travelling from a transmitter to a receiver propagate via multiple paths due to reflection and diffraction (Bisnath and Langley, 2001). The multipath effect introduces errors in both pseudorange and carrier-phase measurements. The magnitude of range error can reach up to 10 to 20 m for the pseudorange measurements and up to 5 cm for the carrier-phase measurements (Wells *et al.,* 1999). The pseudorange noise comes from the receiver electronics itself or is picked up by receiver's antenna.

Since PPP uses only a single GPS receiver, no data differencing between two receivers can be used to eliminate satellite specific errors such as the clock and orbital errors and atmospheric errors. It is therefore necessary to use the most precise satellite and clock corrections and satellite orbits and estimate the atmospheric errors. Figure 1.1 illustrates the precision of the International GNSS Service (IGS) Final GPS orbits over the past 15 years. The precise orbit product has been improved from an accuracy of 30 cm to approximately 1-2 cm, with a similar improvement in the IGS Final combined orbit product. The GPS satellite clock estimates that are included in the IGS orbit products

since 1995 are now within the standard deviation range of 0.02 - 0.06 ns or 1 - 2 cm, which is consistent with the orbit precision (Kouba, 2009).

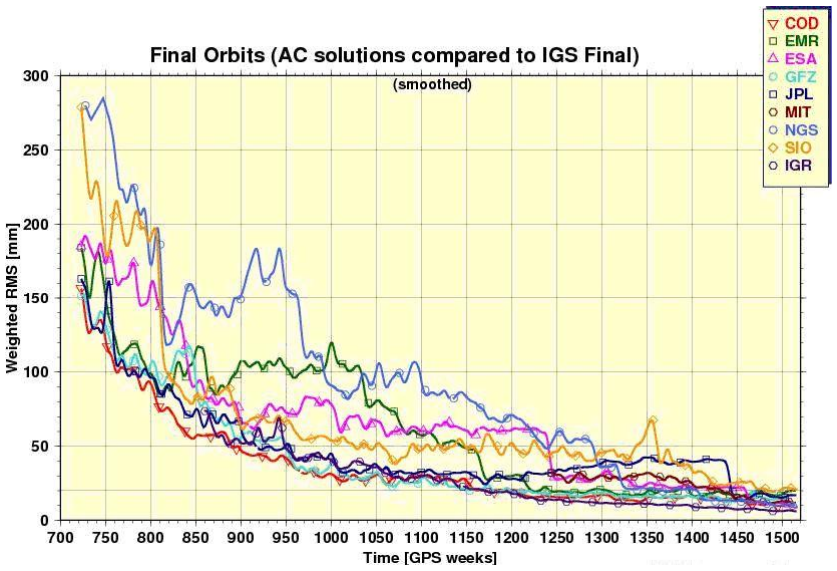

Figure 1.1: Weighted orbit rms of the IGS Rapid (IGR) products and AC Final orbit solutions during 1994-2009 with respect to the IGS Final orbit products. (Kouba, 2009)

1.3 Current PPP Research

This section discusses research in the field of PPP data processing being carried out by academia, industry and governments. The following sub-section, arranged in terms of magnitude of possible improvement to PPP, discuss current research in the areas of ambiguity resolution, integration of PPP and INS, merging PPP and NRTK, using multi-GNSS constellations and processing data collected with low-cost single-frequency receivers. The improvements that these different methods to PPP can be categorized in

terms of reduction of the initial and re-convergence period of PPP and improvement in solution accuracy. There has been a lack of research activities in the area of PPP pseudorange uncertainty management, further increasing the desire to examine possible methods to mitigate the pseudorange multipath and noise, which, if efficiently accounted for, may provide improvements in the rate of convergence.

1.3.1 Ambiguity Resolution

Integer ambiguity resolution of undifferenced carrier-phase observables has been a difficult task in GPS processing and even more troublesome in PPP, where the undifferenced carrier-phase observable is used (Collins *et al.,* 2010; Ge *et al.,* 2008; Geng *et al.,* 2010; Leandro *et al.*, 2006; Shi and Gao, 2010). In relative GPS data processing, through the double-differencing operator, the satellite and receiver clock biases are eliminated to make the ambiguity term an integer and easily resolvable. In PPP, the fractional-cycle biases in the GPS measurements are absorbed by the undifferenced ambiguity estimates and their integer properties are no longer present (Collins, 2008). If the ambiguity term is successfully resolved there will be improvements in the convergence period and solution accuracy.

The integer ambiguity resolution at a single receiver can be implemented by applying the improved satellite products, where the fractional biases have been separated from the integer ambiguities in a network solution. One method of deriving such products is to

estimate the biases by averaging the fractional parts of the steady-state float ambiguity estimates (Ge *et al.,* 2008), and the other is to estimate the integer-recovery clocks by fixing the undifferenced ambiguities to integers in advance (Collins, 2008; Laurichesse *et al.*, 2009).

Ambiguity resolution focuses on reducing the initial convergence period of PPP and improving the solution accuracy. The results reported by Ge *et al.* (2008) showed improvements in solution accuracy from 3.1, 4.1 and 8.3 mm to 3.0, 2.8 and 7.8 mm, in north, east and up, respectively. The reduction in convergence period was presented by Collins *et al.* (2008), Laurichesse *et al*, (2009) and Geng *et al.* (2010). Collins *et al.* (2008) and Laurichesse *et al*, (2009) saw improvements in hourly position estimates by 2 cm and Geng *et al.* (2010) saw noticeable hourly improvements from 1.5, 3.8 and 2.8 cm to 0.5, 0.5, 1.4 cm for north, east and up, respectively.

1.3.2 Integration of PPP and INS

GPS-INS integration refers to the use of GPS satellite signals in the correction of a solution from an Inertial Navigation System (INS) or vice versa. The two systems are reliant on each other, compensating for the limitations of the other. An INS provides accurate high-rate solutions for a short time period, but the solution drifts depending on the quality of the IMU. The GPS positioning solution provides accurate absolute position which can be used to correct the INS solution and reduce the solution drift. With GPS, a

solution provided while there is visibility to the GPS constellation. The INS maintains the availability of the navigation solution during GPS outages (Geodetics Inc., 2010). The Integration of PPP and INS does not assist in reducing the initial convergence period of PPP but offers improvement in re-convergence period as the INS provides an accurate solution for a short time period which can be used to re-initialize the PPP filter. This is important for real-time kinematic applications, as frequent signal outages are common (Bisnath and Gao, 2009).

Du and Gao (2010) and Kjørsvik *et al.* (2010) analyzed the integration of PPP and INS in loosely and tightly-coupled systems. Du and Gao (2010) used a low cost IMU in contrast to Kjørsvik *et al.* (2010) using an typical IMU sensor used in many direct geo-referencing applications, with a reasonable cost/performance trade-off. It has been proven both theoretically and empirically that the tightly-coupled GPS aided INS has superior integrity and error detection capabilities compared to the loosely-coupled differential GPS-INS (Kjørsvik *et al.*, 2010). Du and Gao (2010) and Kjørsvik *et al.* (2010) examined datasets collected by terrestrial vehicles. The terrestrial vehicle dataset highlighted the difficulties of PPP in environments with frequent GNSS outages. The dataset examined by Kjørsvik *et al.* (2010) had the frequent re-initialization which prevented proper convergence of the carrier-phase float ambiguities, and use of a high quality IMU. The loosely-coupled PPP-INS yields no significant improvement over a pure PPP solution;

however, the position accuracies of a few decimetres were demonstrated using a tightly-coupled strategy, an improvement of 30-40%.

Unlike Kjørsvik *et al.* (2010), it was shown by Du and Gao, (2010) that both the tightly-coupled and loosely-coupled system was able to offer high-quality solutions, which was comparable to the DGPS-INS system. The tightly-coupled system offered slightly better results than the loosely-coupled system, because the GPS and INS information were more rigorously modelled in a tight integration than a loosely-coupled system (Du *et al.*, 2010).

The difference in the results presented by Kjørsvik *et al.* (2010) and Du and Gao (2010) may be a result of the quality of the datasets used. But it is clear that integrating PPP and INS can significantly improve PPP re-convergence, not the initial convergence period due to the inaccuracies of pseudorange observations which affects the estimation of the INS navigation states and user position.

1.3.3 Moving from GPS towards GNSS

Several advantages that could be gained from the modernized GPS, GALILEO, COMPASS and GLONASS include more visible satellites, greater signal power level and more potential observable combinations, potentially resulting in improved positioning accuracy, availability and reliability (Shen and Gao, 2006). For the combined GPS and GLONASS processing, two receiver clock offsets must be estimated, one with respect to GPS time and the other with respect to GLONASS time. This is an offset existing

between GPS and GLONASS system times causing a bias between GPS and GLONASS measurements (Moudrak *et al.*, 2005; Cai and Gao, 2007). Another limiting factor is the accuracy of the satellite orbits and clocks for GLONASS. In the study carried out by Cai and Gao (2007) the satellite orbits was 15 cm and has now been improved to approximately 10 cm (IGS, 2009). As reported by Cai and Gao (2007) with the inclusion of GLONASS, there was not any significant improvement in the receiver clock estimation and the estimated zenith wet tropospheric delay. During the convergence period, when the GLONASS satellites were included thus the geometry also improved resulting in an improvement of the convergence period in the east and up direction. The major constraint of the Cai and Gao's (2007) study was there were typically only two or three GLONASS satellites being observed.

Tolman *et al.* (2010) and Li *et al.* (2009) both stated that using GLONASS with GPS is beneficial, when there are only a few (less than five) GPS satellites available. However, the lower precisie GLONASS orbit and clock products can even decrease the positioning accuracy in some cases (Tolman *et al.*, 2010). According to Cai and Gao (2007), using GLONASS with GPS can improve the solution accuracy by 28%, 40% and 24% and the corresponding convergence period by 24%, 21% and 19% for the north, east and up coordinate components, respectively. These results were observed based on the test data from seven different IGS stations. According to the previous work, it is difficult to

conclude if using GLONASS with GPS is beneficial, compared to using GPS alone. This is due to the differences in the error corrections and models used in different papers.

Shen and Gao (2006)'s results indicated that the combined system has a greater accuracy than the current GPS system, a 75% improvement in both horizontal and vertical. The combined system has a greater improvement in convergence period. The simulated results showed that the convergence period was reduced by more than half compared to the current GPS PPP. As the constellation grew from the data examined by Cai and Gao (2007) and Cai (2009) it was observed that the quality of the results improved. It would be expected that as all potential error sources are more efficiently mitigated, the quality of the results would become similar to that of simulated results presented by Shen and Gao (2006).

1.3.4 From PPP to so-called PPP-RTK

In conventional PPP, the ambiguities are solved as part of the unknown state with real numbers and not fixed to integers (Zumberge *et al.,* 1997; Kouba *et al.,* 2001). As a result, several tens of minutes of initial data are needed when processing to allow the ambiguities to reach a steady state and the solution to converge. For real-time applications using NRTK (Network Real-Time Kinematic), observations from a reference station together with network-derived parameters to describe distance dependent errors or a virtual reference station are transmitted to GPS users in the field using the RTCM

standards (Wubbena *et al.,* 2005). Based on this methodology, Wubbena *et al.* (2005) saw precise absolute positioning based on a NRTK network (termed PPP-RTK) as a practicable concept. Essentially, PPP-RTK is the augmentation of PPP estimation with precise un-differenced atmospheric corrections and satellite clock corrections from a reference network, allowing an instantaneous ambiguity fixing for users within the network coverage (Li *et al.,* 2011).

Wubbena *et al.* (2005), Geng *et al.* (2011) and Mervart *et al.* (2008) presents three important benefits of PPP-RTK: significant reduction in initialization period from 20-30 minutes to a few seconds; improved real-time static and kinematic solution accuracy; and greater inter-station distances of bases from several tens of kilometres to several hundred kilometres.

Geng *et al.* (2011), Mervart *et al.* (2008) and Zhang *et al.* (2011) show that ambiguity resolution is possible, but not always instantaneous as described by Li *et al.* (2011) in their experimental case study. Similar to Mervart *et al.* (2008), Geng *et al.* (2011) showed a successful ambiguity resolution with the significant improvement in the accuracy of position estimates from 7.1, 13.7 and 11.4 cm to 0.9, 0.8 and 2.5 cm for the north, east and up components, respectively, but a few tens of minutes was required to achieve the first ambiguity-fixed solution. Zhang et al. (2011) stated that the dual-frequency PPP-RTK performance required less than 30 epochs (15 mins) to converge with the ambiguity resolution, typically occurring within the first 10 epochs (5 mins). The corresponding

accuracy of the ambiguity-fixed positioning was approximately 1 cm and 5 cm for the horizontal and vertical components, respectively, while the accuracy of the ambiguity-float positioning ranged from 2 - 4 dm within the first 15 minutes.

The PPP-RTK proposed by Geng *et al.* (2011) and Mervart *et al.* (2008) is still useful in some highly kinematic environment like a buoy or an airplane at a significant distance (several 100 to 1000 km) from the reference network, where the required solution performance is not as critical as that in instantaneous positioning, such as near-real-time GPS meteorology. One of the limitations of PPP-RTK not being instantaneous may possibly lead to a bottleneck on the server end, which prohibits many real-time users who require instantaneous precise positioning from applying the PPP-RTK model (Geng *et al.*, 2011).

1.3.5 Low-Cost Receivers

Extensive research has been done in PPP with data collected by dual-frequency, geodetic-quality GPS receiver. Lower cost receivers are more affordable to the general public thus stimulating interest in possible applications through processing by PPP. The use of low-cost, single-frequency GPS receivers creates a challenge as the ionosphere, noise, multipath and other measurement error sources are managed.

The ionospheric effect is the largest error source after the satellite orbits and clocks in PPP. Using a single-frequency receiver makes it a lot more challenging to effectively

correct for the ionospheric delay. Chen and Gao, (2005) describes single frequency GPS receivers as the most popular type of receivers and the driving force for research in this area due to their broad range of application.

The simplest method for ionospheric effect mitigation is by using the Klobuchar model with ionospheric coefficients, which only mitigates for 50% to 60% of the total ionospheric effects. Also, the IGS has been providing the total electron content of ionosphere on a global scale since 1998 (Schaer *et al.*, 1998). Ovstedal (2002) showed that the IGS model known as Global Ionospheric Model (GIM) could provide better results than the Klobuchar model using the same GPS dataset and ephemeris, but only a couple of metres position accuracy has been obtained since only the pseudorange measurements were used. The use of the GIM model will also be limited by the low spatial and temporal resolution and significant latency (Chen *et al.*, 2005). The ionosphere-free observables known as GRAPHIC (GRoup And PHase Ionospheric Correction) (Yunck, 1996) can be formed via a combination of the pseudorange and carrier-phase observations. A positioning accuracy of 1.5 m has been demonstrated for LEO (Low Earth Orbit) satellite orbit determination in Montenbruck (2003). When applying GRAPHIC, an estimation process using cumulative measurements has to be applied and a long time period of 2-4 hours is also required for the float ambiguity parameters to converge (Héroux *et al.*, 2004). Beran *et al.* (2007) showed the positioning accuracy at a couple of metres using single-frequency observations from a static geodetic

receiver with one or two (a bias and a drift) zenith ionospheric parameters being estimated.

As reported in Chen and Gao. (2005) the ionospheric estimation model with horizontal gradients estimated and GIM offer better performance than the Klobuchar model. The ionospheric estimation model and GIM provide a comparable accuracy at mid-latitude stations. The Klobuchar model can be implemented in real-time mode, while GIM is obtainable only in post-mission using the IGS Final ionospheric products with a latency of currently 11 days. GIM is slightly more accurate at high-latitude stations, while the ionospheric estimation model is much better at equatorial stations.

Beran *et al.* (2007) collected data with a Garmin GPS 12XL handheld receiver with a Garmin GA27C low-profile remote automobile antenna. IGS rapid and final ionospheric grid maps were used in the tests. During the kinematic experiment, the Garmin receiver encountered difficulties with GPS signal tracking for both pseudorange and carrier-phase measurements. The low-cost GPS receiver point positioning depended on the receiver tracking capabilities, i.e., hardware-based-limit and handling of measurement errors. The technique worked for static and kinematic applications and approximately 50 cm 3D error rms was achieved. The obtained positioning results were worse than those of the high-quality GPS receiver, but they were still within the few dm accuracy level (horizontal rms) (Beran *et al.*, 2007).

1.4 Problem Statement

As stated, PPP requires a relatively long initialization period (few tens of minutes at least) for the carrier-phase ambiguities to converge to constant values and for the solution to reach its optimal precision. This situation is primarily caused by the estimation of the carrier-phase ambiguity from the relatively noisy pseudoranges. The result is that PPP can take full advantage of the precise but ambiguous carrier-phase observations; however, the length of time it takes to reach the optimal solution is a major disadvantage to the wider use of the technique. If the pseudoranges were more precise then there would be a reduction in the convergence period. As can be seen from the previous section, no current PPP research has focused on the pseudoranges.

Given this problem, this study seeks to improve the management of pseudorange observable error. Pseudorange multipath and noise together is the largest remaining unmanaged error source in PPP. By reducing the effects of the multipath and noise on the pseudorange observable, carrier-phase ambiguities will reach a steady state at an earlier time, thus reducing the initial convergence and re-convergence period of PPP. This study seeks to address this short coming of the technique.

1.5 Thesis Objectives

The general objective of this study is to significantly reduce the initial convergence period of PPP by reducing the effects of pseudorange multipath and noise. The initial

phase of research requires the development of a PPP software of comparable scientific standard. This work is followed by the examination of the causes of PPP convergence period (e.g., initial pseudorange-based solution, filtering techniques, parameter estimations, unmodelled errors) and defining convergence period quantitatively (using a literature-based and RAIM approach to be discussed later). The final phase is the mitigation of the pseudorange multipath and noise to improve initial solution accuracy (through RAIM pseudorange / carrier-phase residual analysis and rejection) and reduce filter convergence period (through pseudorange multipath modelling and stochastic de-weighting).

1.6 Research Contributions

This research has been fueled by the ideas presented in Bisnath and Gao (2009) as concepts which may improve convergence as well as improve the integrity monitoring within PPP. The concepts discussed include RAIM and using the multipath observable to mitigate the pseudorange multipath and noise from the P1 and P2 observable. These two methods shall be augmented into the standard PPP software.

RAIM provides rigorous analysis of the post-fit residuals, assisting in detecting outliers within the residuals, which in some cases have been previously overlooked by standard PPP residual rejection. Unlike RAIM, the current standard method for rejecting residuals is based on analyzing the maximum pseudorange and carrier-phase post-fit residuals. For

example, in the NRCan PPP code (NRCan, 2010) if the carrier-phase residual is greater than 4.47 cm (an empirically set value), then the measurement for the respective satellite is rejected and the epoch is reprocessed.

If pseudoranges were more precise, there would be a reduction in the convergence period. Pseudorange multipath and noise together is the largest remaining unmanaged error source in PPP. By reducing the effects of the multipath and noise on the pseudorange observable, carrier-phase ambiguities will reach a steady state at an earlier time, thus reducing the initial convergence and re-convergence period of PPP. The multipath linear combination was calculated to mitigate the raw pseudorange observable and stochastically de-weight pseudorange observables based on the magnitude of the pseudorange multipath and noise present. To correct the raw observables three different methods were applied; these included: 1) running average 2) previous day multipath observable, and 3) the same day multipath observable.

The running average filters the pseudorange multipath and noise in real-time. Its major limitation is the requirement of several epochs of data to successfully average the ambiguity term. A simple recursive algorithm is used to average the ambiguity term. Filtering the pseudorange observables may introduce the uncertainty of the ambiguity term present in the running average. Significant improvements were not observed while using this multipath observable from the previous day because of the pronounced effect of the pseudorange noise. While improvements were minimal, it is beneficial to make use

of data from the previous day if the information is available, while it is important to take note of this method's primary limitation is a repeated multipath environment is required.

The final method applied is the use of the multipath observable from within the same day. This method is possible by post-processing the dataset, generating the multipath observable which is then fed into the PPP processor. This method was most effective as it allowed the ambiguity term to be accurately removed and therefore accurately removed the pseudorange multipath and noise from the pseudorange measurements. Also, unlike the running average, using the same day multipath observable provides corrections during the first epoch, thus improving the initial coordinates which is critical for reducing convergence period in PPP.

The benefits of either de-weighting using the elevation angle or the multipath observable were observed when compared to the standard PPP solution, which used no weights on the pseudorange measurements. Of all the methods presented, the stochastic de-weighting using the pseudorange measurements is recommended to become a component of the standard PPP processor. The strength of this model is it allows for real-time compensation of the effects of the pseudorange multipath and noise in the stochastic model, as long as realistic stochastic models are applied for each epoch in the position estimation process. Its performance is comparable to elevation weighting but with further tuning of the weighting strategy it is expected to show improvement performance as was seen for individual sites.

1.7 Thesis Outline

Chapter 2 provides details on the development of the PPP processor entitled, York-PPP. This description is followed by a brief overview of the used observation and correction models and the architecture and functionalities of the software. The chapter is concluded with significant processing results from the York-PPP software designed to verify that the software is of high scientific standard.

Chapter 3 provides an overview of different methods to define the initial convergence period in PPP. These methods include: 1) required convergence period based on the application; 2) when the solution attains a steady state; 3) a modified version of horizontal protection level (HPL). PPP requires a relatively long initialization period (few tens of minutes at least), implementing RAIM is expected to improve initialization thus reducing the convergence period.

Chapter 4 discusses the pseudorange multipath and noise, which is the largest remaining unmanaged error source in PPP. This is followed by novel implementation different techniques implemented to mitigate pseudorange multipath and noise and quantifies the magnitude of improvement found in using each of the technique.

Finally, Chapter 5 summarizes all the findings and provides recommendations for future work.

2.0 Development and Testing of York-PPP Software

The PPP processor entitled, York-PPP, was developed based on the processing software engine used by the on-line CSRS-PPP service (NRCan,2010). Presented in this chapter is a brief overview of the observation and correction models used within York-PPP. This is followed by an overview of the architecture and functionalities of the software. The chapter is concluded with results of GPS data processed by York-PPP verifying that the software is of high scientific standard.

2.1 Single Point Positioning

In single point positioning, the coordinates of a receiver at an "unknown" point are sought with respect to a geodetic datum by using the "known" positions of the GPS satellites being tracked. Single point positioning (also referred to as absolute positioning or point

positioning) is the most basic GPS solution obtained with epoch-by-epoch least-squares estimation. For point positioning, GPS provides two levels of services, the Standard Positioning Service (SPS) with the access for civilian users and the Precise Positioning Service (PPS) with the access for the authorized users. In SPS, only the C/A-code is available. The achievable real-time SPS 3D positioning accuracy is ~ 10 m at the 95% confidence level. The pseudorange at an epoch can be modelled by equation 2.1 (Hofmann-Wellenhof *et al.*, 2001)

$$R_i^j(t) = \rho_i^j(t) + c\Delta\delta_i^j(t) + d_{iono} + d_{tropo} \quad 2.1$$

where, $R_i^j(t)$ is the measured pseudorange between the observing site *i* and the satellite *j*, $\rho_i^j(t)$ is the geometric distance between the satellite and the observing point and *c* is the speed of light, d_{iono} and d_{tropo} represent the delays caused by ionosphere and troposphere refraction. $\Delta\delta_i^j(t)$ is the clock bias, which represents the combined clock offsets of the receiver and the satellite clock with respect to GPS time. The receiver location to be calculated is determined relative to the distance$\rho_i^j(t)$, which can be explicitly written as

$$\rho_i^j(t) = \sqrt{(X^j - X_i)^2 + (Y^j - Y_i)^2 + (Z^j - Z_i)^2} \quad 2.2$$

where X^j, Y^j, Z^j are the components of the geocentric position vector of satellite j at epoch t and X_i, Y_i, Z_i are the three unknown Earth-Centred-Earth-Fixed (ECEF)

coordinates of receiver i. The above observation equation is non-linear function of the unknowns. In order to most efficiently solve the problem, the model can be linearized about the given initial position vector $(X_{i_0}, Y_{i_0}, Z_{i_0})$. The iterated least-squares solution is obtained from

$$x = x_0 + \Delta x \tag{2.3}$$

Where X is the state estimate, x_0 is the a priori estimate and

$$\Delta x = (A^T A)^{-1} A^T w \tag{2.4}$$

In the above equation, A is the Jacobian matrix which consists of the partial derivatives of measurement model with respect to unknown parameters, and w is the misclosure vector of differences between the actual measurements and the modelled observation vector.

$$A = \begin{bmatrix} \frac{\partial \rho_1}{\partial X_i} & \frac{\partial \rho_1}{\partial Y_i} & \frac{\partial \rho_1}{\partial Z_i} & 1 \\ \frac{\partial \rho_2}{\partial X_i} & \frac{\partial \rho_2}{\partial Y_i} & \frac{\partial \rho_2}{\partial Z_i} & 1 \\ \vdots & \vdots & \vdots & 1 \\ \frac{\partial \rho_n}{\partial X_i} & \frac{\partial \rho_n}{\partial Y_i} & \frac{\partial \rho_n}{\partial Z_i} & 1 \end{bmatrix} \tag{2.5}$$

$$w = \begin{bmatrix} R_1 - \rho_1 \\ R_2 - \rho_2 \\ R_3 - \rho_3 \\ \vdots \\ R_4 - \rho_4 \end{bmatrix} \tag{2.6}$$

where

$$\frac{\partial \rho_i^j}{\partial X_i} = \frac{(X^j - X_i)}{\sqrt{(X^j - X_i)^2 + (Y^j - Y_i)^2 + (Z^j - Z_i)^2}} \quad 2.7$$

$$\frac{\partial \rho_i^j}{\partial Y_i} = \frac{(Y^j - Y_i)}{\sqrt{(X^j - X_i)^2 + (Y^j - Y_i)^2 + (Z^j - Z_i)^2}} \quad 2.8$$

$$\frac{\partial \rho_i^j}{\partial Z} = \frac{(Z^j - Z_i)}{\sqrt{(X^j - X_i)^2 + (Y^j - Y_i)^2 + (Z^j - Z_i)^2}} \quad 2.9$$

where X^j, Y^j, Z^j are the GPS satellite coordinates and X_i, Y_i, Z_i are the approximate receiver coordinates. The terms in the vector w, R_1 and ρ_1 represent the measured pseudorange and the modelled range, respectively.

2.2 Precise Point Positioning

As described in the previous section, PPP is a positioning technique in which a single receiver is used to determine coordinates using precise satellite orbits and clocks in the data processing. PPP is currently able to provide few centimetre-level results in static mode and decimetre-level results in kinematic mode. The results presented in Bisnath and Gao (2009) indicates that it takes approximately 20 to 30 minutes for the positioning solution to converge to the centimetre-level. After convergence, the horizontal component is accurate at the sub-centimetre level and centimetre to few centimetres in the vertical component.

It is necessary when processing data with PPP to mitigate all potential error sources in the system. As a result of the un-differenced nature of PPP, all errors caused by the space segment, propagation, environment and receiver directly impact the positioning solutions. The mitigation can be carried out by modelling, estimating or eliminating (through linear combination) each error term. Each of these error sources and their mitigative strategy are discussed in more detail in the following section.

The standard PPP observation model is presented in equations 2.10 and 2.11. The term standard is used as the four major publically available online PPP services: CSRS-PPP (NRCan, 2010), GAPS (Leandro *et al.*, 2007), APPS (Farmer, 2010) and magicGNSS (GMV, 2010) use this model, with ionospheric-free combination of pseudorange and carrier-phase. Though proprietary differences exist between them that may not always be published. Leandro (2009) indicated that one difference amongst online PPP services is the estimation process of the residual neutral atmosphere delay, e.g., as random walks, or fixed values for given time intervals.

Assuming that PPP related errors such as phase wind-up, relativity, antenna phase centre offset and geophysical effects have been properly mitigated for (discussed in more detail in Section 2.3), the un-differenced observation equations can be written as follows (Mohamed *et al.*, 2002). Where the pseudorange measurement in eq'n 2.10 is measured in units of distance and the carrier-phase measurement in eq'n 2.11 is measured in units of cycles which is converted to distance.

$$P_{L_i} = \rho + c(dr - dT) + d_{orb} + d_{iono} + d_{tropo} + d_{multi_{(P_{L_i})}} + b^r_{P_{L_i}} - b^s_{P_{L_i}} + \varepsilon(P_{L_i}) \quad 2.10$$

$$\phi_{L_i} = \rho + c(dr - dT) + d_{orb} - d_{iono} + d_{tropo} + \lambda_{L_i} N_{L_i} + d_{multi_{(\phi_{L_i})}} + b^r_{\Phi_{L_i}} - b^s_{\Phi_{L_i}} + \varepsilon(\Phi_{L_i}) \quad 2.11$$

Where

P_{L_i} - measured pseudorange on L1 or L2 (m)

ϕ_{L_i} - measured carrier-phase range on L1 or L2 (m)

ρ - true geometric range (m)

c - speed of light (ms^{-1})

dt - receiver clock error (s)

dT - satellite clock error (s)

d_{orb} - satellite orbit error (m)

d_{iono} - ionospheric delay (m)

d_{trop} - tropospheric delay (m)

λ_{L_i} - wavelength on L1 or L2

N_i - non-integer phase ambiguity on L1 or L2 (cycle)

$d_{multi_{(P_{L_i})}}$ - pseudorange multipath effect on L1 or L2 (m)

$d_{multi_{(\phi_{L_i})}}$ - carrier-phase multipath on L1 or L2 (m)

b^*_* - hardware biases (m)

$\varepsilon(*)$ - measurement noise (m)

The linearization of the observation equations 2.10 and 2.11 around the a priori parameters and observations becomes the matrix form

$$A\delta + W - V = 0 \tag{2.12}$$

where A is the design matrix, δ is the vector of corrections to the unknown parameters X, W is the misclosure vector and V is the vector of residuals. The design matrix A consists of the partial derivatives of the observation equations with respect to X, consisting of four types of parameters: station position (X_i, Y, Z_i), receiver clock offset (dt), troposphere zenith path delay (zpd) and carrier-phase ambiguities.

$$A = \begin{bmatrix} \frac{\partial \rho^1}{\partial X_i} & \frac{\partial \rho^1}{\partial Y_i} & \frac{\partial \rho^1}{\partial Z_i} & \frac{\partial \rho^1}{\partial t_i} & \frac{\partial \rho^1}{\partial zpd} & 0 & 0 & \dots & 0 \\ \frac{\partial \phi^1}{\partial X_i} & \frac{\partial \phi^1}{\partial Y_i} & \frac{\partial \phi^1}{\partial Z_i} & \frac{\partial \phi^1}{\partial t_i} & \frac{\partial \phi^1}{\partial zpd} & \frac{\partial \phi^1}{\partial N_{if,1}} & 0 & \dots & 0 \\ \vdots & \vdots & \vdots & \vdots & \vdots & 0 & 0 & \dots & 0 \\ \frac{\partial \rho^n}{\partial X_i} & \frac{\partial \rho^n}{\partial Y_i} & \frac{\partial \rho^n}{\partial Z_i} & \frac{\partial \rho^n}{\partial t_i} & \frac{\partial \rho^n}{\partial zpd} & 0 & 0 & \dots & 0 \\ \frac{\partial \phi^n}{\partial X_i} & \frac{\partial \phi^n}{\partial Y_i} & \frac{\partial \phi^n}{\partial Z_i} & \frac{\partial \phi^n}{\partial t_i} & \frac{\partial \phi^n}{\partial zpd} & 0 & 0 & \dots & \frac{\partial \phi^n}{\partial N_{if,n}} \end{bmatrix} \tag{2.13}$$

The misclosure vector is the difference between the observed carrier-phase or pseudoranges and their modelled values, computed with the parameter values as known at the time of the update. The elements of the misclosure vector are computed as follows

$$w_{\phi_{L_{if}}} = \phi_{L_{if}} - \rho_i - cdT^j + cdt_i - T_{zpd} - \lambda_{L_{if}} N^j_{L_{if}} \tag{2.14}$$

and

$$w_{P_{L_{if}}} = P_{L_{if}} - \rho_i - cdT^j + cdt_i - T_{zpd} \quad 2.15$$

resulting in

$$W = \begin{bmatrix} w^1_{P_{L_{if}}} \\ w^1_{\phi_{L_{if}}} \\ \vdots \\ w^n_{P_{L_{if}}} \\ w^n_{\phi_{L_{if}}} \end{bmatrix} \quad 2.16$$

$$X^T = \begin{bmatrix} x & y & z & dt & zpd & N^j_{j=1,nsat} \end{bmatrix} \quad 2.17$$

$$P = \begin{bmatrix} 1 & & & & & \\ & 100 & & & & \\ & & \ddots & & & \\ & & & 1 & & \\ & & & & 100 & \end{bmatrix} \quad 2.18$$

And the weight metric, P, is given by 2.18 as pseudorange measurements are approximately 100 times less precise than carrier-phase measurements. The least-squares solution with a priori weighted constraints (P_x) to the parameters is given by:

$$\Delta \mathrm{x} = (A^T P A + P_x)^{-1} A^T P W \quad 2.19$$

The estimated parameters are

$$\hat{X} = x^0 + \Delta \mathrm{x} \quad 2.20$$

The adjustment procedure represents a sequential filter that requires the user's input to specify whether the receiver's dynamics is static or kinematic. The station position may be constant or change over time depending on the user dynamics. The receiver clock will drift according to the quality of the oscillator. The zenith path delay will vary in time by a relatively small amount, in the order of a few cm/h and the non-integer carrier-phase ambiguities (N) will remain constant as long as the carrier-phases are free of cycle-slips (Héroux *et al.*, 2004).

2.3 GPS Error Sources

The following sections look at additional correction terms that are significant for carrier-phase point positioning. As mentioned before, there are a few corrections which have to be applied to carrier-phase and pseudorange measurements in addition to other commonly known effects (such as relativistic correction in order to have a complete (adequate) observation model in PPP. This aspect is a limiting factor to achieve cm-level accuracy, as it is possible today, with PPP. All corrections accounted for are listed below and discussed.

2.3.1 Satellite Ephemeris and Clock Errors

This is the errors in each satellite's reported position against its actual position. The accuracy of precise IGS (International GNSS Service) final orbit has steadily improved between 1992 and 2009 (Kouba, 2009). The IGS GPS final orbit accuracy in 2009 was of order 2.5 cm. GPS satellites carry highly stable atomic clocks to generate accurate timing

signals. Although the onboard atomic clocks are stable, the inability of the onboard oscillator to maintain synchronisation with GPS time results in a clock error. The deviation between the atomic time and GPS time is known as the satellite clock error (Wells *et al.*, 1999). The GPS clock rms error is ~75 ps with a standard deviation of ~20 ps (IGS, 2009).

2.3.2 Ionospheric Refraction

The ionosphere is the uppermost layer of the Earth's atmosphere between the heights of 50 km to 1000 km above the Earth's surface. The density of free electrons and ions is high enough to influence the propagation of satellite signals. GPS ranging can vary from a few metres to more than twenty metres within a day, depending on the user's location and time plus variations in the ionosphere (Wells *et al.*, 1999), but can reach over 150 m under extreme solar activities at midday and near the horizon (El-Rabbany, 2006). The ionospheric effect refracts the pseudorange and carrier-phase differently (Hofmann-Wellenhof *et al.*, 2001; Leick, 2004), but given that the ionosphere is a dispersive medium it is possible to use an ionosphere-free pseudorange and carrier-phase combination to eliminate common ionospheric biases.

The ionospheric delay is greater at the L2 carrier frequency than that of the L1 carrier frequency. Up to 99.9% of the ionospheric delay can be eliminated through linear combination of GPS observables on L1 and L2 frequencies (Hofmann-Wellenhof *et al.*,

2001; Collins, 2008). Though Elsobeiey *et al.* (2009) showed that neglecting the second-order ionospheric delay introduces an error in the order of 2 cm.

When measurements from both L1 and L2 frequencies are available, the following ionosphere-free linear combination can be formed for the pseudorange and carrier-phase in units of distance:

$$P_{IF} = \frac{f_1^2 P_1 - f_2^2 P_2}{f_1^2 - f_2^2} \quad 2.21$$

$$L_{IF} = \frac{f_1^2 L_1 \lambda_1 - f_2^2 L_2 \lambda_2}{f_1^2 - f_2^2} \quad 2.22$$

where f_1 = 1575.42 MHz and f_2 = 1227.60 MHz are the frequencies of the L1 and L2 signals, respectively, and λ_1 = 19.0 cm and λ_2 = 24.4 cm are the wavelengths of the L1 and L2 signals, respectively. A negative side effect of the iono-free combination is that the measurement noise is approximately tripled versus the noise on L1 or L2 (Leandro, 2009).

2.3.3 Troposphere Refraction

The troposphere extends from the surface of the Earth up to about 50 km. It delays both the pseudorange and carrier-phase signals by the same magnitude. The dry or hydrostatic component represents approximately 90% of the delay and wet component 10%. It is difficult to alleviate the troposphere delay completely, as the troposphere delay depends on the satellite elevation angle, receiver altitude, atmospheric temperature, pressure and

humidity. GPS ranging can vary from a few metres to more than twenty metres if the troposphere is not properly modelled.

Boehm and Werl, *et al.*, (2007) compared different tropospheric mapping functions (such as Isobaric Mapping Functions (IMF), Vienna Mapping Functions (VMF) and the Niell Mapping Functions (NMF)) for GPS and very long baseline interferometry and indicating closer to the equator and at higher latitude coefficients have deficiencies, which could influence the mean station height by as much as 4 mm. Apart from using a tropospheric model Kouba and Héroux (2001) suggested to estimate the wet component along with the other parameters in PPP processing to reduce the residuals of the wet tropospheric delay.

2.3.4 Relativistic Effects

The velocity of a GPS satellite in an Earth inertial frame is high enough that it will significantly affect the precision of position determination. Haustein (2009) indicated if these effects were neglected, an error of 12 km per day for position determination or 39 μs for time determination would occur. Three primary effects of the relativity on GPS are:

Fixed Frequency Offset Effect - There is a fixed frequency offset in the satellite's clock rate when observed from Earth. Most of the effect is purposely removed by slightly offsetting the satellite clock in frequency prior to launch (O'Keefe, 2000).

Sagnac delay- The Sagnac effect arises from the rotation of the Earth during the GPS signal propagation. The Sagnac effect is a correction for adapting the dilation of time caused to a clock carried by a rotating object on non-inertial frames (Ashby and Spilker, 1996). This relates to the fact that a moving clock tends to be slower than one at rest or moving slower. This results in a frequency offset that may be interpreted as a distance (ICD-GPS-200, 2000).

Periodic Clock Error Effect - The GPS satellite orbit is not truly circular. The slight eccentricity of each satellite orbit causes an additional periodic clock error that varies with the satellite position in its orbital plane. This correction must be applied to the broadcast time of the signal transmission (Ashby and Spilker, 1996). This additional effect is cancelled on the case of double-differencing, while it would bring a maximum of 23 ns for an eccentricity of 0.01 to single point positioning, an equivalent to 6.9 metres in distance (O'Keefe, 2000).

2.3.5 Multipath and Noise

Multipath occurs when signals travelling from a transmitter to a receiver propagate via multiple paths due to reflection and diffraction (Bisnath and Langley, 2001). This error is often caused by the reflected GPS signals from surrounding objects and terrain such as the ground, buildings, trees, canyons, and fences. The reflected signals increase the measured distance between the receiver and satellite resulting in inaccurate positions. The

multipath effect produces errors in both pseudorange and carrier-phase measurements. The magnitude of range error can reach up to 10 to 20 metres for pseudorange measurements and up to 5 cm for carrier-phase measurements (Wells *et al.,* 1999). Bisnath and Langley (2001) discussed four classes of multipath mitigation techniques:

Cautious antenna placement- Selection of low-multipath environment for antenna placement.

Hardware solutions - Hardware compensation rests with antenna design. The use of microwave absorbing material and receiver tracking augmentation. The extended ground planes and choke rings can reduce antenna susceptibility to ground bounce multipath, and gain-pattern-forming techniques reduce antenna sensitivity to multipath at low elevation angles.

Software solutions - Algorithms have been developed to diminish unknown measurement error sources, including multipath, ranging from the application of GPS satellite elevation angle masks to the use of receiver autonomous integrity monitoring scheme (RAIM).

Hybrid solutions – Combination of hardware and software components to estimate multipath due to the spatial correlation of the measurements received from an array of antennas, but requires the array to be static (see, e.g., Ray *et al.*, 1999).

2.3.6 Antenna Phase Centre Offset and Variation

Receiver Antenna - The receiver electrical phase centre is not a physical centre and is neither well defined nor fixed. For any given GPS antenna, the variation of the phase centre depends on the direction change of the incoming GPS satellite signals, and it is a function of the antenna phase pattern, known as the Phase Centre Variation (PCV). The receiver antenna phase centre offset (PCO) can cause a positioning error up to 10 cm in the vertical component and a few centimetres in the horizontal component (Mader, 1999).

Satellite Antenna - The satellite antenna phase centre offsets originate from the separation between the GPS satellite centre of mass and the electronic phase centre of its antenna. Force models used by the IGS community for satellite orbit modelling refer to the satellite centre of mass. Subsequently, the resulting IGS precise satellite orbit and clock correction products also refer to the satellite centre of mass, and not the antenna phase centre (Zhu *et al.*, 2002).

2.3.7 *Phase Wind-Up*

Phase wind-up error is a problem associated with the satellite and receiver antenna orientation due to the nature of circularly polarised waves intrinsic in the GPS signals. The phase wind-up error only affects the carrier-phase measurements. GPS satellites transmit right circularly polarised waves, thus the observed carrier depends on the mutual orientation of the satellite and receiver antennas. The phase wind-up error has generally been ignored in most of the high-precision relative GPS applications, but cannot be in

absolute PPP. It has been shown that the error can reach up to 4 cm for a 4000 km baseline (Kouba *et al.*, 2001).

2.3.8 Solid Earth Tide

The earth is composed of three basic components: solid (i.e., rock), liquid (i.e., ocean) and the atmosphere, which constantly interact with each other making the Earth pliable and subject to deformation. Globally, a station undergoes periodic movement reaching a few decimetres, which are generally not considered in the International Terrestrial Reference Frame (ITRF) position (Kouba, 2009). These are typically referred to as "site displacement effects".

The "solid" Earth is far from rigid and is pliable enough to respond to the same gravitational forces that generate the ocean tides. The tides are caused by the gravitational attraction and temporal variations of the Sun and Moon orbital motion. While the ocean tides are strongly influenced by the coastal outlines, the solid Earth tides can be computed quite accurately from simple Earth models (Leick, 2004). The effect of the tidal variation is larger in the vertical component and can reach as much as 30 cm (Kouba, 2009). For horizontal component, its effect can reach about 5 cm (Leick, 2004). Neglecting this error in point positioning would result in systematic position errors of up to 12.5 cm and 5 cm in the radial and north directions, respectively (Kouba, 2009).

2.3.9 Ocean Tide Loading

The ocean loading tides are the deformation of the sea floor and coastal land that results from the redistribution of seawater, which occurs from the ocean tides. While the ocean loading is almost an order of magnitude smaller than the solid Earth tides, it is more localised. For stations that are located far from the ocean (>1000 km) with the, point positioning at 5 cm precision level, or static positioning over 24 hour periods, the ocean loading effects can be safely ignored (Kouba, 2009). However, for stations that are located along the coastline with an observation length shorter than 24 hours, this effect needs to be taken into account. Otherwise, this error will be mapped into the tropospheric ZPD and station clock solutions. The magnitude of the surface displacement caused by the ocean tide loading can reach up to 5 cm in the height and 2 cm in the horizontal direction (Kouba and Héroux, 2001).

2.3.10 Polar Tides

Polar tides are periodical deformations caused by the changes of the Earth's spin axis with respect to the Earth's crust, i.e., the polar motion. In order to achieve a sub-centimetre point positioning accuracy and be consistent with the ITRF frame, this bias is required to be considered during data processing. This is because most of the IGS Analysis Centers (ACs) utilises these correction terms to generate the precise satellite orbit and clock corrections, and thus, the precise products are consistent with the station

position corrections. The polar tide displacements can reach about 7 mm in the horizontal direction and 25 mm in the height (Kouba, 2009).

2.3.11 Atmosphere Loading

The gravitational forces of the Sun and Moon affect the solid Earth tides, the ocean and atmosphere in different ways due to the different properties of material involved (Urquhart, 2009). The atmospheric mass above the Earth's surface causes a load on the Earth's surface. This results in horizontal and vertical displacements, which can be as large as 20 mm for the vertical component and 3 mm for the horizontal component (Petrov and Boy, 2004). The displacement caused by the atmospheric tides varies according to atmospheric pressure variations, as well as geographic location. The results in the study carried out by (Urquhart, 2009) showed an improvement in the PPP solution by 3.6% to 5.9% for six out of eight of the examined sites, indicating that while improvement was noted the benefits of atmospheric load modelling would become more apparent as the PPP technique improves.

2.3.12 Differential Code Bias (DCB)

L1-L2 (P1-P2) DCB - The differences between L1 and L2 frequencies which are consistent with the P1 and P2 pseudorange measurements, hence the term P1-P2. In general, the satellite DCBs are nearly constant in time, but differ from satellite to satellite. The magnitude of this bias can reach up to 12 ns. If left unaccounted, this may have detrimental effects on the estimated PPP solutions (Kouba, 2009).

P1-C1 DCB - The P1-C1 DCBs are the differences between the pseudorange observations. The magnitude of the P1-C1 biases is quite constant, i.e., in the order of 2 ns (60 cm), but they are unique for each satellite and receiver. The values of the P1-C1 biases are regularly estimated by the IGS ACs as part of their precise satellite clock corrections estimation process (Collins *et al.*, 2005).

P2-C2 DCB - As part of the modernization of GPS, the satellites which belong to the Block IIR-M have a new open civil pseudorange called L2C or C2 in the RINEX 2.11. There is a bias between the P2 and C2 pseudorange measurements called P2-C2 DCB. Leandro *et al.*, 2007 results shows the bias ranging from 0 to 20 cm.

2.3.13 Ambiguity Term

The ambiguity term within the carrier signal is the unknown number of whole wavelengths in an unbroken set of measurements from the satellite to a receiver. The initial estimate of the real ambiguities is mainly based on the GPS C/A-code information (Geng *et al.*, 2010). The reliability is very low because the C/A-code has metre level ranging accuracy (Hofmann-Wellenhof *et al.*, 2001). The ambiguity parameter in PPP includes the satellite clock, receiver clock and hardware bias, and in relative positioning it is mitigated by double-differencing, to remove all common bias existing amongst the two receivers and satellites. It was reported by Geng *et al.* (2010) that fixing the ambiguities to integers in PPP can significantly improve the positioning quality, especially for the east component, whereas keeping float ambiguities will potentially jeopardize the final

solutions, such as introducing amplified unauthentic signals into the long-term position time series.

2.4 Overview of York-PPP software

The York-PPP processor was implemented in C++, MATLAB and DOS batch scripts, capitalizing on the advantages that exist in each of the programming languages. The processing core of York-PPP consists of approximately 110 functions and over 32,000 lines of C++ code translated from the original Fortran code provided by NRCan, (2010). The source code is used by the on-line CSRS-PPP service. MATLAB was used in the design of the graphical user interface (GUI) of the software, as well as plotting of output data of the processor. The DOS batch scripts were used to automate the downloading of the input (observation, and precise orbits and clocks) files and to initialize the batch processing aspect of York-PPP.

One standard 24 hour long observation file with a 30 secs data rate takes approximately 2 minutes to process on an Intel Core Duo 2.10 GHz laptop. The software was designed to allow batch processing of datasets which has proven to be an asset. The dataset used for this research consists of 560 observation files collected from 81 sites accompanied with all required input files (i.e., precise orbits and clocks, ocean loading coefficient and ANTEX file). York-PPP is capable of running independently to process the dataset, storing all necessary output files for later analysis. Each scenario takes approximately 10

hours with a minimum of 30 scenarios examined within this research, for a total of 13 days of consistent processing by York-PPP.

Figure 2.1 is a general overview of architecture of York-PPP. It consists of three core modules – the data interface, sequential least-squares module and correction computation. Before the actual computation takes place, the user defines processing parameters and input files through the GUI. All incoming data are converted into an internal format and plausibility checks (such as making sure all necessary data are available for each satellite, types of observable present and number of satellites present for each epoch) are carried out. Also, coefficients required for interpolating satellite orbits and clock corrections are generated.

Depending on the user's input, different algorithms will be selected. Out of these parameters the corrections for each observation are calculated according to the algorithms discussed in Section 2.3. The correction module accesses the required data supplied from the user in form of an observation file, precise satellite orbits and clocks, ocean loading coefficients and the ANTEX file. The corrected observations together with the computed satellite positions are then fed into the sequential least-squares module. Within this module the actual position estimation takes place. The accuracy and quality of the parameters are provided to the user. For the subsequent evaluation and comparison of different settings, the significant results and intermediate data are stored in files. Currently, this first version only supports post-processing; future work would consist of expanding the functionality of the software to work in real-time.

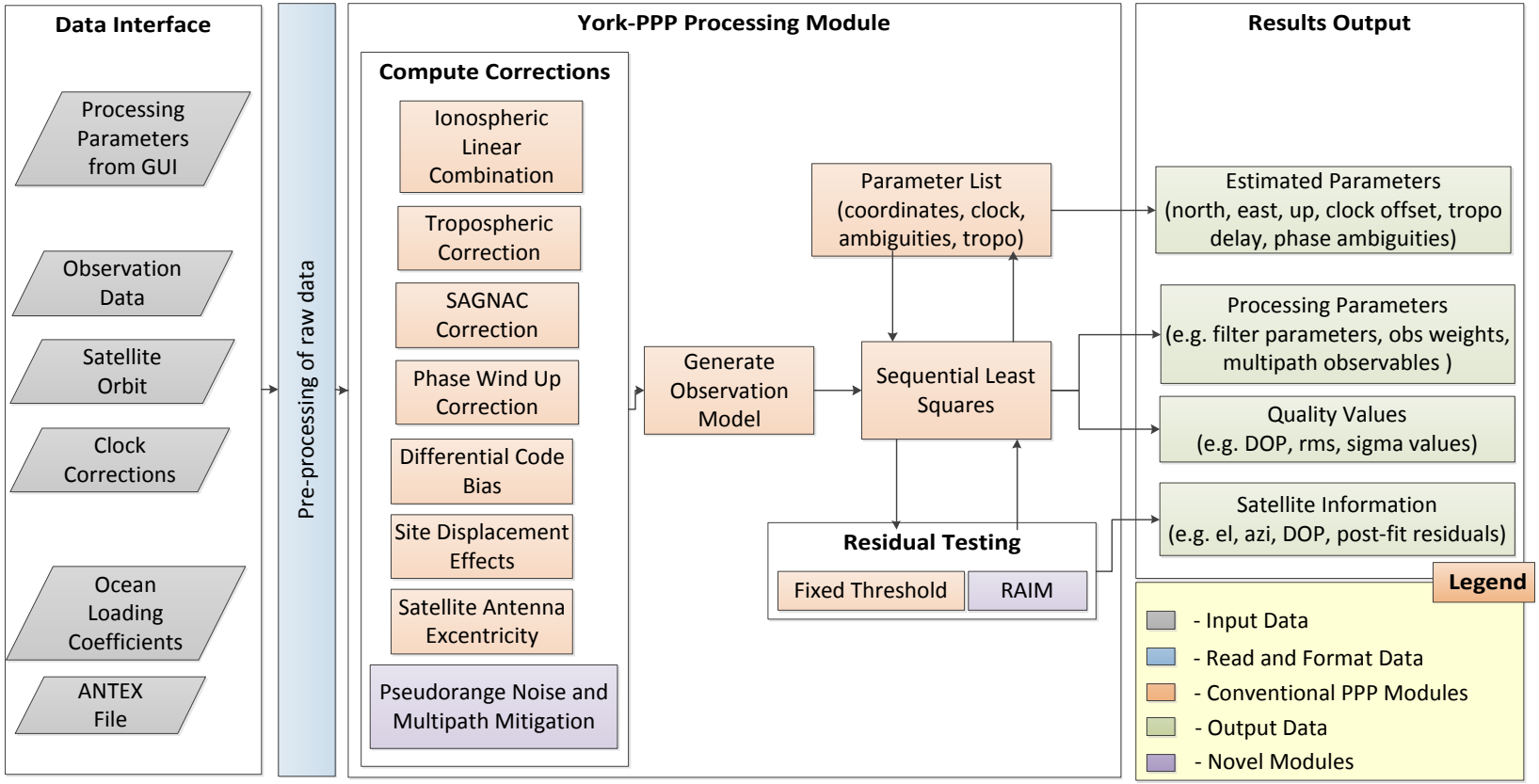

Figure 2.1: Architecture of York-PPP

2.5 Dataset and Processing Parameters

Data from 81 IGS stations observed during the days of 244 to 250 in 2011 were used in the validation of the York-PPP software. The sites chosen were a subset of those processed regularly by most IGS ACs, represents a good global distribution. The distribution of the sites is illustrated in Figure 2.2 below. Dual-frequency receivers tracking either the C/A or P(Y) pseudorange on L1 were used. Settings used for the evaluation the ionosphere-free combination of L1 and L2 data, 2 m and 15 mm a priori standard deviations for pseudorange and carrier-phase observations, and 10° elevation cut-off angle.

IGS Final 5 minute orbits, 30 second clocks and Earth rotation parameters products were used. The reference stations are analyzed in static PPP mode. Receiver clocks were estimated epoch-by-epoch. The zenith tropospheric delays were estimated every 60 minutes with an initial STD of 1 m and a power density of 2 cm/sqrt (h). The station coordinates was estimated with an initial constraint of 1 km. The IGS relative antenna model was used. The ocean loading and solid Earth tides were obtained from Scherneck (2011) for each of the sites being processed.

The accuracy of York-PPP is validated in Section 2.6 and the quality of the solution is compared to other PPP processors. PPP is not restricted to only static data, the quality of PPP results in kinematic mode are discussed in Section 2.7.

Figure 2.2: Distribution of the selected 81 IGS stations

2.6 Static Results

To analyze the accuracy of the solution being produced by the developed York-PPP processing software, the estimated positions were compared with the IGS weekly SINEX solution (Crustal Dynamics Data Information System, 2012). The primary factors that affect the convergence period and the accuracy of PPP are the limited precision of current precise orbit and clock products and the effects of unmodelled error sources. Solution here refers to the solution generated after processing the entire 24 hour dataset.

The distribution of the York-PPP solutions in the horizontal and vertical components are illustrated in Figure 2.3 and Figure 2.4 with histogram bin sizes of 2 mm and 5 mm, respectively, for a sample size of 560. Of the 560 datasets processed, 4 of the 7 datasets from the site KIRU, in Sweden converged with significant biases in the final solution. Therefore this site was not included in the generation of any of the following statistics.

KIRU is analyzed in detail in Section 2.8, to examine how the solutions deteriorate and is examined further in Chapters 3 and 4 in an attempt to improve the quality of the results.

PPP has been described as being capable of producing sub-centimetre accuracy in the horizontal component and few centimetres in the vertical (Bisnath and Gao 2009; Ge *et al.*, 2008). The York-PPP results indicate that 99.2% of the data processed had an error in the horizontal component of less than or equal to 2 cm and that 92% of the results had a horizontal error of less than one centimetre. In the vertical component, 99% of the data processed had an error of 5 cm or less. It is expected for the vertical component to be of a lesser accuracy than that of the horizontal component due to satellite geometry (inherent to all modes of GPS/GNSS data processing) and the quality of the models for the solid and ocean loading tides.

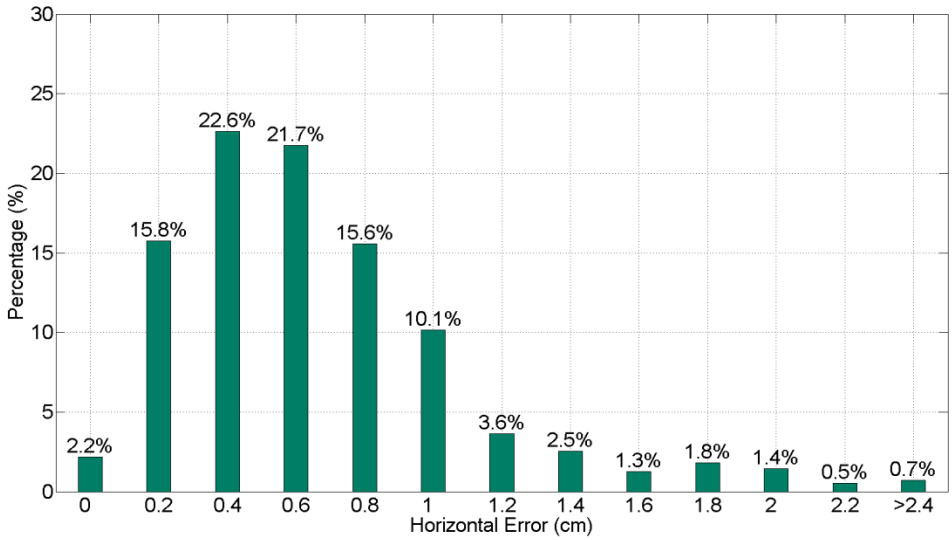

Figure 2.3: Histogram showing absolute horizontal error after 24 hour solution for 80 sites processed in static mode

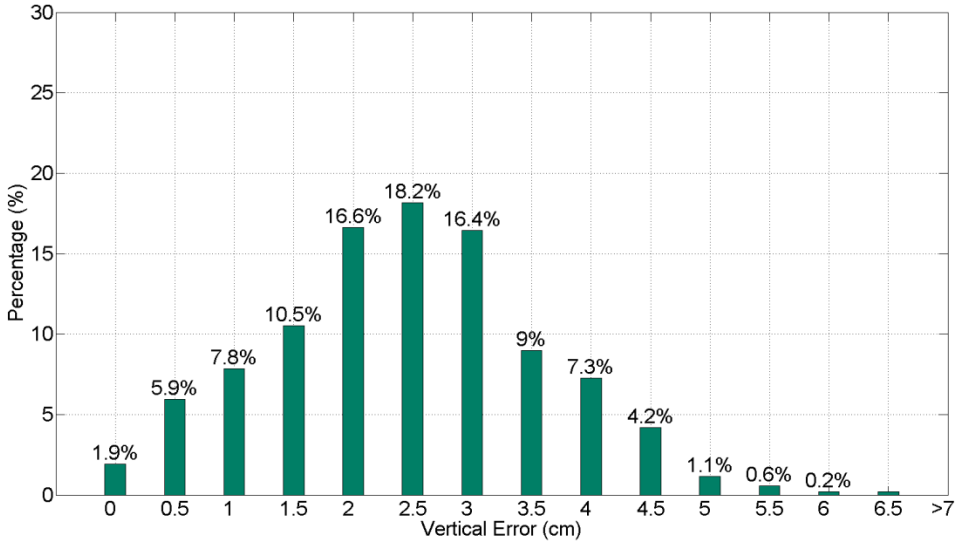

Figure 2.4: Histogram showing absolute vertical error after 24 hour solution for 80 sites processed in static mode

A summary of the statistics of positions estimated by York-PPP are presented in Table 2.1. The solution had an rms of 4, 5 and 26 mm in the north, east and up, respectively. Almost all of the 27mm 3D rms error is due to the 24mm vertical bias. The horizontal component of the software was comparable to the results presented by Ge *et al.,* (2008) with an rms 3 and 4 mm in north and east. In the up component the rms published by Ge *et al.,* (2008) was three times smaller in magnitude with a value of 8mm. Ge *et al.,* (2008) carried out a 7-parameter Helmert transformation when comparing their results against the SINEX coordinates. This quenstionable coordinate adjustment would most likely have further reduced the biases from their results, and may explain why their up component accuracy is not typical of PPP. The 7-parameter Helmert transformation between the two products allows the evaluation and removal of systematic differences

caused by reference frame realizations that are slightly different (Mireault *et al.*, 2008). Though this transformation is not required to be carried out as the solutions produced would have been in the same coordinate system as the IGS weekly satellite orbit and coordinate products.

Absolute point positioning is calculated relative to a well-defined global reference system, in contrast to relative positioning, where the coordinates are in relation to some other fixed point. Eckl *et al.* (2001) describes the accuracy of static relative positioning with a geodetic-grade receiver is typically 5 mm + 0.5 ppm (rms) for the horizontal component and 5 mm + 1 ppm (rms) for the vertical component. This is the highest accuracy possible for static relative positioning, as the fixed point would have an uncertainty associated with it. To determine if it is possible to replace static relative positioning by PPP, the statistics calculated from the solution estimated by York-PPP were compared to the specifications published by Eckl *et al.* (2001). In the horizontal component York-PPP had an accuracy of 7 mm which is comparable to static relative positioning. In the vertical component, the accuracy of relative positioning is three times greater than that of York-PPP. The significant vertical bias may be due to limitations within solid and ocean loading models and satellite (receiver geometry and point positioning).

Given the comparison between York-PPP and the published results from Ge *et al.* (2008) and accuracy specfications from Eckl *et al.* (2001), the software has been verified as being comparable to the scientified standards.

Table 2.1: Final solution produced by York-PPP from 24 hour datasets from 80 sites for DOY 244-250, processed in static mode for a total sample size of 560

Position Component	Bias (mm)	Std dev (mm)	rms (mm)
North	4	1	4
East	5	2	5
Horizontal	7	2	7
Vertical	24	11	26
3D	25	11	27

2.7 Kinematic Results

The York-PPP processor is also capable of processing kinematic datasets. To examine the kinematic mode of the software, the same static dataset was used to simulate kinematic data. This method of analysis was chosen due to the limited availability of reference solutions for kinematic results with a higher precision than PPP. Presented in Figure 2.5 and Figure 2.6 are the horizontal and vertical kinematic results, respectively. It is important to note, the kinematic mode of the processing was not the main focal point of this study and was included for completeness to show the functionality and effects of receivers motion in the data processing.

The difference between static and kinematic mode in PPP primarily exists in the variation of the process noise models in the sequential least-squares (in this case) or kalman filter. The process noise for the coordinates serves as a priori weighted constraints (Px) to the parameters (refer to equation 2.20 for more detail). The quantity of process noise can be scaled based on the user dynamics such as stationary, walking, driving and satellite motion with process noise values of 0 ms^{-1}, 1 ms^{-1}, 10 ms^{-1} and 10000 ms^{-1} respectively. A process noise equivalent of that of a terrestrial vehicle in motion was used, even though overly pessimistic, it serves to better analyze the contrast in the quality of the results from static and kinematic mode and the variation of convergence, which is discussed in more detail in Section 2.8.

In the horizontal component, 99% of the data processed had an error in the horizontal component equal to or less than 9 cm and in the vertical component, 14 cm or less. A summary of the statistics of positions estimated by York-PPP are presented in Table 2.2 In static mode, the horizontal component the rms was 8 mm in contrast to kinematic mode which was 54 mm and in the vertical component 29 mm in static mode and 102 mm in kinematic mode. The solution quality deteriorated because of the magnitude of the process noise used, adding large uncertainties to each parameter, allowing the solution to converge freely based on individual measurements, whereas in static mode the parameters are tightly constrained, thus a significantly higher accuracy of results is achieved through the power of averaging. It was noted that the final solution from the

kinematic and static solution had biases of equivalent magnitude, but the standard deviation increase from few millimetres to few centimetres.

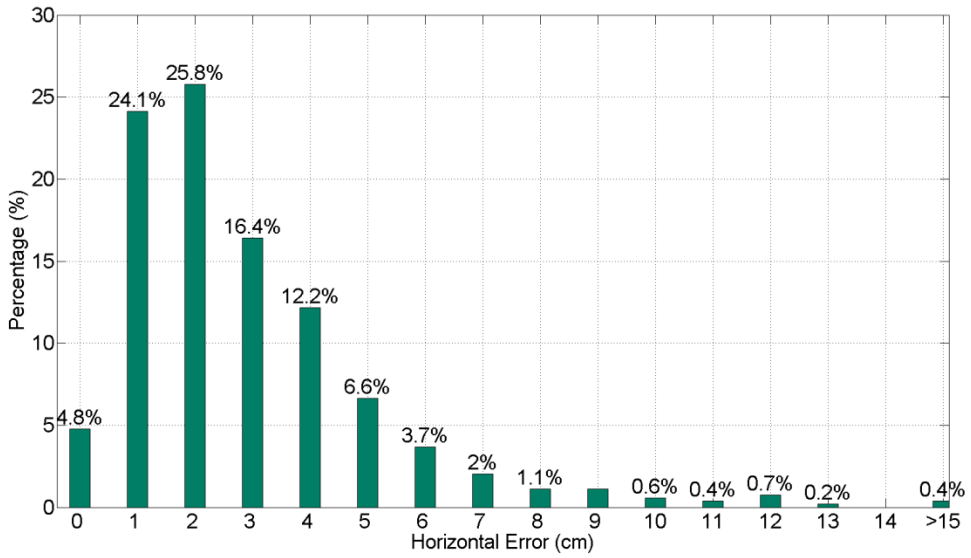

Figure 2.5: Histogram showing absolute horizontal error after 24 hour solution

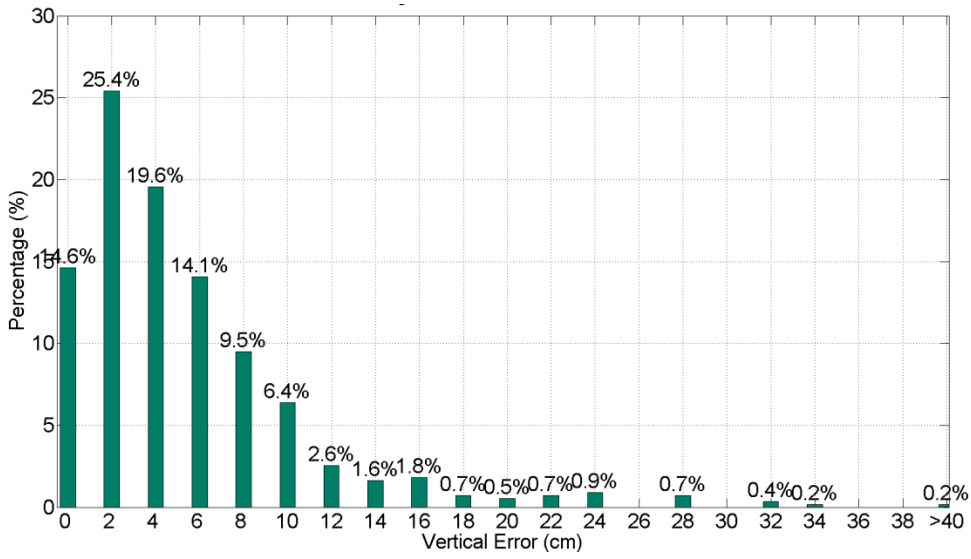

Figure 2.6: Histogram showing absolute vertical error after 24 hour solution

Table 2.2: Final solution produced by York-PPP from 24 hour datasets from 80 sites for DOY 244-250, processed in kinematic mode for a total sample size of 560

Position Component	Bias (mm)	Std dev (mm)	rms (mm)
North	2	40	40
East	0	36	36
Horizontal	2	54	54
Vertical	-27	83	87
3D	27	99	102

3.0 PPP Convergence Period and Initialization

This chapter provides an overview of different methods to define the initial convergence period in PPP. These methods include: 1) Required convergence period based on the application; 2) When the solution attains a steady state; and 3) A modified version of horizontal protection level (HPL). Finally, a RAIM algorithm is implemented, as it is expected to reduce initialization error, thus reducing convergence period.

3.1 Convergence

PPP definitely presents advantages for many applications in terms of operational flexibility and cost-effectiveness. One of its major limitations is its relatively long initialization time as carrier-phase ambiguities converge to constant values and the solution reaches its optimal precision. PPP convergence depends on a number of factors

such as the number and geometry of visible satellites, user environment and dynamics, observation quality and sampling rate (Bisnath and Gao, 2009). As these different factors interplay, the period of time required for the solution to reach a pre-defined precision level will vary.

The site ALBH (Albert Head) located in British Columbia, Canada illustrates "good" PPP convergence over a 24 hour period. One week's convergence in the horizontal component in static mode is illustrated in Figure 3.1 and kinematic mode in Figure 3.2. The rate of convergence was consistent throughout GPS days 244-250. There was a slight spike between hours 2 – 4 in Figure 3.1, which was common throughout the results for the week. This spike illustrates the correlation between rate of convergence and static user environment together with satellite geometry. The highest rate of convergence was within the first 5 minutes, with a steady state being achieved after 10 minutes resulting in a bias of 15 cm and a standard deviation of 10 cm.

In kinematic mode, the convergence period of the solution increased from a few minutes to tens of minutes. Also, after the fifth hour when the ambiguity terms would have been successful estimated, there is still relatively high uncertainty in contrast to static mode, due to the high uncertainty attached to each parameter. There also was a significant variation in the final solution. In static mode, the solution had an rms of 4 mm, 4 mm and 26 mm in the north, east and up components, respectively, in contrast to 19 mm, 18 mm

and 21 mm in the north, east and up components, respectively, in kinematic mode. These statistics are summarized in Table 3.1.

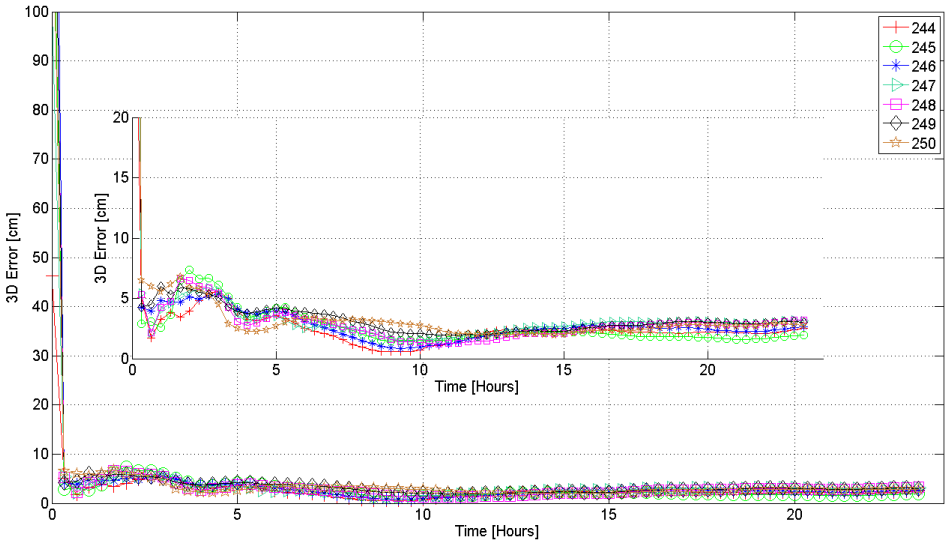

Figure 3.1: Site ALBH for DOY 244-250, processed in static mode showing typical convergence static mode

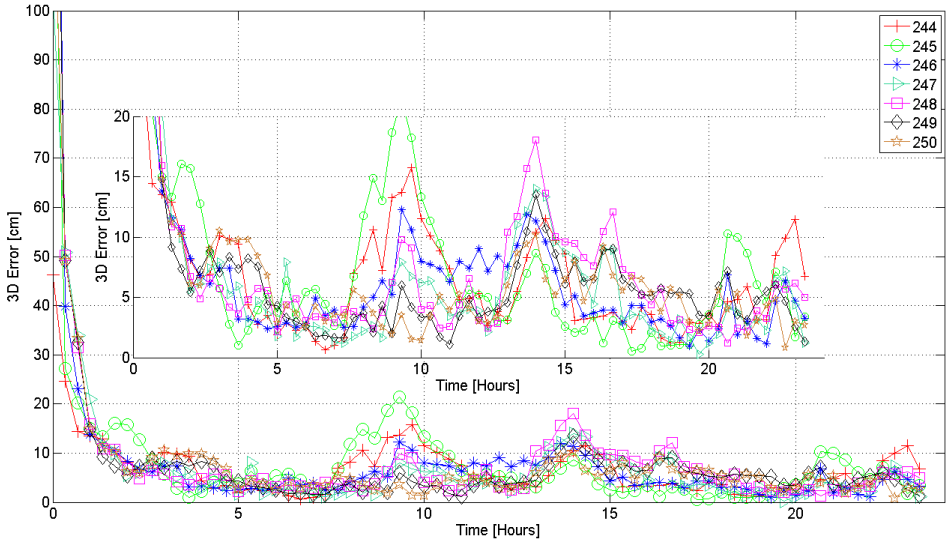

Figure 3.2 : Site ALBH for DOY 244-250, showing typical convergence in kinematic mode

The data obtained from the site KIRU (Kiruna) located in Sweden, was the one outlier present from the 81 stations processed. In the horizontal component, there was an error of 2.8 cm and greater for 5 of the 7 days for that GPS week. The convergence time series for GPS days 245 to 250 are given in Figure 3.3. On day 244 and 249, the solution took approximately 16 and 10 hours, respectively, to converge to sub-centimetre horizontal accuracy. Typical PPP convergence was noted for GPS days 245 and 250. On days 246, 247 and 248 the solution did achieve a steady state within 2 hours of convergence, but the final solution had a 3D error of 62, 38 and 26 cm respectively.

Table 3.1: Final solution produced by York-PPP from 24 hour datasets for the site ALBH for DOY 244-250, processed in static and kinematic mode

Site (mode)	Statistic (mm)	North	East	Horizontal	Up	3D
ALBH (static)	Bias	3	0	3	26	26
	Std dev	3	4	5	4	6
	rms	4	4	6	26	27
ALBH (kinematic)	Bias	5	4	6	5	8
	Std dev	18	18	25	20	33
	rms	19	18	26	21	34

When the processing mode was changed to kinematic at KIRU, the solution for days with noticeable biases (DOY 246-249) got significantly worst as illustrated in Figure 3.4. In the horizontal component, the solution has a standard deviation of 1557 cm with maximum values of 10 m. This quality of solution is equivalent to a standard point positioning solution using single-frequency pseudorange observables. There is unusually

high pseudorange multipath and noise present at the site (discussed in more detail in Chapter 4) there may have also been a receiver malfunction as the largest induced error on the pseudorange observable by multipath is 5 cm.

Table 3.2: Final solution produced by York-PPP from 24 hour datasets for the site KIRU for DOY 244-250, processed in static and kinematic mode

Site (mode)	Statistic (mm)	North	East	Horizontal	Up	3D
KIRU (static)	**Bias**	33	104	109	92	143
	Std dev	126	186	224	125	257
	rms	130	213	250	155	294
KIRU (kinematic)	**Bias**	841	49	842	394	930
	Std dev	1174	1023	1557	1901	2457
	rms	1444	1024	1770	1941	2627

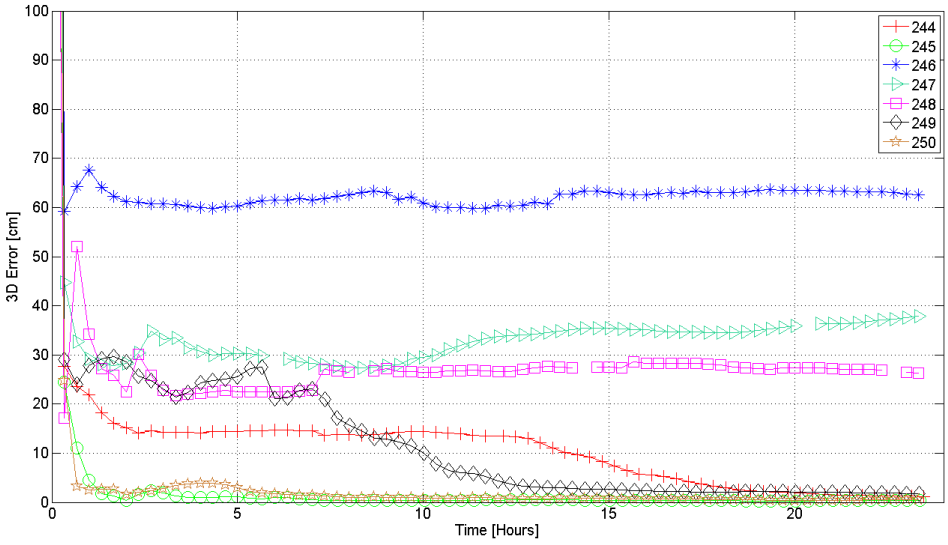

Figure 3.3: Site KIRU showing poor convergence static mode

PPP has been described by Bisnath and Gao. (2009) to take approximately 20 to 30 minutes for the positioning solution to converge to the decimetre-level. To verify this behaviour, the datasets processed were reinitialized every hour. The results increased in sample size from 560 data sets to approximately 13 300. The cumulative histogram presented in Figure 3.5 with a bin size of 5 minutes illustrates the required time for the data processed to reach 20cm horizontal threshold in static and kinematic mode.

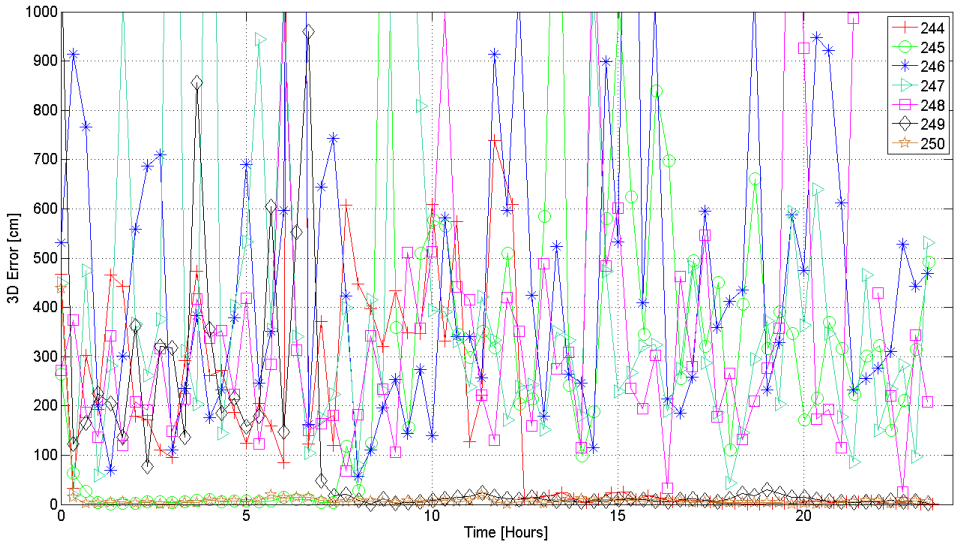

Figure 3.4 : Site KIRU showing poor convergence kinematic mode

The variation in convergence period is easily visible between static and kinematic modes as a result of the difference in the process noise applied. In static mode the estimated parameters are constrained allowing the ambiguities to be estimated within a shorter time period. In static mode an exponential trend was observed in contrast to the quasi-linear trend in kinematic mode. In static mode, 9% of the solutions had an initial horizontal

error of 20 cm or less, and 5% in kinematic mode. Within 10 minutes 71% of data processed had converged to a horizontal accuracy of 20 cm or less but took an additional 15 minutes for 96% of the data to converge to 20 cm. The solution took approximately 25 minutes for 70% of the data to converge in kinematic mode and 55 minutes for 96% of data. For various applications of PPP, it would be recommended to collect an initial 15 minutes of data while the receiver is stationary, after which the receiver can be moved to collect data at various locations. The initial 15 minutes can be processed in static mode allowing solution to converge within a shorter time period, after which the convergence mode can be switched to kinematic.

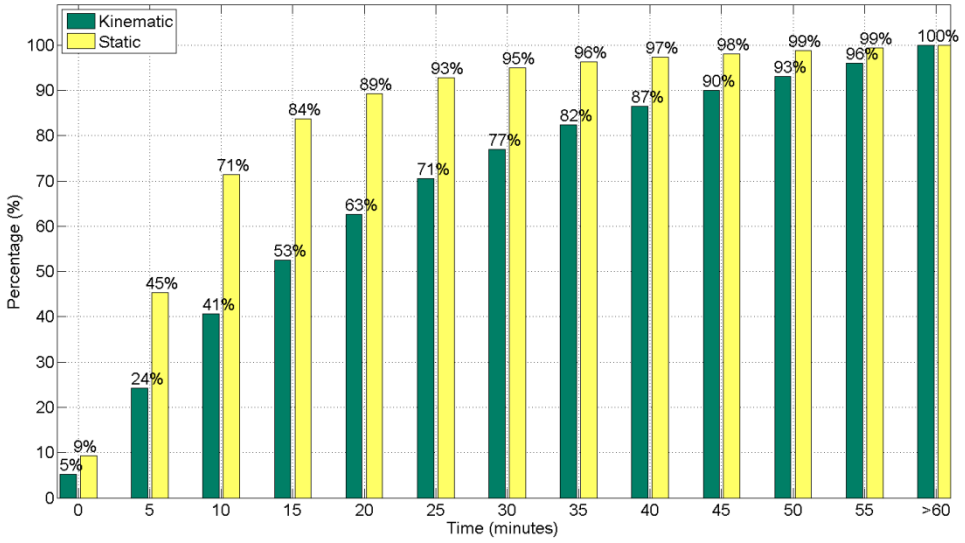

Figure 3.5: Cumulative histogram showing convergence period to 20 cm horizontal accuracy for static and kinematic PPP

3.2 Convergence Period for PPP Applications

Presented in the following sub-section are different applications of PPP and the period required for the solution to converge to different levels of accuracy. Some of the applications examined include the agricultural industry for precision farming, marine applications (for sensor positioning in support of seafloor mapping and marine construction) and airborne mapping. In rural areas where precise positioning and navigation is required and no reference stations are available, PPP proves to be an asset allowing the user to establish a geodetic control station. The major limitation of PPP for these applications is the initial convergence period and re-initialization. Re-initialization occurs when the receiver loses lock on a minimum number of satellites which requires the processing filtering to re-initialize, resulting in tens of minutes of greater than decimetre resolution positioning, until filter re-convergence. This may occur when an airplane "banks" or a vehicle passes under a bridge (Bisnath and Gao 2009).

3.2.1 Precision Agriculture

Precision agriculture enables real-time data collection with sufficiently accurate positioning information being used for enhancement of agricultural production. GPS and Geographic Information System (GIS) assists farmers to analyse data collected during soil sampling, crop scouting and yield monitoring, and establish efficient farming plans when carrying out tasks such as tractor guidance and variable rate applications (Pierce and Nowak 1999). The benefits of precision agriculture include improved efficiency of

water usage, time, fuel and fertilizer which leads to increased productivity and net profit (Reid *et al.*, 2000).

As discussed by Wang and Feng (2009), the accuracy requirements for precision agriculture for various farming are compiled in Table 3.3 (columns one through three). These specifications were used as the horizontal accuracy levels to examine the required convergence period in static mode, before initiating field work. Figure 3.6 illustrates the data processed over 1 hour periods. The data were binned at 5 minute time intervals. Using the information presented in Figure 3.6, recommended convergence period for each farming operation was developed and included in Table 3.3. Farming operations such as plowing and controlled traffic farming was not included in the analysis because a required horizontal accuracy of 1-2 cm was required. While PPP is capable of achieving this horizontal accuracy level, the required time for the solution to converge may not be practical for this particular application.

Recommendations for the quantity of data to be logged are based on the time 95% of the datasets took to achieve the specified horizontal accuracy level. At the 5 and 10 cm horizontal accuracy level a quasi-linear trend is shown, indicating a longer convergence period of 50 minutes is required. At the 20 cm horizontal accuracy level, an exponential trend is observed, thus a significant reduction in the convergence period to 25 minutes. Lower horizontal accuracy levels at 50 and 100 cm required 10 and 5 minutes of data, respectively.

Table 3.3: Horizontal accuracy requirements and recommended PPP convergence periods for precision farming operations

Farming operation	Farming stage	Horizontal accuracy (cm) 2σ	PPP period (minutes)
Rough	Yield Mapping	50-100	5-10
	Soil Sampling	50	10
	Weed Scouting	50	10
Fine	Pesticide Application	10-20	35-50
	Soil Cultivation	10-20	35-50
	Automated Machine Guidance	10-20	35-50
Precise	Spraying	5	60
	Cultivation	5	60
	Seeding	5	60
	Plowing	1*	-
	Controlled Traffic Farming	2*	-
	Harvesting	5	60

*- not plausible application of PPP requiring convergence within an hour Source: Wang *et al.* (2009)

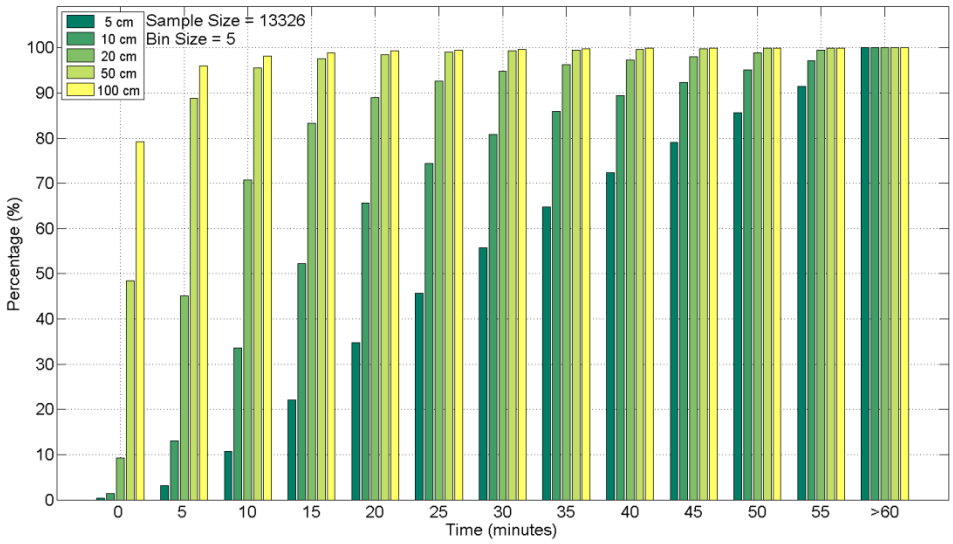

Figure 3.6: Horizontal convergence period for precision agriculture in static mode

3.2.2 Hydrographic Surveying

Hydrographic surveying is the measurement and description of water depths, geographical features, hazards to navigation, man-made and natural features that aid navigation, tides, currents and water levels, and sea bottom characteristics (Fisheries and Oceans Canada, 2012). Hydrographic surveying requirements presented by the International Hydrographic Organization (2005) were summarized in Table 3.4 and used as the horizontal accuracy levels to examine the required convergence period. Figure 3.7 illustrates the convergence period from the data processed over 1 hour periods. The data were binned at 5 minute time intervals.

Also included in Table 3.4 is a summary of the recommended time period for data to be logged for at these different applications within hydrographic surveying in static mode before initiating the survey. A quasi-linear trend is show at at the 5 and 10 cm horizontal accuracy level indicating a longer convergence period of 50 minutes is required. At the 20 cm horizontal accuracy level, an exponential trend is observed, thus a significant reduction in the convergence period to 25 minutes. Quick convergence is seen at horizontal accuracy levels 50 and 100 cm such as 10 and 5 minutes of data, respectively, are required.

Table 3.4: Horizontal accuracy requirements and recommended PPP convergence periods for hydrographic surveying operations

	Hydrographic surveying grouping (cm)			Recommended PPP convergence period (mins)		
	Special Order	**Order 1**	**Order 2**	**Special Order**	**Order 1**	**Order 2**
Primary control	10	100	100	50	5	5
Secondary stations	50	-	-	10	-	-
Altimetric surveys	5	10	10	60	50	50
Conspicuous objects	20			25		
Isolated signal or object	50			10		

Source: International Hydrographic Organization (2005)

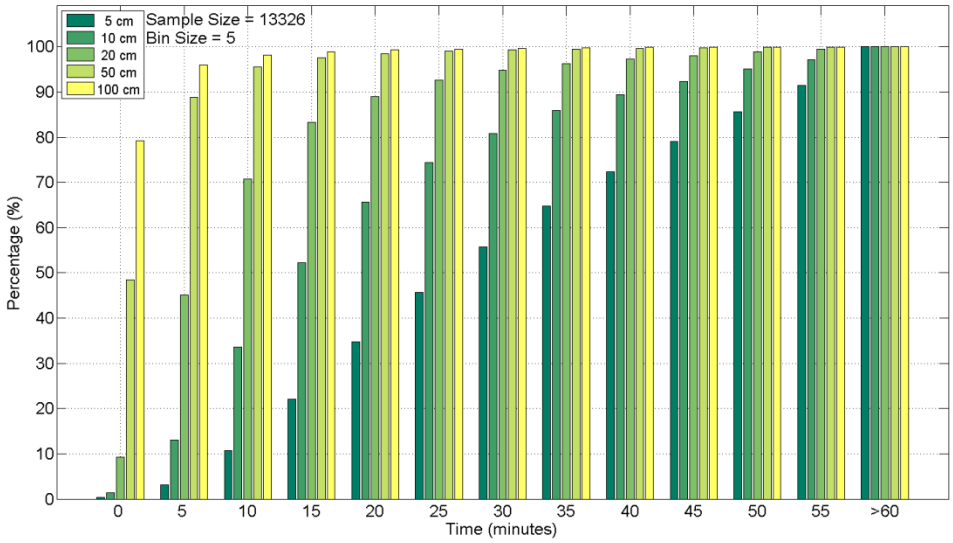

Figure 3.7: Horizontal convergence period for hydrographic surveying static mode

3.2.3 Remote Sensing

Remote sensing is the measurements of an object's properties on the Earth's surface using data acquired from aircrafts and satellites. Some of the applications of remote-sensing technology include environmental assessment and monitoring, global change detection and monitoring, agriculture, mapping, military surveillance and reconnaissance (Schowengerdt, 2006). It is critical to have accurate positioning and time to accompany collected measurements for ground target positioning. Depending on the application and scale of the information to be presented, the GPS positioning requirements may vary (Nassar *et al.*, 2005).

Remote sensing surveying requirements presented by the Federal Geographic Data Committee (1998a) were summarized in Table 3.5 and used as the horizontal accuracy levels to examine the required convergence period. Figure 3.8 and 3.9 illustrates the results of the data processed over 1 hour periods. The data were binned at 5 minute time intervals. Remote sensing operations requiring a horizontal accuracy of 1.8 to 5.4 cm was not included.

Recommendations for the quantity of data to be logged are based on the time 95% of the datasets took to achieve the specified horizontal accuracy level. The examined horizontal accuracy level ranged from a minimum of 7 cm and a maximum of 212 cm. At the highest specified accuracy level a quasi-linear trend was noted amongst the percentage of data to converge within the examined 1 hour period with a recommended convergence period of 55 minutes. As the horizontal accuracy level decreased, ranging from 14 cm to

21 cm an exponential trend is observed indicating the required time for the solution to converge has significantly decreased, such that a recommended convergence period is 25 minutes. Horizontal accuracy levels greater than 35 cm require few minute convergence. A recommendation of 15 minutes for a horizontal accuracy level of 35 cm and when further decreased to 53, 106.1 and 212.1 cm a recommendation of 12, 7 and 3 minutes where made, respectively.

Table 3.5: ASPRS planimetric feature coordinate accuracy requirement for well-defined points and recommended PPP convergence periods

Target Map Scale	ASPRS Limiting Horizontal rms error (cm)			Recommended convergence period (mins)		
Ratio m/m	**Class 1**	**Class 2**	**Class 3**	**Class 1**	**Class 2**	**Class 3**
1:50	1.8 *	3.5 *	5.4 *	-	-	-
1:100	3.5 *	7.1	106.1	-	55	7
1:200	7.1	14.1	21.2	55	25	25
1:500	17.7	35.4	53	25	15	12
1:1000	35.4	70.7	106.1	15	12	7
1:2000	70.7	141.4	212.1	12	5	3

*- not plausible application of PPP requiring convergence within an hour. Source: Federal Geographic Data Committee (1998a)

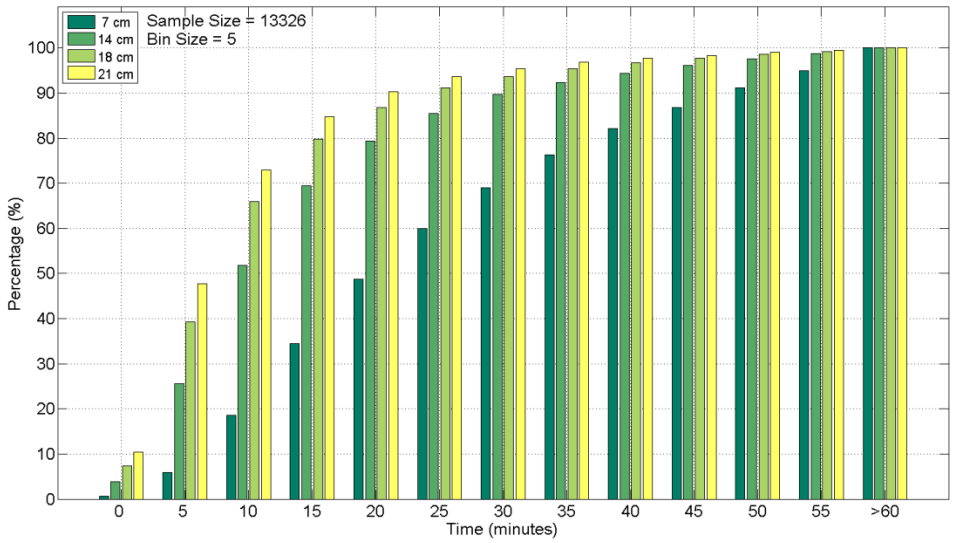

Figure 3.8: Horizontal convergence period for remote sensing, threshold 7-21 cm in static mode

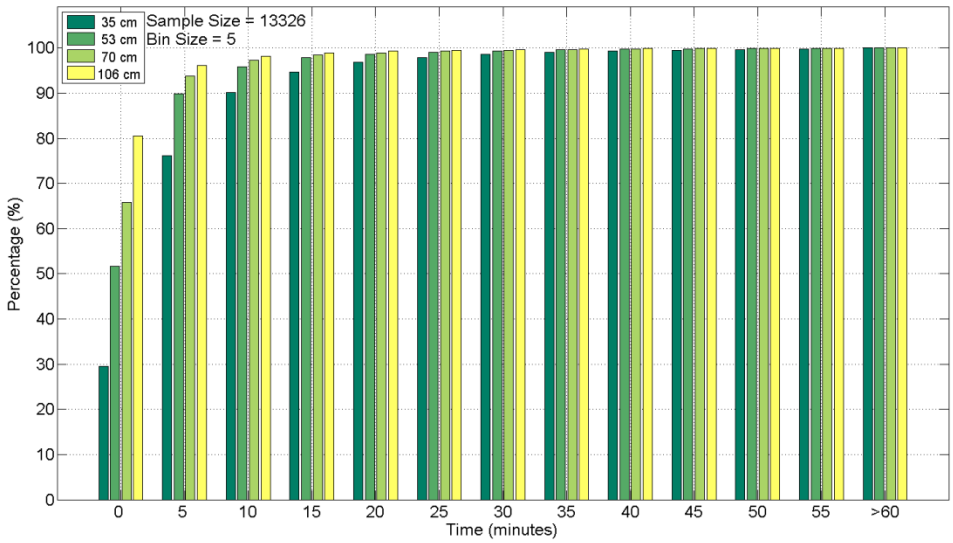

Figure 3.9: Horizontal convergence period for remote sensing, threshold 35-106 cm in static mode

3.2.4 Geodetic Control Surveying

Geodetic control surveys are usually performed to establish the basic positional framework from which supplemental surveying and mapping are performed. Geodetic control surveys are distinguished by use of redundant, interconnected, permanently monumented control points. Geodetic control surveys are performed to far more rigorous accuracy and quality assurance standards than those for local control surveys for general engineering, construction, or topographic mapping purposes (Federal Geographic Data Committee, 1998b).

Presented in Table 3.6 are the different accuracy classifications with 95% confidence requirements, as well as a proposed recommendation for the required convergence period for the solution to reach the specified horizontal accuracy level in static mode (Federal Geographic Data Committee, 1998b). Accuracy requirements at 1-2 mm are used for global and regional deformation measurements which is not possible with PPP. At the 5 mm accuracy classification, these monuments are used to establish a national geodetic reference system, as well as regional geodynamics and deformation measurements. 1-5 cm accuracy classification are included as part of the national geodetic reference system with varying accuracy specifications, which are dependent on the control surveys to meet mapping, land information, property and engineering requirements.

Figure 3.10 illustrates the results of the data processed over a 24 hour period. The data were binned at hourly intervals. For geodetic control requiring an accuracy of 0.5, 1 and 2 cm a minimum of 12 hours data are recommended to be logged. At a 2 cm horizontal

accuracy level an exponential trend was observed, in contrast to the quasi-linear trend observed for 0.5 – 1 cm horizontal accuracy level. Recommendations for the quantity of data to be logged are based on the time 95% of the datasets took to achieve the specified horizontal accuracy level. For a 2, 1 and 0.5 cm horizontal accuracy level it's recommended a minimum of 9, 23 and 24 hours of data be logged. These specified thresholds are the most stringent of the different applications listed thus the long convergence period.

Table 3.6: Horizontal accuracy requirement and required convergence period

Accuracy Classification (cm)	95% Confidence (cm)	Recommended PPP convergence period (hours)
0.1*	0.1	-
0.2*	0.2	-
0.5	0.5	24
1	1	23
2	2	9

*- not applicable for PPP. Source: Federal Geographic Data Committee (1998b)

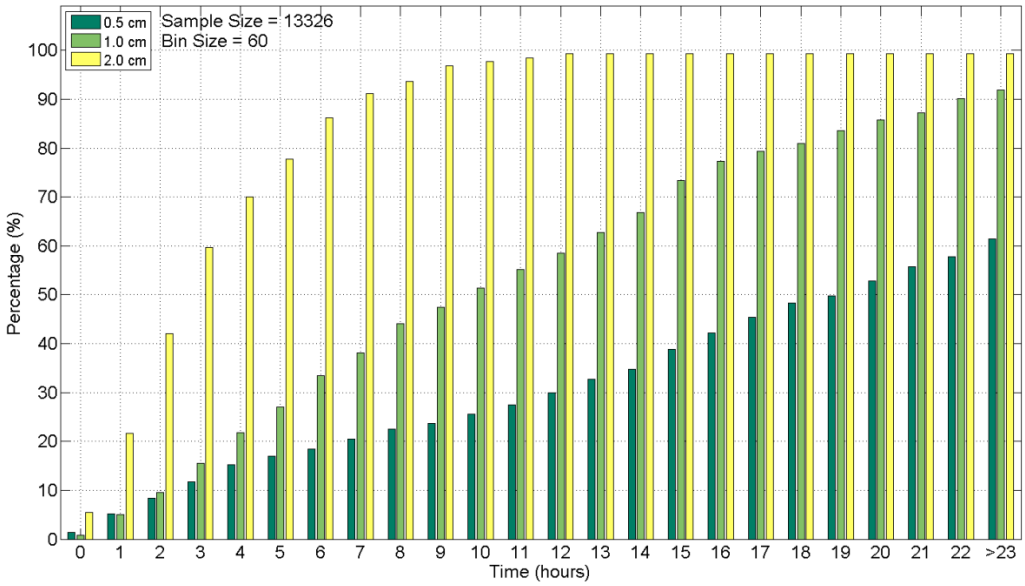

Figure 3.10: Convergence period for geodetic control in static mode

3.3 Definition of steady state

PPP convergence can be qualitatively provided as Section 3.1 or specified by application as Section 3.2, but it can also be defined as when the positioning time series reaches a steady state. It is important to analyze each solution returned by the processor for all time instants $t \geq t_0$, where t_0 represents the initial time when the PPP processing has begun. The PPP solution consists of two components: a transient response and a steady state response (Sinha, 2007), such that

$$y(t) = y_{tr}(t) + y_{ss}(t) \tag{3.1}$$

The transient response is present in the short period of time immediately after the PPP processing starts. If the solution convergence is asymptotically stable, the transient response disappears, which can be represented as

$$\lim_{t\to\infty} y_{tr}(t) = 0 \tag{3.2}$$

If the system is unstable, the transient response will exponentially increase in time and in most cases the PPP solution would be practically unusable. Even if the PPP solution is asymptotically stable, the transient response should be carefully monitored since some undesired phenomena such as a poorly modelled error source will introduce biases into the final solution.

Assuming the system is asymptotically stable, the system response in the long run would be determined by its stead state component only. It is important that steady state response values as to the "truth" or reference solution (when available) as possible. In control

systems, there exists three types of second order responses: a) the critically damped case b) the over-damped case, and c) the under-damped case. These three examples are illustrated in Figure 3.11.

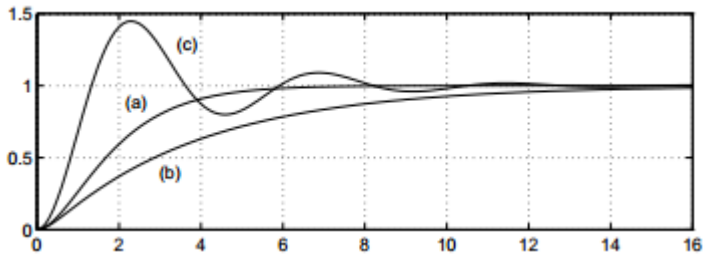

Figure 3.11: Responses of second order systems. Source: (Sinha, 2007)

PPP is an example of the under-damped case and is the most common case in control system applications. A magnified figure of the system step response for the under-damped case is presented in Figure 3.12. The most important transient response parameters are the rise time, peak time, overshoot and settling time indicated by t_r, t_p, OS and $t_{s,}$, respectively. The rise time refers to the time required for the solution to change from a specified low value to a specified high value. In PPP, the low value is zero (the true solution) and the high value is the peak or the maximum value at which the solution converges from. It is difficult to define a rise time in PPP as the range of which solutions converge from varies. The peak time is the time that the solution took for the response to reach the first peak of the overshoot. The overshoot is when the solution reaches a maximum value and the settling time is the time the solution enters a steady state (Sinha, 2007).

The response of an asymptotically stable linear system is in the long run determined by its steady state component. During the initial time interval the transient response decays to zero. The system response is represented by the steady state component for the remainder of the time series with an rms of a few centimetres which proportionally decreases with time (Sinha, 2007). In PPP it is important to have the steady state as close as possible to the reference solution so that the so-called steady state errors, which represent the differences between the steady state of the PPP solution and reference solution, can be defined.

Presented in Figure 3.13 is an example of the first 30 minutes of a typical PPP horizontal position solution which illustrates the four second order response from components in Figure 3.12. The rising time is difficult to define as in PPP there is not a specified low and high value defined in PPP, as convergence varies with each dataset, therefore assumed to be zero. The overshoot occurs at a peak time of 3 minutes with a value of 23.9 cm. The settling time occurs after 36 minutes of processing, after which the solution enters a steady state.

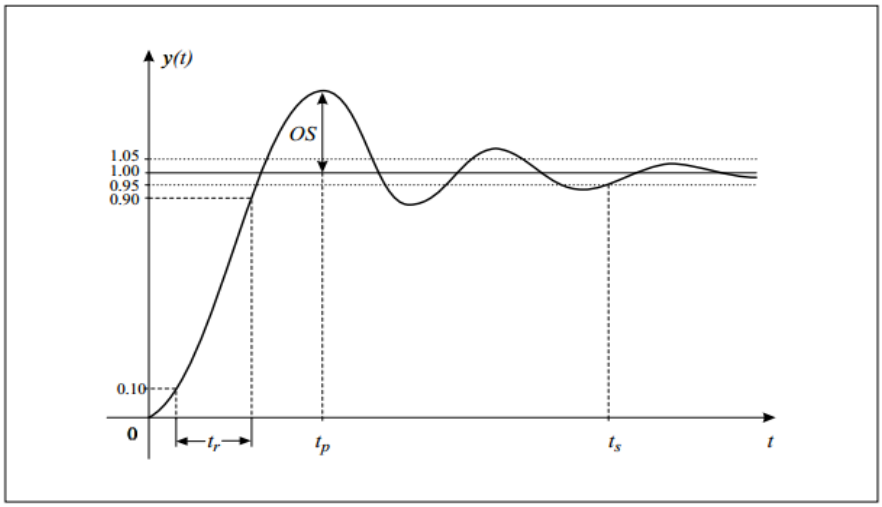

Figure 3.12: Response of an under-damped second-order system. Source: (Sinha, 2007)

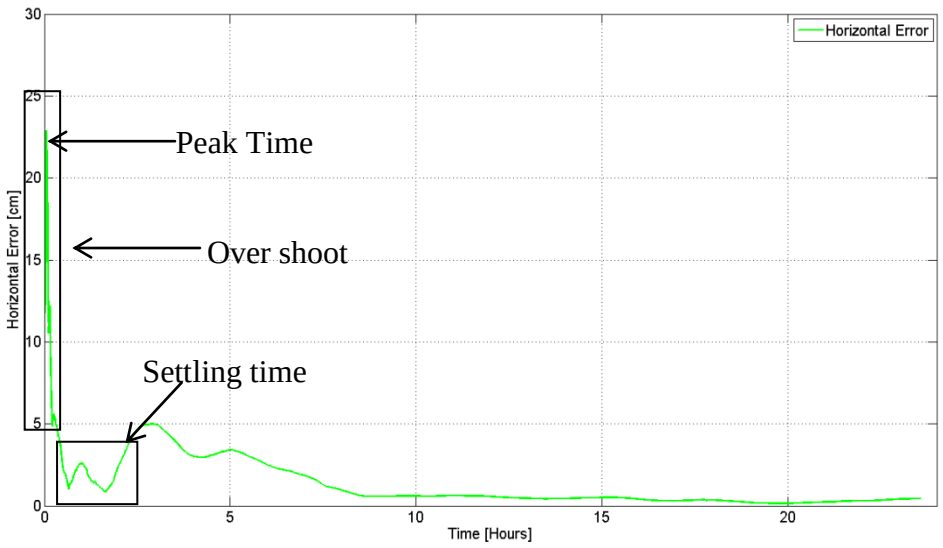

Figure 3.13: Typical PPP convergence, an example of an under-damped system processed in static mode

Figure 3.14 shows the average rate of convergence in the horizontal component for approximately 13 000 datasets, which are distributed globally to rigorously test the YORK-PPP software under varying conditions such as ionospheric refraction, solid and

ocean tides and relativistic effects that are dependent on generalized models to correct these station dependent errors. These averaged values were calculated each minute and are accompanied by the associated standard deviation. The data processed were sampled at 30 second epoch intervals. The averaged value at the first minute consisted of three epochs as data logging began at 12:00 am each day.

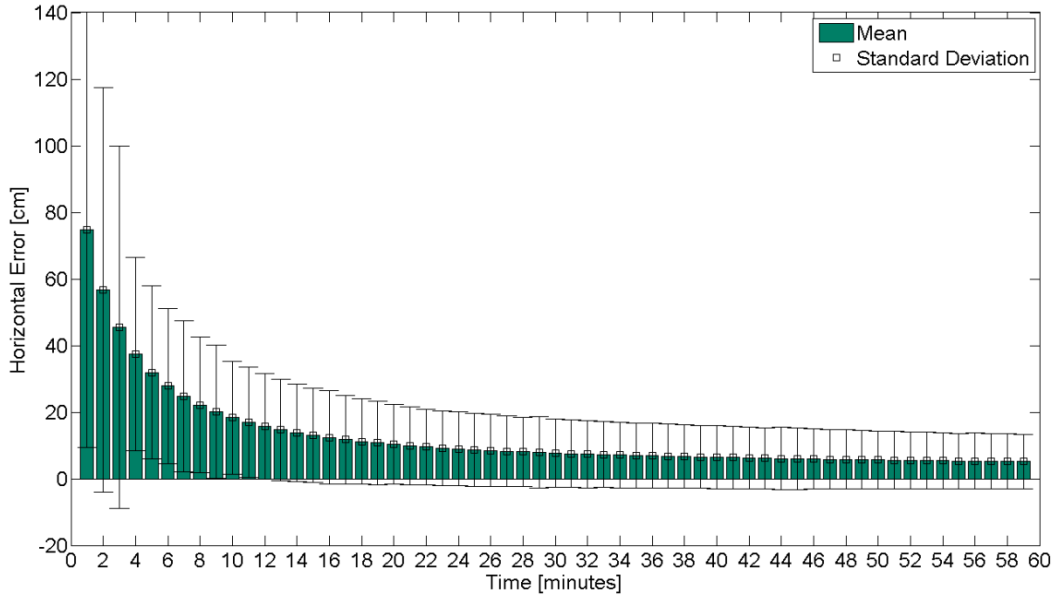

Figure 3.14: Horizontal mean and standard deviation for hourly re-initialization for a sample size of 13 300

During the first minute of processing the solution is still primarily a pseudorange only solution, as the linear combination of the P1 and P2 observables are used to initialize the carrier-phase float ambiguities. The average difference in the horizontal component for the first minute is 74.8 cm ± 65.2 cm. The rate of convergence can be seen to exponentially decrease with the greatest rate of change being observed within the first 20 minutes, after which the solution achieves a steady state with an average value of 10.3 cm ± 12 cm. After the 20th minute the solution continues converging at a lower rate to an average horizontal difference of 5.1 cm ± 8.2 cm after 60 minutes of processing. It can be

seen that the solution consistently has a larger standard deviation than the mean, which can be attributed to the large variation in number, quality and geometry of measurements from individual stations.

One of the limitations of PPP is its inability to assure to the user 100% accuracy of the solution. For comparison purposes two sites are presented to show variation in PPP convergence. The PPP processor was reinitialized every hour. At the site KIRU in Figure 3.15 illustrates unsatisfactory convergence in PPP, while Figure 3.16 shows typical PPP convergence. The general trend at which the mean values converged between KIRU and ALBH were similar such that they both exponentially decreased with respect to time with the greatest rate of change occurring within the first 10 minutes. The precision of the solution at ALBH was 8 times greater than that at KIRU.

At KIRU the initial mean was 110 cm, which decreased to 90 cm by the second minute while the initial standard deviation was 70 cm and increased to 160 cm. After 10 minutes both the mean and standard deviation achieved a steady state with a 50 cm bias present in the solution which remained constant for the entire 60 minute period. This was likely due to a site induced error which was not taken into consideration, the site log file was reviewed and the institution that maintains the site KIRU was contacted, there were no recorded problems present at the site during this GPS week.

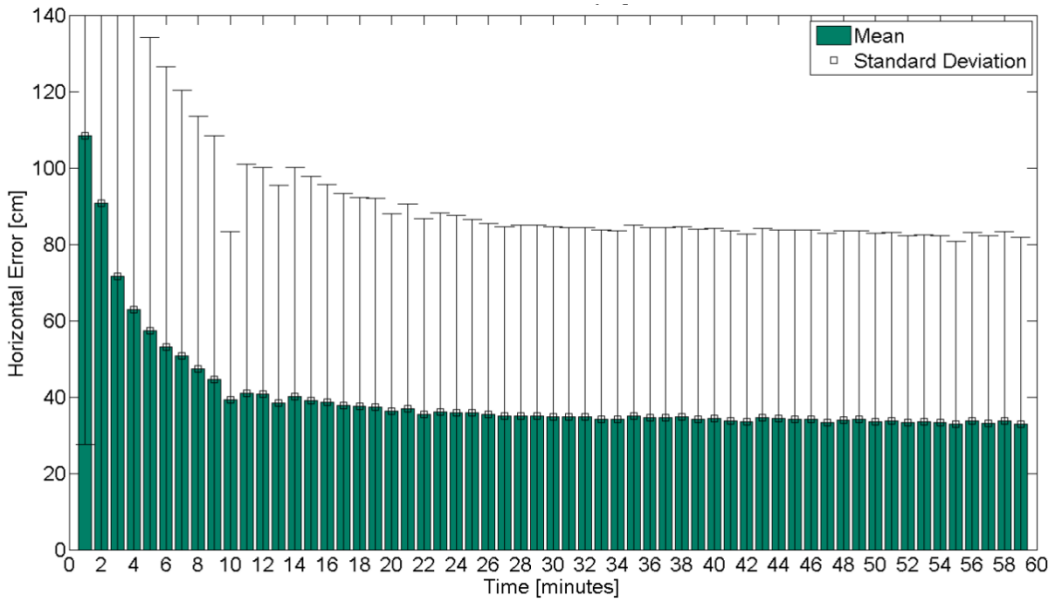

Figure 3.15: Horizontal mean and standard deviation for hourly reinitialization for the site KIRU

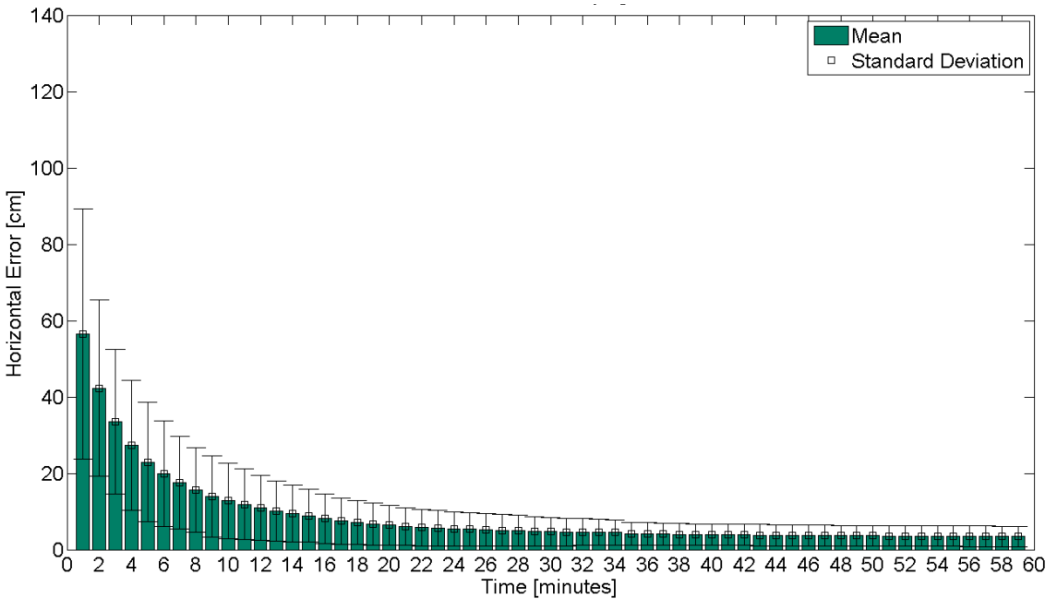

Figure 3.16: Horizontal mean and standard deviation for hourly reinitialization for the site ALBH

3.4 Horizontal Protection Level (HPL)

Horizontal Protection Level (HPL) was designed and used for GNSS-based aircraft rovers. It represents the radius of a circle in the horizontal plane with its centre being at the true position, which describes the region that is assured to contain the indicated horizontal position (Federal Aviation Administration, 2011). Presented in this section is a modified version of HPL, adapted to indicate to the user when convergence is attained.

HPL is a function of the visible GPS satellites, user geometry, and expected error characteristics. The goal of an integrity algorithm is to provide a position solution within HPL. If the position integrity cannot be guaranteed to be protected within HPL with the given probabilities, the user will be notified and the position for that epoch will be rejected. Thus HPL is a very important part of an integrity method. The performance of GPS RAIM algorithms (Section 3.5) is mainly measured by HPL. The purpose of HPL is to make use of horizontal position error and screen out bad satellite constellation geometry. Poor geometries are detected and excluded by comparing HPL to the horizontal alert limit (HAL). The Horizontal Alert Limit (HAL) is the maximum horizontal position error allowable for a given navigation mode without an alert being raised.

The position error Δx_{XYZ}, which is defined in a 3D Cartesian coordinate system is converted to a local topocentric coordinate system, Δx_{ENU}. A position vector at (φ, λ, h) given in the (X,Y,Z) system is used to transform the coordinates to the easting, northing

and up (E,N,U) system through multiplication by the orthogonal transformation matrix F (Borre, 2009):

$$\mathrm{F} = \begin{bmatrix} -\sin\lambda & \cos\lambda & 0 \\ -\sin\varphi\cos\lambda & -\sin\varphi\sin\lambda & \cos\varphi \\ \cos\varphi\cos\lambda & \cos\varphi\sin\lambda & \sin\varphi \end{bmatrix} \tag{3.3}$$

For failure detection purposes, the satellite whose bias error causes the largest slope is the one that is the most difficult to detect (typically the lowest in horizon) and produces the largest error for a given test statistic. The method used to calculate the maximum slope is presented below (Brown, 1992; Borre, 2009). The matrix M0 calculated in equation 3.4 is resized to take into consideration only the X,Y,Z parameters, which are transformed to E,N,U in equation 3.5. The slope values are calculated for each satellite for the pseudorange and carrier-phase observables in equation 3.6. The maximum slope value is used to calculate the HPL, equation 3.7.

$$M0 = (\mathrm{A}^{\mathrm{T}}PA + Px)^{-1}A^{T}P \tag{3.4}$$

$$M = \mathrm{F} * M0(:,1:3) \tag{3.5}$$

$$\alpha(i) = \sqrt{\left(\frac{\mathrm{M}_{1\mathrm{i}}^{2}+\mathrm{M}_{2\mathrm{i}}^{2}}{\mathrm{S}_{\mathrm{ii}}}\right)} \tag{3.6}$$

$$\alpha_{max} = \mathrm{MAX}[\alpha] \tag{3.7}$$

The S matrix represents the corresponding covariance matrix of the residuals. The maximum slope value is scaled by σ which represents a realistic noise for the pseudorange and carrier-phase measurements.

$$HPL = \alpha_{max} * \sigma \tag{3.8}$$

This modified HPL offers the user a dynamic indicator of when a steady state is achieved based on the user's defined HPL threshold. Typically, the HPL is based on the single receiver point positioning. Presented in Figure 3.17 is an example of HPL calculations and the position update for the horizontal position Δx_{EN} coordinates at the site ALBH for DOY 244. As expected, the convergence is seen in both HPL and Δx_{EN}. The modified HAL is set to a radius of 2 cm, to indicate to the user when a steady state is achieved. The user is notified in real-time when the radius of the HPL is less than or equal to 2 cm, which occurs after 26 minutes at the site ALBH day 244.

Presented in Figure 3.18 are different HPL threshold values ranging from 1 to 5 cm and the time taken at which these HPL values are achieved on average for the data processed. The tighter the HPL threshold, the higher the precision guaranteed to the user, but the longer convergence period required. At a 5 cm threshold, 95% of the data had an HPL radius of 5cm or less at the 35 minute bin. The modified version of HPL is a good metric to define PPP convergence as it indicates to the user in real-time when a steady state is attained.

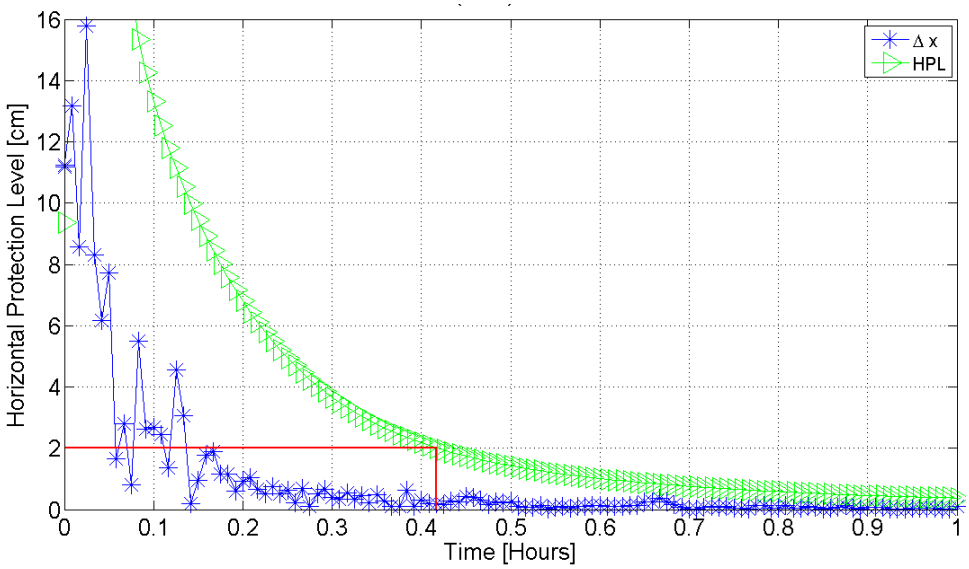

Figure 3.17: Using HPL as a real-time indicator of PPP convergence

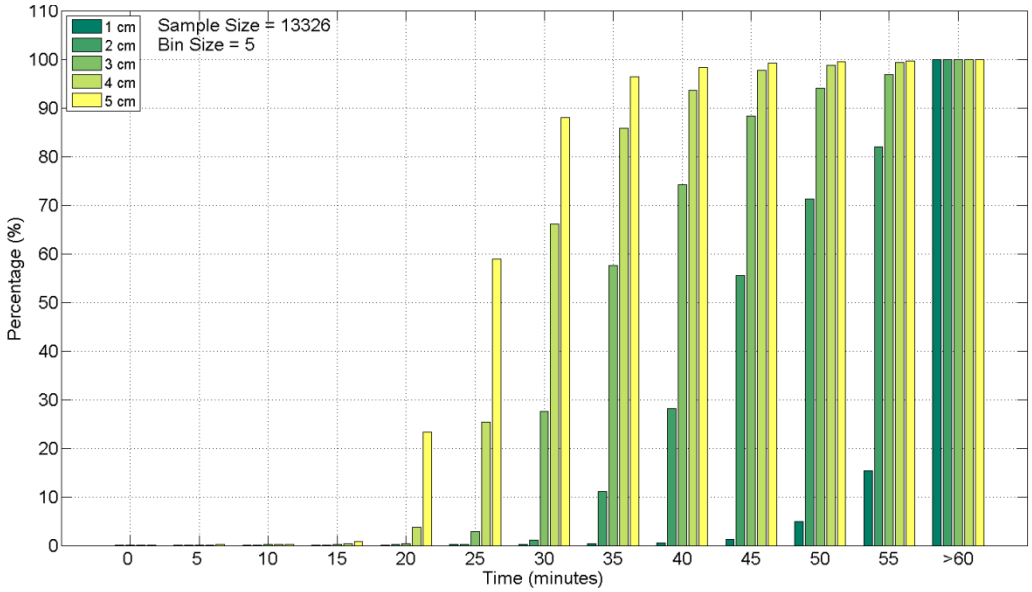

Figure 3.18: Histogram showing time taken to achieve different HPL threshold

3.5 Receiver Autonomous Integrity Monitoring (RAIM)

Integrity monitoring is an essential component of any positioning / navigation system. In PPP processing some parameters are estimated, modelled or eliminated without referring

to any nearby reference stations. This is additional reason why providing integrity information for PPP single receiver estimates is important. Post-fit residuals from PPP epoch solutions could be analyzed to detect individual measurement outliers, or more significant problems (Bisnath and Gao 2009).

RAIM is a receiver-internal technique to assess the integrity of GPS signals and plays a significant role in safety-critical GPS applications (Irsigler, 2008). There are many possible errors which only affect the user, these include: excessive multipath, receiver error, and localized ionosphere or troposphere effects. RAIM is easily implemented and requires no additional hardware (Walter and Enge 1995). RAIM was originally designed to be incorporated as part of a standard point positioning processor for data collected by a code-only receiver. It was modified to be implemented within the PPP software for this thesis because it offers increased integrity monitoring the analysis of the residuals takes into consideration the number of satellites and geometry for each epoch potentially allowing for improved solution initialization, resulting in potentially reduced convergence period.

A RAIM algorithm should provide a procedure for detection of a navigation failure, and a procedure for screening out geometries that may be satisfactory for navigation purposes, but cannot provide failure detection within the required specifications. The typical steps are outlined below (Brown, 1992) and in Figure 3.19.

1) Determine number of visible satellites N.
2) Calculate observation matrix A.

3) Select proper threshold corresponding to number of visible satellites N.

4) Determine whether geometry is admissible.

5) If geometry is admissible, calculate test statistic is calculated. If geometry is inadmissible, give appropriate warning.

6) Compare of the test statistic with pre-computed threshold. If the test statistic is greater than threshold then declare 'failure', otherwise declare 'no failure'.

7) Continue to next sample point in time, and repeat of steps 1 to 6.

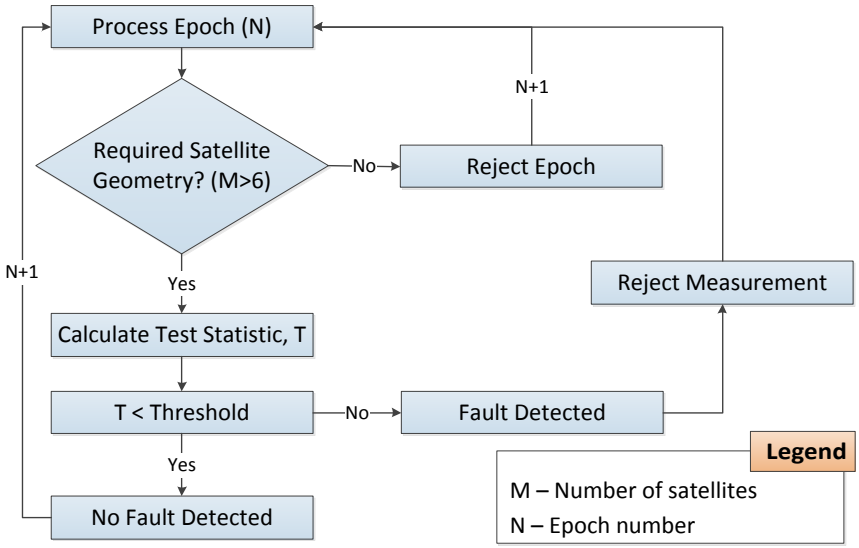

Figure 3.19: General overview of RAIM

There are several possible RAIM implementations which can be divided into methods for Fault Detection (FO) and Fault Detection and Exclusion (FOE). The Least-squares Residual Method is an example of FOE, as it is able to identify the affected signal and exclude it from navigation processing. The proposed standard RAIM scheme as discussed by Brown (1992) is based on a unified theory that says "under the condition of equal

alarm rates, the least-squares-residuals, parity, and range-comparison RAIM methods all yield identical results". The Least-squares Residual Method was modified here to fit the sequential least-squares model used within the York-PPP software (Brown, 1992).

The least-squares estimate $\hat{x}$ is calculated by the sequential filter given in equation 2.19. The least-squares solution is used to calculate the residuals of the 2N measurements. This process is the linear transformation that takes the range measurement error into resulting residual vector (Kuusniemi, 2007) given in equation 3.9. The vector $\hat{e}$ has the dimension 2N x 1 and is the measurement error vector due to usual receiver noise, anomalies in propagation, imprecise knowledge of satellite position, satellite clock error and unexpected errors due to satellite malfunctions (Kuusniemi, 2007) (Kouba *et al.*, 2001).

$$\hat{e} = (\mathrm{I} - \mathrm{A}(\mathrm{A}^{\mathrm{T}}\mathrm{PA} + \mathrm{Px})\mathrm{A}^{\mathrm{T}}\mathrm{P})\mathrm{W} \tag{3.9}$$

The sum of the squares of the residuals plays the role of the basic observable in the Least-squares Residual Method and is called the SSE in the equation below (Brown, 1992).

$$\mathrm{SSE} = \hat{e}^{\mathrm{T}}\hat{e} \tag{3.10}$$

Brown (1992) states that it is more convenient to use as a test statistic (T), the quantity that is outlined in equation 3.11, rather than SSE, as it is a function of both SSE and the number of satellites available, where N is the number of satellites and U is the number of unknowns.

$$\mathrm{T} = \sqrt{\frac{\mathrm{SSE}}{\mathrm{N-U}}} \tag{3.11}$$

This basic observable has three very special properties that are important in the least-squares residuals decision rule (Kuusniemi, 2007).

1. The SSE is a non-negative scalar quantity, which makes for a simple decision rule. The calculated threshold sets two conditions for the SSE, either failure or pass (Parkinson and Spilker 1996).
2. If all the elements of $\hat{e}$ have the same independent zero mean Gaussian distributions, then the statistical distribution of SSE is completely independent of the satellite geometry for any N. This makes it especially simple to implement a constant alarm algorithm. All that is required is to pre-calculate the thresholds that yield the desired alarm rate for the various anticipated values of N. Then the real algorithm sets the threshold approximately for the number of satellites in view at the moment.
3. For the zero mean Gaussian assumption mentioned in two, SSE has an unnormalised chi-squared distribution with (N - U) degrees of freedom.

The proposed standard scheme involves the formation of a simple scalar test statistic from the redundant measurements. This statistic is then compared with a pre-computed threshold (Broughton, 2003).

$$Td = \left[\frac{F\mathcal{X}^2_{N-U}(1-P_{FA})\sigma}{N-U}\right] \quad 3.12$$

$$F\mathcal{X}^2_{N-U}(z) = \int_0^z \frac{e^{-\left(\frac{s}{2}\right)} s^{\left[\frac{N-U}{2}\right]-1}}{2^{\frac{N-U}{2}}\Gamma\left(\frac{N-U}{2}\right)} \quad 3.13$$

$F\mathcal{X}^2_{N-U}$ - inverse of the central $\mathcal{X}^2$ distribution function

P_{FA} - maximum allowable false alarm rate

σ - realistic noise

$\Gamma(z)$ - Gamma Function

RAIM provides rigorous analysis of the post-fit residuals which may assist in detecting outliers residual, which may have been previously overlooked by standard PPP residual rejection. Unlike RAIM, the current standard method for rejecting residuals is based on ad hoc or empirically set value for rejecting the maximum pseudorange and carrier-phase post-fit residual. For example, in the PPP-CSRS code from NRCan (2010), if the carrier-phase residual is greater than 4.47 cm, the measurement for the respective satellite is reject and the epoch is reprocessed, and if the pseudorange measurement is greater than 4.47 m the epoch is not reprocessed, but the satellite is rejected for the following epoch.

Illustrated in Figure 3.20, is the sample results for the site ALGO DOY 244 showing the maximum phase residual for each epoch processed and the phase threshold. The results presented in Figure 3.21 illustrate the modified RAIM test statistic calculated for each epoch and the associated carrier phase residual threshold. The benefits of RAIM are visible in these two figures as RAIM offers a dynamic tightened form of residual rejection, more observables are more. 5 measurements are rejected in Figure 3.21, in contrast to 1 in Figure 3.20.

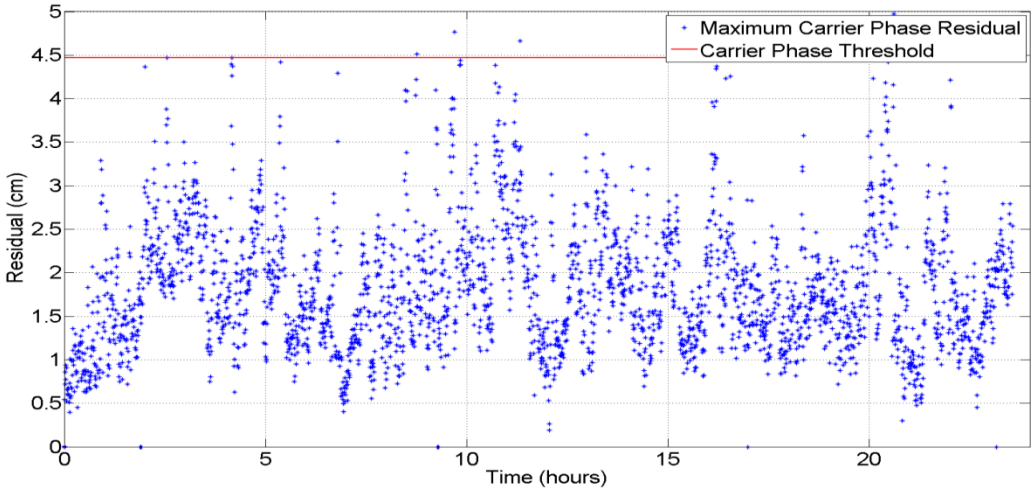

Figure 3.20: Fixed threshold residual rejection

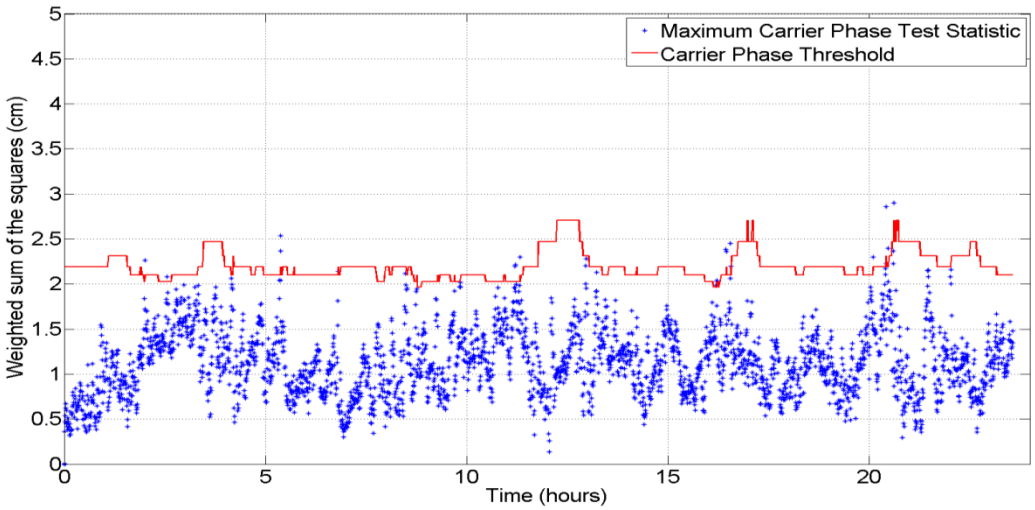

Figure 3.21: RAIM based residual rejection

Rejecting residuals that are greater than the specified threshold for the initial epoch could have a significant impact on the rate of convergence. Presented in Figure 3.22 is a histogram of the initial PPP solution, for four different scenarios. The scenario, "no residual rejection" is used as the worst case scenario. The scenario, "fixed threshold," is a component of PPP-CSRS code from NRCan (2010) and is used as the control to examine

the benefits RAIM has on the initialization of the PPP solution. The final scenario, "maximum residual rejection," scenario uses the measurements that have the 5 smallest residuals to initialize the solution.

Examining Figure 3.22, no residual rejection, fixed threshold and RAIM showed no significant variation. All 3 methods had a mean ranging from 210 to 213 cm and a standard deviation ranging from 184 to 193 cm. The scenarios fixed threshold and RAIM were expected to show significant improvement over no residual rejection being used. Further analysis of datasets has shown there was not significant residual rejection occurring. This may be due to, the data used for this study was collected by high-quality geodetic receivers used by the IGS network which consists of high-grade antennas and cables to reduce measurement noise and multipath are situated in clear open areas.

The scenario, maximum residual rejection was attempted as PPP convergence is reliant on the precision of the pseudorange observables. By selecting the satellites that have the highest level of precision to initialize the solution, could show improved rate of convergence. As illustrated in Figure 3.22, the initial solution quality deteriorated which would result in an increased convergence period. This may be possibly due to poor geometry as the 5 lowest residuals were selected to initialize the solution. Satellites at lower elevation would have larger residuals as the signal passes through a larger portion of the atmosphere, producing more signal refraction. Also, the signal may be more susceptible to multipath (discussed in more detail in section 4.2).

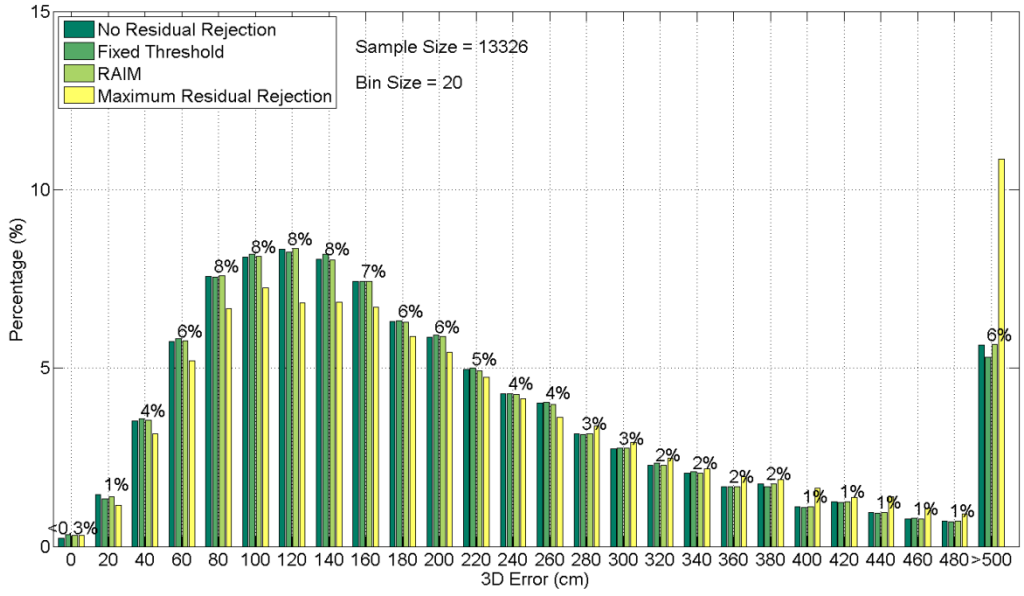

Figure 3.22: Distribution of the 3D position error used to initialize the PPP filter

3.6 Summary

In precision agriculture, hydrographic surveying and remote sensing the horizontal positioning accuracy specifications ranged from 10 to 100 cm. At an accuracy requirement of 10 cm or less, a minimum 50 minute convergence period is required. As the accuracy requirements decrease, the convergence period also exponentially decreases. To attain 15, 25 and 100 cm requires 25, 20 and 7 minutes, respectively. The most stringent is geodetic control surveying with horizontal positioning accuracy requirements of 0.5, 1 and 2 cm, with a convergence period of 24, 23 and 9 hours, respectively.

The greatest rate of change of PPP convergence is observed on average within the first 20 minutes followed by the solution achieving a steady state, with an average value of 10.3 cm ±12 cm.

A modified version of HPL adapted to indicate to the user in real-time when a steady state is attained.

To enhance the integrity monitoring and improve initialization of PPP, a modified version of RAIM was implemented and rigorously tested. However, significant improvements were not seen over the standard PPP residual rejection. This was attributed to the fact that the data were collected from high-quality geodetic receivers. If data were collected from lower-quality receivers, the value of RAIM would more likely be observed due to the larger magnitude of carrier-phase pseudorange multipath and noise present.

4.0 Mitigating Pseudorange Multipath and Noise

The convergence period in PPP is due to the carrier-phase ambiguities converging to constant values and allowing the solution to reach its optimal precision. This is primarily due to the estimation of the carrier-phase ambiguities from relatively noisy pseudoranges. If the pseudoranges were more precise, there would be a reduction in the convergence period. Pseudorange multipath and noise, together is the largest remaining unmanaged error source in PPP. By reducing the effects of the multipath and noise on the pseudorange observables, the carrier-phase ambiguities will reach a steady state at an earlier time, thus reducing the initial convergence and re-convergence period of PPP. This section provides an in depth review of the causes of pseudorange multipath and noise as well as different methods of hardware and software mitigation to reduce this

error source. This is followed by a review of the different techniques to be implemented within the PPP software and processing of the entire dataset to quantify the improvements.

4.1 Pseudorange Noise

The quality of a GPS receiver is based essentially how precisely it can measure the pseudorange and carrier-phase observables and aside from the inherent nature of each observable, is largely dependent on how much noise accompanies the signals in the receiver's tracking loops (Langley, 1997). This noise comes from the receiver electronics itself or is picked by up the receiver's antenna. The different sources of noise generated by natural causes and within the receiver are presented below.

Thermal noise: This noise represents the most basic kind of electrical noise produced by the random movement of the electrons in the electronic components such as the resistors and semi-conductors in a GPS receiver. The voltage has a zero average, but the power associated with it, which is proportional the square of the voltage, although small, is non-zero. Langley (1997) provides an example of a receiver situated in an environment at 290 K (16.85 ºC) with a 1 MHz bandwidth has power generated from noise of 4×10^{-15} watts. Where the power a received radio signal regenerates at an antenna's terminals can be quite small, e.g., the GPS C/A-code signal generates only about 10^{-16}.

Antenna Temperature: The sky and ground noise also have a pronounced effect on GPS receivers, requiring the source of the temperature to extend over the entire antenna. For hypothetical isotropic types (i.e., unit gain in all directions), the antenna temperature for

the sun subtended an angle of 0.5° is less than 0.5 K when solar activity is low and ~ 6 K at most when the Sun is disturbed. GPS antennas are typically omnidirectional. The gain has a non-directional pattern in the azimuth, but as the elevation angle decreases, so does gain. This aids in reducing the noise and multipath on the pseudorange and carrier-phase measurements (Langley, 1997; Kunysz, 1998).

System Noise: The antenna noise temperature is one of two components of the overall system noise performance of a GPS receiver. The other component is the receiver's equivalent noise temperature, which consists of a combination of cable losses and the noise internally generated in the receiver. The antenna noise temperature must be corrected for the contribution by the cable between the antenna and the receiver or antenna preamplifier input. As the signal travels through the cable, the electrical energy passing through the cable dissipates. For a signal travelling through an attenuated cable, not only does the signal dissipate, it also adds to the noise. A receiver's noise temperature represents that of a noise source at the input of an ideal noiseless receiver that would produce the same level of output noise as the actual receiver's internal noise. To reduce the internal noise, the receivers are constructed as a number of stages, each with its own gain contributing to its own noise and interconnected by cables or other circuitry (Langley, 1997).

4.2 Pseudorange Multipath

Among the numerous potential sources of GPS signal degradation, multipath takes on a prominent position. Unlike other errors like ionospheric or tropospheric path delays

which can be modelled or significantly reduced by differential techniques, multipath influences cannot be mitigated by such approaches.

Multipath occurs when the satellite signal is reflected by objects in the vicinity of a receiver, so that not only the direct signal enters the receiver, but rather a composite signal consisting of the line-of-sight (LOS) signal plus one or several multipath signals. It is also possible that the LOS signal is completed obstructed, so that the receiver only processed the multipath component. Multipath distorts the correlation function and leads to the pseudorange and carrier phase errors that degrade the solution performance (Irsigler, 2010).

The signature feature of multipath is an oscillation that occurs in all three observation types. The amplitude of the multipath induced errors in carrier-phase observations is limited to a quarter wavelength or about 5 cm, but is typically well below 2 cm. Pseudorange multipath can have a magnitude of up to 10 to 20 m as it depends directly on the distance to the reflector (Dixon, 1991). Thus, one approach to reducing pseudorange multipath is simply to apply so-called "carrier smoothing" to pseudorange observations, which will be discussed in section 7.7. This approach is quite effective in the absence of cycle-slips and loss of carrier lock (Axelrad *et al.*, 2005).

Figure 4.1 illustrates the simplified geometry for a fixed antenna and a large tilted planar reflector at a distance, h, from the surface. The angle of incidence of the signal with respect to the reflector plane is γ and the angle of the plane with respect to the local level is β. Since the GPS satellites are very distant, all lines of sight can be considered parallel.

The reflected signal arrives at the antenna delayed, phase shifted, and attenuated with respect to the direct signal. Figure 4.2 illustrate the pseudorange correlation function, where τ_m is the pseudorange tracking error, which is a result of multipath and noise on the pseudorange measurement (Axelrad *et al.*, 2005).

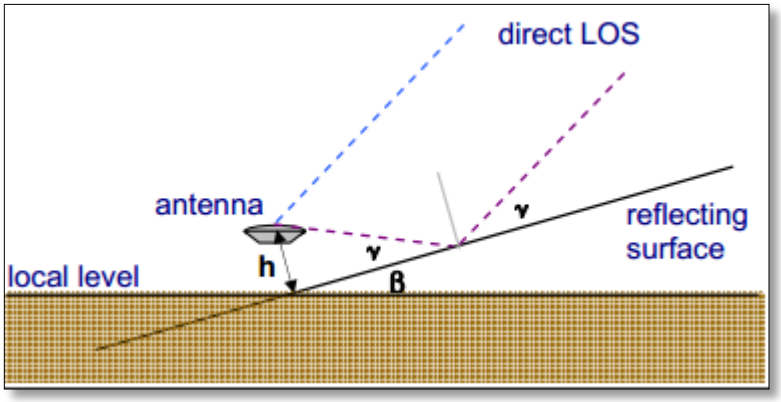

Figure 4.1: Simplified reflector geometry. The antenna is at a distance h, normal to the surface. The satellite line of sight is incident at angle, γ, to the surface. Source: (Axelrad *et al.*, 2005)

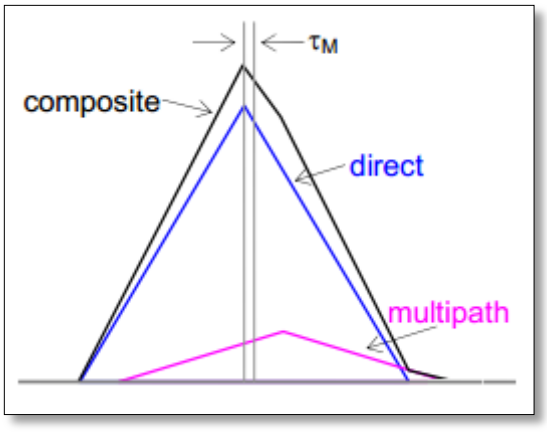

Figure 4.2: Effect of multipath on pseudorange measurement. The pseudorange tracking error is τm. Source: (Axelrad *et al.*, 2005)

4.3 Multipath Mitigation Techniques

Ground Plane: A simple form of multipath mitigation uses a metallic disk in the horizontal plane, centred at the GPS antenna's base referred to as an extended ground plane. This shields the antenna from most signals arriving from below the antenna, such as those bouncing off the ground. This method is not entirely effective due to characteristic of electromagnetic waves. A wave can induce horizontally travelling surface waves on the disk's top side, which then travel to the antenna, thus compromising the disk's usefulness. Also, not all multipath signals arrive from the below the antenna, thus limiting this method's effectiveness (Weill, 1997; Gao *et al.* 2012).

Choke Ring: The choke ring is essentially a ground plane containing a series of concentric circular troughs one-quarter wavelength deep. The troughs act as transmission lines shorted at the far end, and at their tops exhibit a very high impedance at the GPS signal frequency. This architecture mitigates surface waves from forming, protecting the antenna from ground bounce and multipath signals arriving from near-horizontal directions. The major disadvantage is the size, weight and cost of such antennas. The choke ring antenna is not as effective against multipath arriving above the horizontal, such as from reflections from tall building (Weill, 1997; Gao *et al.*, 2012).

Right Hand Circularly Polarized (RHCP): The GPS antenna is designed for RHCP signals transmitted by the GPS satellite, which assists in improving the immunity of antenna from multipath signals due to reflections. A RHCP signal becomes a left handed

circularly polarized signal (LHCP) upon complete reflection (Weill, 1997; Kalyanaraman, 1999).

Antenna Location: One simple, yet very effective, method of reducing multipath effects is by placing the antenna where it is less likely to receive reflected signals.

Long-term Signal Observation: If a receiver observes a signal for a sufficiently long time from a static location, the multipath observable (discussed in more detail in section 4.5) can be accurately calculated to characterize pseudorange multipath and noise at a static site. At these static sites, the same satellites from one day to the next are repeated, each advancing approximately four minutes per day, referred to as sidereal lag (discussed in more detail in section 4.6) (Axelrad *et al.*, 2005; Kalyanaraman, 1999; Weill, 1997).

Receiver technology: One of the most effective methods to reduce multipath effects is the use of real-time signal processing within the receiver. This includes methods such as narrow spacing correlators and extending the multipath estimation delay lock loop (MEDLL) (Weill, 1997). The benefit of narrow spacing correlators is a result of extending the lag by 0.1 C/A - code chips or ~100 ns forward and backward. The reduction in the correlators spacing not only makes the pseudorange measurement 10 times more accurate, but pseudorange multipath error is also reduced by approximately 1/10 in magnitude. MEDLL takes multiple correlators spaced at narrow intervals across a C/A-code chip, which allows the correlation triangle (from figure 4.2) to be recreated almost instantaneously, almost eliminating long delay multipath errors resulting in a multipath error comparable to that of the GPS P-code (Kumar, 2006).

4.4 Hatch Filtering

One of the earliest techniques of GPS pseudorange filtering was described by Hatch (1982). Making use of the pseudorange and carrier-phase measurements, this technique is commonly referred to as the Hatch filtering or, inaccurately, phase smoothing. This method is based on the concept that the change in pseudorange between observations at different points of time (epochs) equals the change in carrier range, and that the change in carrier range can be determined with far more accuracy than the change in pseudorange (Kim *et al.*, 2007).

In principle the more epochs of data that are used in the filtering process, the more precise the filtered pseudorange should become, and eventually approach the precision of the carrier range. Since the ionosphere delays the pseudorange and advances the carrier phase, the change in pseudorange does not equal the change in carrier phase resulting in what is referred to as ionospheric divergence. If the receiver channel loses lock on the satellite momentarily, or if the range rate of change is too high, the carrier-phase integration process is disrupted, resulting in a 'cycle slip', and an incorrect change in carrier range, and the filtering process has to be re-initialized (Kim *et al.*, 2007). Presented in equation 4.1 is the filtered pseudorange for a series of N observations of pseudorange (P) and carrier phase data (ϕ). N equations for P_N are formulated which are used to determine the filtered value of P_N, which should be more precise than the raw observation P_N.

$$P_N = \frac{P_N}{N} + (P_{N-1} + \phi_N - \phi_{N-1}) * (N - 1) \qquad 4.1$$

Illustrated in Figure 4.3 and Figure 4.4 are the residuals of the pseudorange measurements generated by the York-PPP software. Figure 4.3 shows the non-Hatch filtered residuals consisting of a white noise structure ranging from ±5 m with an average residual of 70 cm and standard deviation of 10 cm. Figure 4.4 shows the Hatch-filtered results with a convergence period as the ambiguity term reaches a stead state, the residuals range from ±3 m with an average residual of 24 cm and standard deviation of 6 cm. The PPP solution was re-initialized every hour, thus the visible convergence period noted in the residuals due to the Hatch filter also being re-initialized.

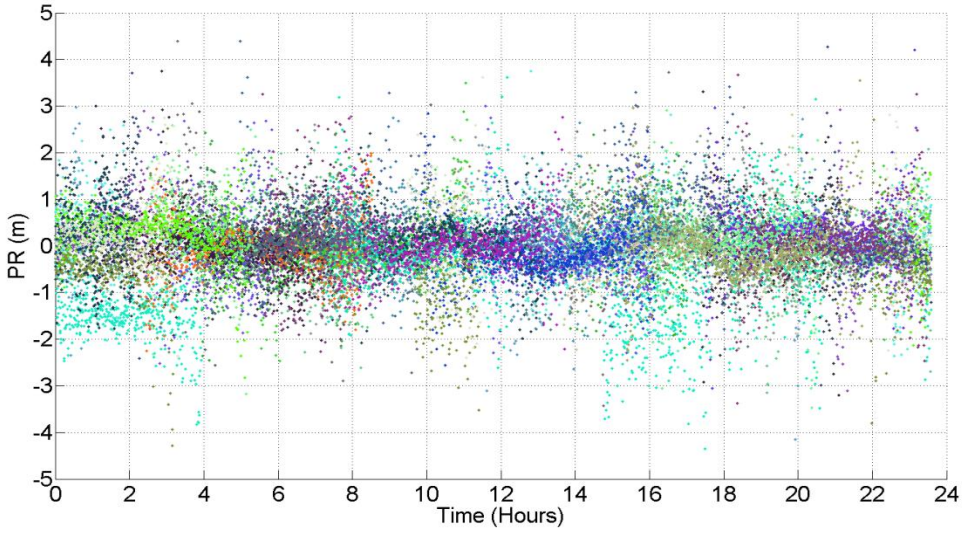

Figure 4.3: Pseudorange residuals with no Hatch filtering

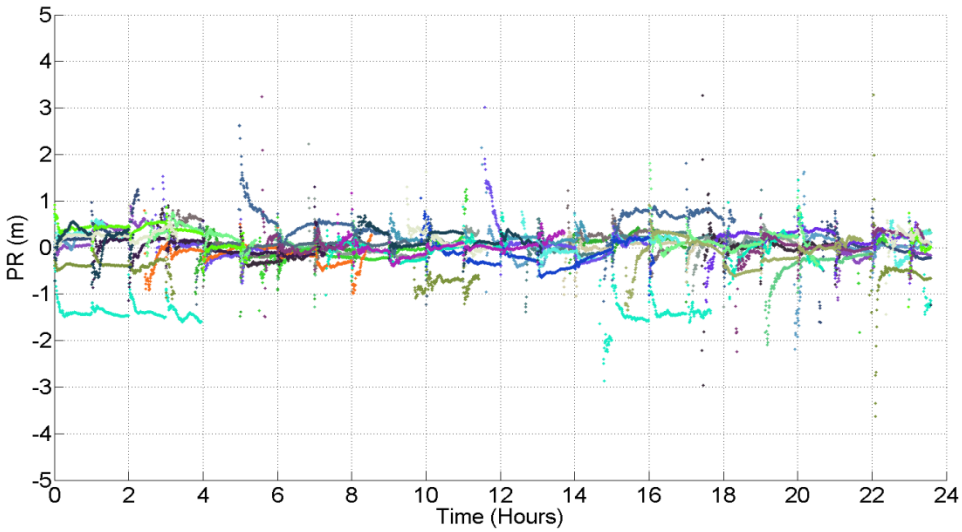

Figure 4.4: Pseudorange residuals with Hatch filtering

To quantify the improvements of the Hatch filter in PPP processing, two scenarios were generated with the Hatch filter turned off and on in Figure 4.5. The same dataset from Chapter 2 consisting of 81 sites reinitialized every hour for a sample size of approximately 13 300. A 3D threshold of 30 cm was set to analyze the varying convergence period of the solution. An exponential trend can be observed in both figures with Hatch on and off, with 95% of the results converging within 28 minutes. There were no significant improvements noted when Hatch filtering was turned on. The convergence period degraded by 9% when compared to Hatch filtering off during the 2 to 8 minute time bins. Within the 16 minute time bin, the same percentage of solutions had converged to meet the threshold.

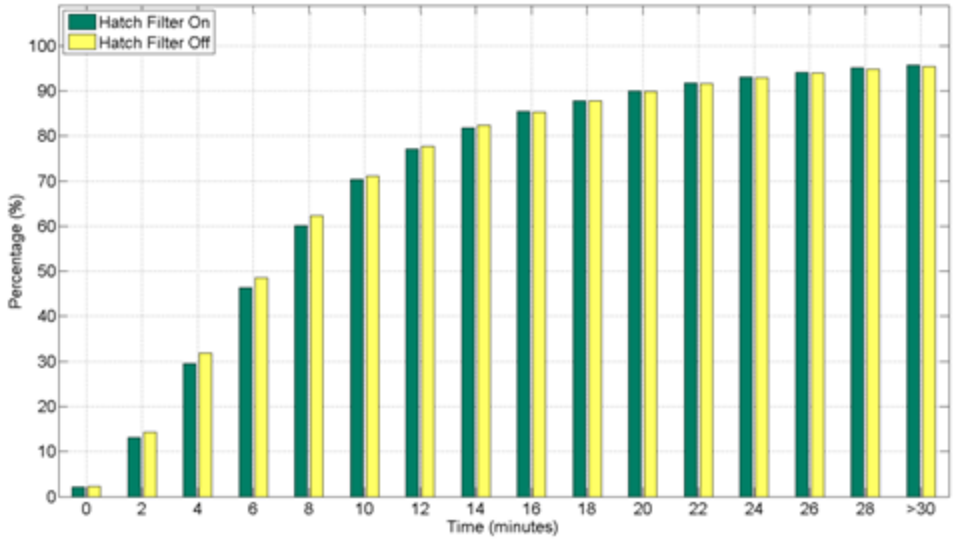

Figure 4.5: Comparing the rate of convergence with and without Hatch filtering with hourly reinitialization for a sample size of 13 300

Hatch filtering filters the pseudorange multipath and noise in real-time. Its major limitation is the requirement of several epochs of data to successfully average the ambiguity term. While Hatch filtering has proven to be useful, in PPP, the Hatch filter requires initialization of the ambiguity. By using a simple recursive algorithm to average estimate the ambiguity term and filter the pseudorange observables may introduce the uncertainty of the ambiguity term present in the Hatch filtering. This may be the reason why at the 16 minute time bin, PPP processing with the Hatch filter on and off presented equivalent results. Using Hatch filtering in PPP to assist in reducing the convergence period of PPP has not proven to be useful. One possible reason for the lack of performance may be attributed to the high-quality geodetic receivers present at these sites. Also, some receivers such as Ashtech have a smoothing correction for the

pseudorange observables available in the raw data (Gurtner, 2002). Ashtech recommends this feature is turned on for full P-code receivers (Gurtner, 2000).

The site KIRU was further examined to determine if the Hatch filter would improve results where there was higher pseudorange multipath and noise present (as illustrated in Figure 4.8), which may have been the cause for the biases introduced into the solution (Figure 2.4). It was anticipated that by using the Hatch filter, the pseudorange multipath and noise would have been reduced thus improving convergence. Presented in Figure 4.6 is the time the solution took to reach a 3D threshold of 30 cm accuracy with hourly re-initialization for days 244-250. On days 246-248 there was significant increase in pseudorange multipath and noise present at the site. After 30 minutes, 15% of the data did not reach the convergence threshold. Scenarios with the Hatch filtering on and off showed similar exponential trends. The rate of convergence was faster with the Hatch filtering off. The most significant difference noted at the 6 minute time bine with a 12% difference. At the site KIRU, DOY 246 between 1am and 2am GPS Time, the solution used to initialize the PPP filter had deteriorated in the Up component by 186 cm when the Hatch filtering was turned on.

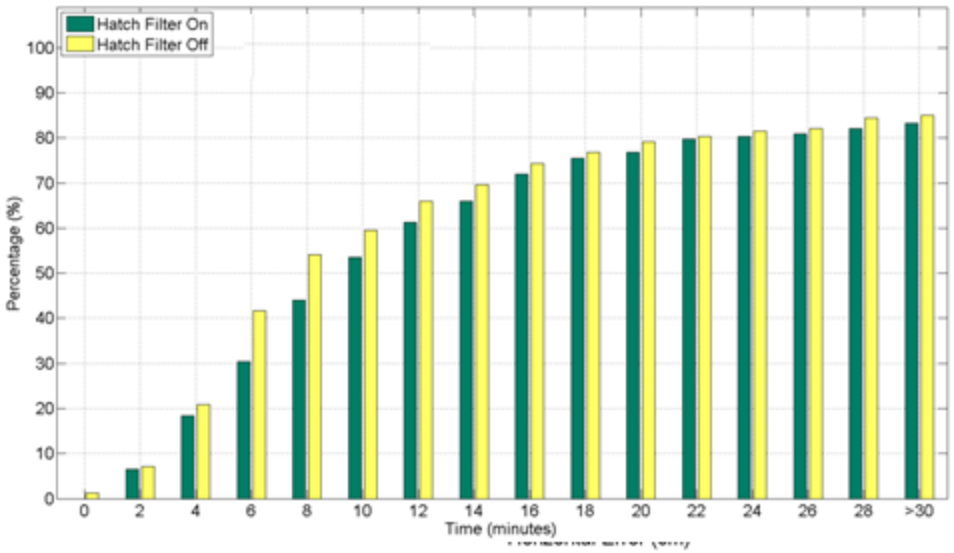

Figure 4.6: Comparing the rate of convergence with and without Hatch filtering at the site KIRU

4.5 Multipath Observable

The coloured noise of the pseudorange consists of multipath and noise, i.e., signal reflections around the satellite and receiver antenna, in cable connectors, and the variations of the instrumental delays possibly due to temperature variations which can occur at different levels: antenna, cables, amplifiers, splitters, receivers, etc. (Defraigne and Bruyninx, 2007).

For each satellite, the pseudorange multipath observable can be computed from the measured pseudorange and carrier-phase measurements in which the phase multipath and noise, significantly smaller than the pseudorange multipath and noise, are neglected (Leick, 2004). The pseudorange multipath/noise on L1 is presented in equation 4.2 and on the L2 in equation 4.3.

$$MP_1 = P_1 - \left(1 + \frac{2}{\alpha - 1}\right) L_1 + \left(\frac{2}{\alpha} - 1\right) L_2 \quad 4.2$$

$$MP_2 = P_2 - \left(\frac{2\alpha}{\alpha - 1}\right) L_1 + \left(\frac{2\alpha}{\alpha - 1} - 1\right) L_2 \quad 4.3$$

where

$$\alpha = \left(\frac{f_1}{f_2}\right)^2$$

f_1: L1 frequency 1.5754 GHz

f_2: L2 frequency 1.2275 GHz

This combination contains only multipath and noise with no possible distinction between both, plus one constant term associated with phase ambiguities, and one term associated with instrumental delays.

Under the conditions that (1) multipath and noise have a zero-mean during a period T_m, (2) the hardware delays are constant during Tm, and (3) no cycle-slips occur during T_m, the multipath and noise can be obtained through equation 4.4.

$$mp_{L1} = MP_1 - MP_{1T_m} \quad 4.4$$

where MP_{1T_m} is the average of MP_1 over the period Tm. The average is removed in order to remove the constant terms, which is mainly a function of scaled carrier phase ambiguities. The quantity mp_{L1} contains the white noise components and multipath

components with periods smaller than T_m. These terms will therefore disappear from the observed pseudoranges when correcting them for mp_{L1} (Defraigne *et al.*, 2007).

Illustrated in Figure 4.7 and 4.8 is the multipath for the PRN 03 at the site ALGO and PRN 15 at the site KIRU, respectively. The multipath time series at the site ALGO, with a standard deviation of 28 cm, illustrates the characteristics of typical ground bounce multipath, as, at lower elevations there is higher multipath and as the elevation of the satellite increases, the multipath decreases. KIRU illustrates high multipath disturbance with a standard deviation of 62 cm. There is little correlation between the multipath observable and the elevation angle of the satellite, suggesting that this disturbance is due to the localized activity at this site.

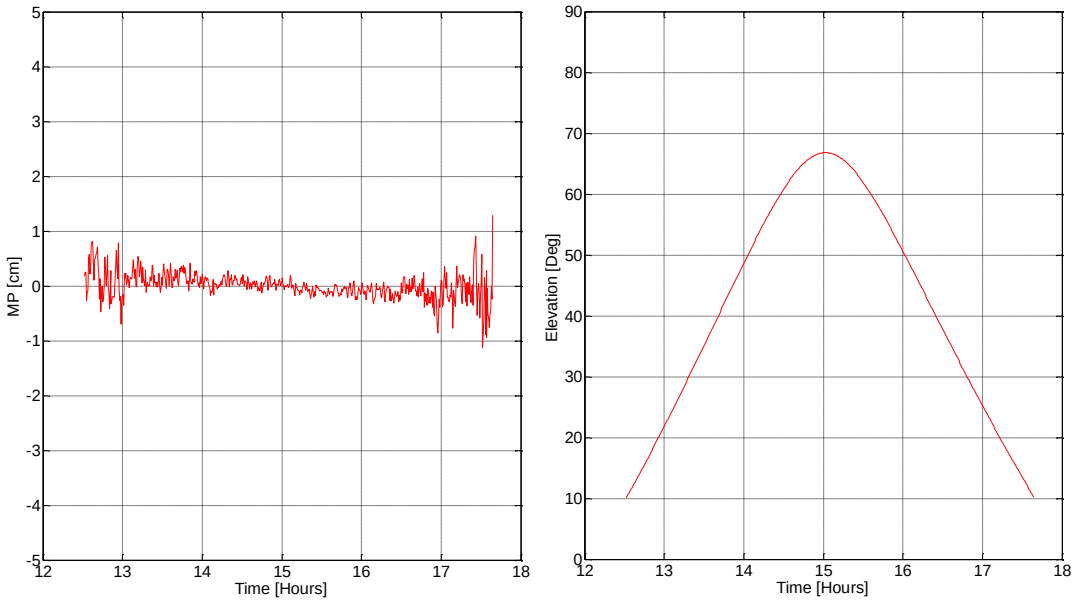

Figure 4.7: Ionospheric free pseudorange multipath observable (left) and elevation angle (right) for PRN 03 at Algonquin (ALGO) on DOY 249

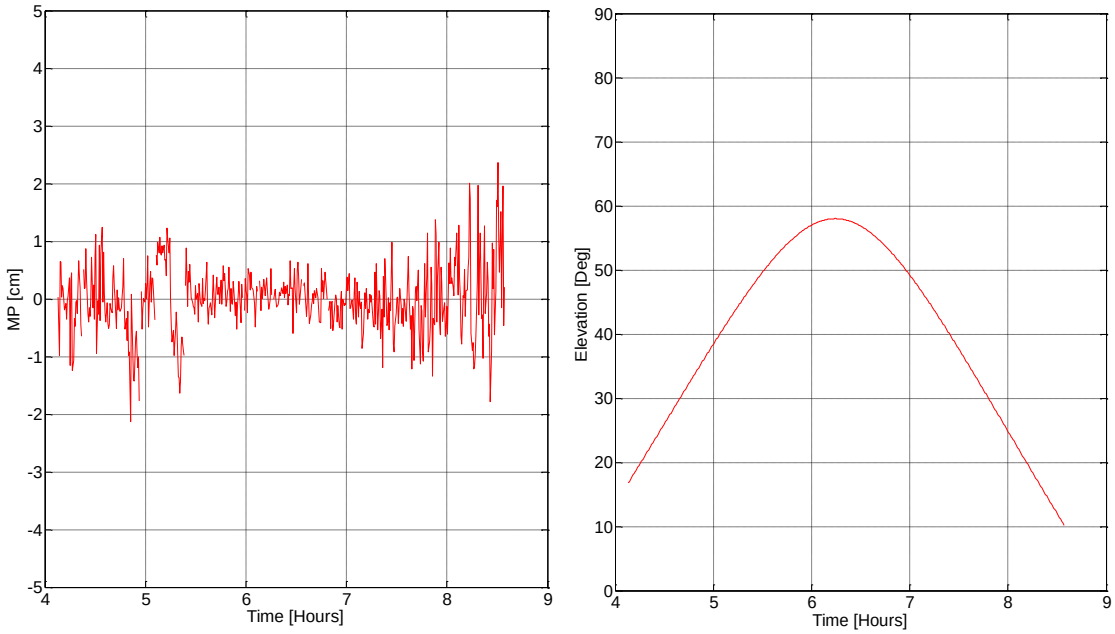

Figure 4.8: Ionospheric free pseudorange multipath observable (left) and elevation angle (right) for PRN 15 at Kiruna (KIRU) on DOY 249

4.6 Satellite Repeat Period

A receiver in static mode, in an unchanged user environment would have a repeated multipath observable if the sidereal lag is removed allowing pseudorange multipath to be corrected for in real-time. Illustrated in Figure 4.9 is the effect of not correcting for the sidereal lag. The GPS satellite orbits have a nominal period of one half of one sidereal day (23 h 56 m 4 s) with a daily repeating ground track. Satellite visibility from any point on Earth is the same from day to day, with the satellites appearing in their positions approximately 4 minutes (236 s) earlier each day due to the difference between the sidereal and solar day (Axelrad *et al.*, 2005). This difference is referred to as sidereal lag. The Earth's oblateness has the largest effect on the ground track repeat at the GPS orbit

altitude, producing a secular nodal drift westward by ~14.665° per year. To compensate for this motion of the orbit plane, the average semi-major axis of the GPS satellite orbits is set slightly lower, such that the orbital period is about 4 s faster than a sidereal half-day and consequently the time shift of the daily repeat for most satellites in the constellation is closer to 244 s (Axelrad *et al.*, 2005).

There are three methods for estimating the sidereal lag for each GPS satellite geometry: 1) compute the period from the semi-major axis given in the broadcast ephemeris or almanac data; 2) compute the repeat time by interpolating precise orbits to the time of equator crossings; and 3) find the actual repeat geometry for a selected location and identify the associated time shift. Presented in Agnew and Larson (2007) and Axelrad *et al.* (2005) are analyses of using these three methods to calculate the sidereal lag. Using the broadcast ephemeris and interpolating the precise orbits presented equivalent results. The method using broadcast ephemeris was used here because of its simplistic design and ease of implementation. The sidereal shift (Ta) is computed using the period from the semi-major axis given in the broadcast ephemeris as follows:

$$T_a = 86400 - 2(2\pi/n) \tag{4.5}$$

Where the mean motion, n, is given by

$$n = \sqrt{\mu_\varepsilon + a^3} + \Delta n \tag{4.6}$$

and a is the semi-major axis and Δn is the mean motion adjustment. μ_ε is the gravitational constant of the Earth specified as $3.986\text{x}10^{14} m^3/s^2$ for use with the broadcast elements.

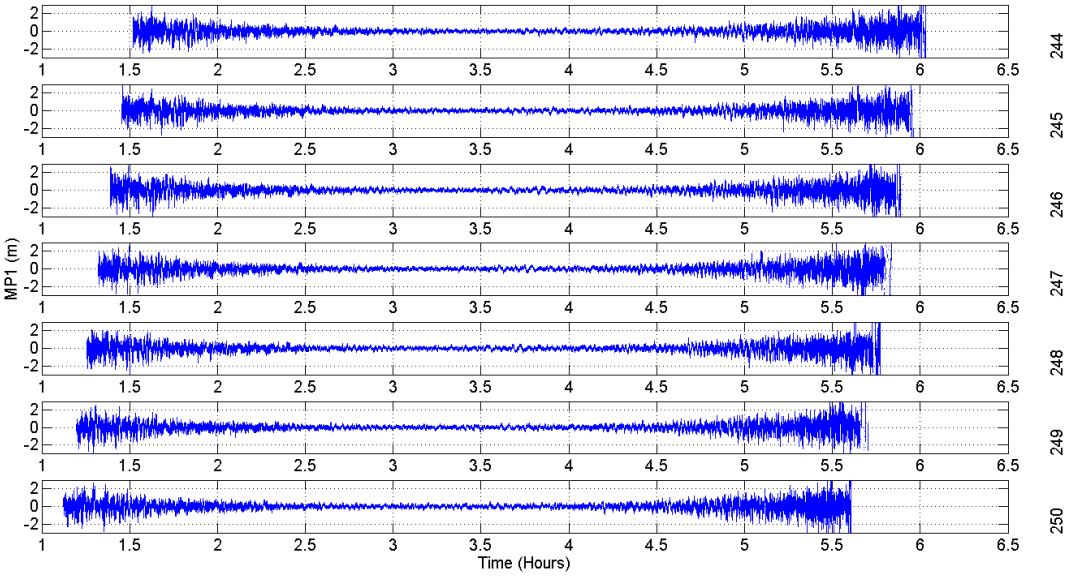

Figure 4.9: Multipath linear combination for DOY 244-250 for the site ALBH PRN 24 showing the daily sidereal lag

4.7 Pseudorange Multipath and Noise Correction

PPP convergence is reliant on the precision of the pseudorange observables. The following methods presented are different techniques to mitigate pseudorange multipath and noise. The following section discusses each of the methods applied and quantifies the reduction of the convergence period.

4.7.1 Testing of the multipath observable

To investigate pseudorange multipath and noise for a fixed ground site, the pseudorange multipath at site ALGO and KIRU are investigated. The results presented in Figure 4.10 and Figure 4.11 illustrates the multipath observable for specific satellites on DOY 248 and 249 with the sidereal shift applied. The multipath observable is generated for the data

between the elevation angle from 10 to 30 ° as this time period is most susceptible to ground bounce multipath. At the site ALGO for PRN 03, typical ground bounced multipath was observed with a standard deviation of 31.2 cm and 29.8 cm on DOY 248 and 249 respectively. When the multipath observable of both days were subtracted, the standard deviation reduced to 20 cm.

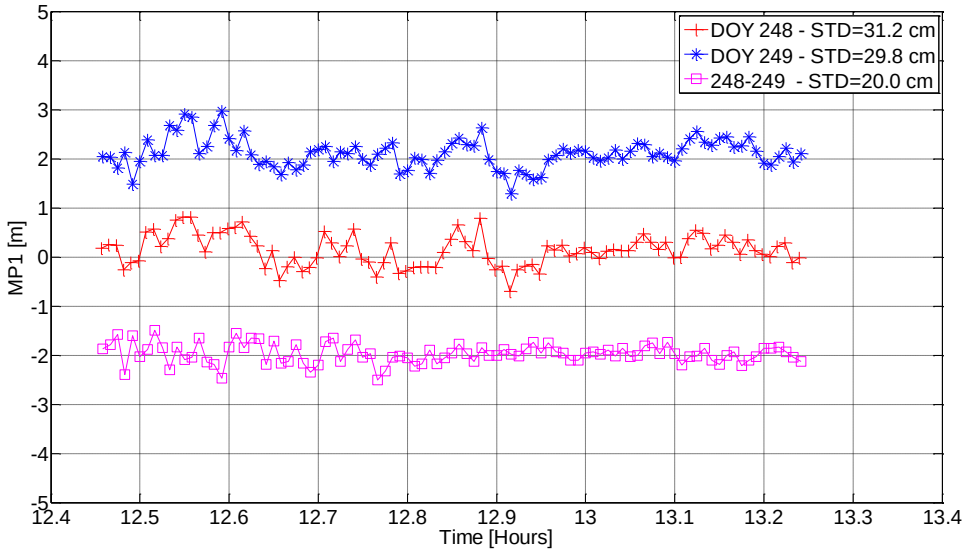

Figure 4.10: Pseudorange multipath for PRN 03 at ALGO, for DOY 248 and 249 in elevation range of 10-30°

At the site KIRU for PRN 15 the multipath observable on DOY 248 and 249 was twice that present at ALGO with a standard deviation of 53.8 cm and 54.2 cm, respectively. With the sidereal shift applied, there was no correlation between the multipath observables for both days. When the two observables were subtracted the standard deviation increased to 65.5 cm. This highlights one of the limitations of using the multipath observable from the previous day, even though it offers a method of real-time

multipath mitigation, if there are any changes in the environment this may result in degradation of the convergence period of the PPP solution.

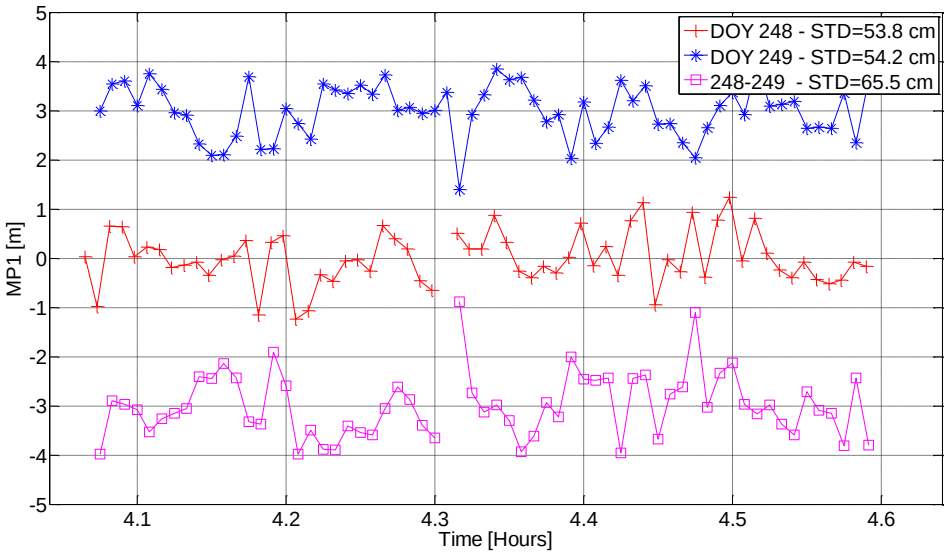

Figure 4.11: Pseudorange multipath for PRN 15 at KIRU, for DOY 248 and 249 in elevation range of 10-30°

Presented in Figure 4.12 and Figure 4.13 illustrates another option for real-time pseudorange multipath and noise mitigation. The running average multipath observable recursively estimates the ambiguity as the more data becomes available, similar to Hatch filtering. The running average is compared to the multipath observable where the ambiguity was averaged out using the entire time where no cycle slip occurred. Using the average of the entire time period has the advantage of being accurate and precise even during the initialization period with a major limitation, such that this is only possible during post-processing of the data. The running average is precise, but requires several epochs of data to increase its accuracy. This can be seen when the difference is calculated

between the average and running-average a convergence period is present during the first few epochs data are collected.

At the site ALGO, the multipath observable with the ambiguity averaged out and the running average had a standard deviation of 31.2 cm and 30.2 cm, respectively, with a difference of 8.1 cm. At KIRU, the multipath observable with the ambiguity averaged out and the running average had a standard deviation of 53.8 cm and 49 cm, respectively, with a difference of 19.3 cm. This highlights one of the advantages of using the running average to mitigate pseudorange multipath and noise rather than the multipath observable from the previous day as a static user environment is not required.

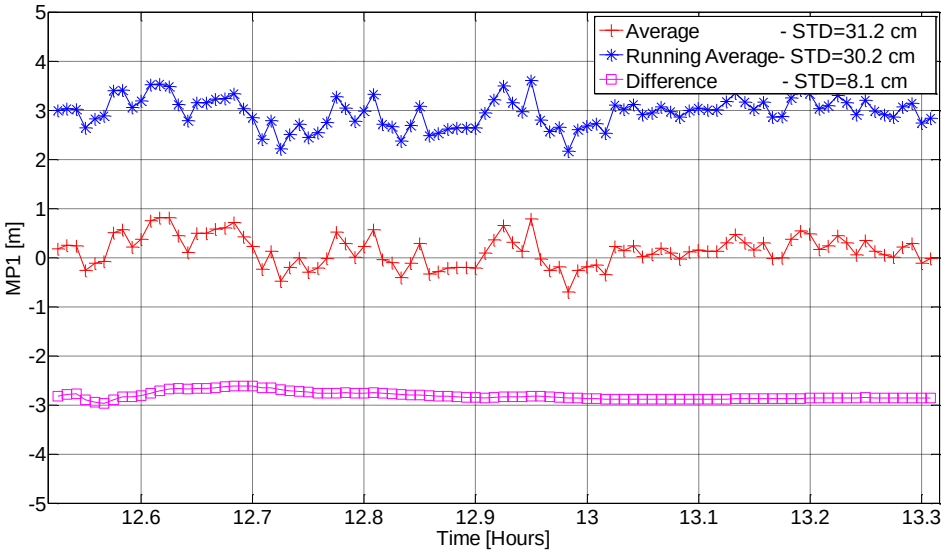

Figure 4.12: Pseudorange multipath for PRN 03 at ALGO, for DOY 249 using running average, in elevation range of 10-30°

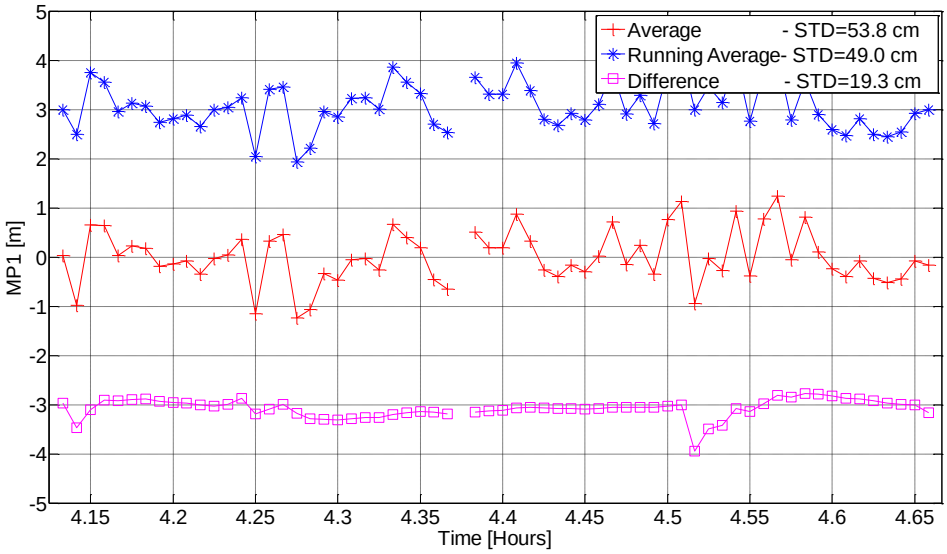

Figure 4.13: Pseudorange multipath for PRN 03 at KIRU, for DOY 249 using running average, in elevation range of 10-30°

4.7.2 Implementation of pseudorange mitigation using multipath observable

The standard PPP software requires dual-frequency measurements to calculate the ionospheric free pseudorange and carrier-phase observables. Illustrated in Figure 4.14 is the measurement processing flow present in the standard PPP software augmented with the multipath mitigation module. The module was designed to function under three different modes of operation, including 1) the multipath observable generated from the previous day 2) the multipath observable generated from the same day, and 3) the multipath observable generated in real-time using a running average. The first step in the module is to obtain the required multipath observable depending on the user defined mode of operation. This is followed by the correction of the raw P1 and P2 measurements by using the respective MP1 and MP2 observables. The final phase is the ionospheric

linear combination of the corrected P1 and P2 and the L1 and L2 observables to give P_{IF} and $L_{IF,}$ respectively.

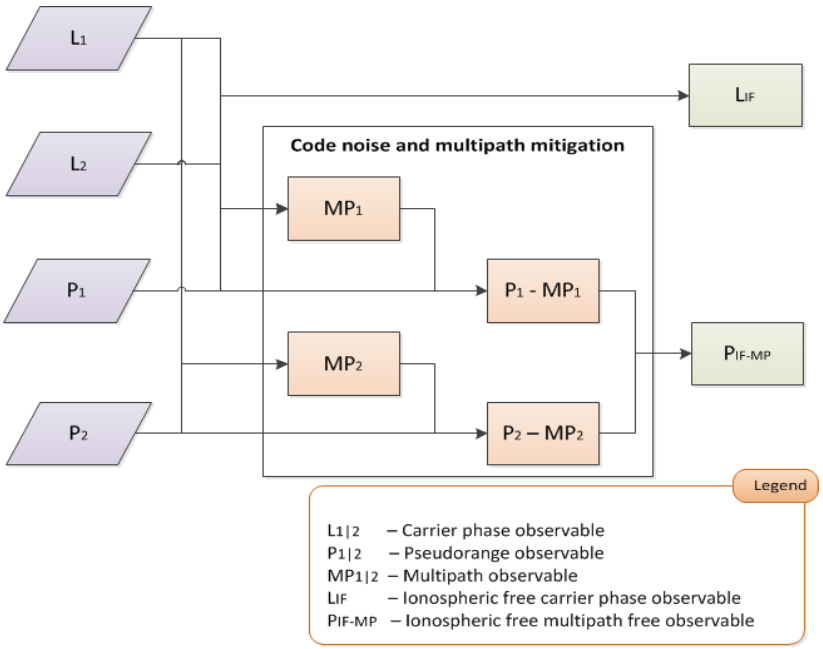

Figure 4.14: Measurement processing flow augmented by multipath mitigation modules

4.7.3 Reduction of convergence period using multipath observable

To quantify each of these methods discussed, Figure 4.15 was generated showing the time the solutions took to converge to a 30 cm 3D accuracy level. In Chapter 2 it was shown that the most critical time for convergence is within the first 20-30 minutes when the carrier phase measurements are as accurate as the pseudorange measurements. This fact is re-iterated in Figure 4.15, at the 30 minute time bin approximately the same percentage of datasets converged to the specified threshold.

Hatch filtering and running average: The least efficient method was the Hatch filter and running average, both producing similar results. This was expected, as conceptually, both methods are reducing the pseudorange multipath and noise in real-time. The lack of performance of this strategy is attributed to the geodetic receivers being used which record observations with a magnitude of multipath and noise lower than that of the accuracy of the pseudorange observables. Also, similar to PPP, both these methods recursively estimate the ambiguity term present in the carrier phase observation requiring several epochs of data to achieve a steady state.

Multipath observable from the previous day: Another method analyzed is the use of the multipath observable from the previous day. Improvements of 1.3, 2.5, 1.6 and 0.7% were seen in contrast to the standard PPP solution for the 0, 2, 4 and 6 minute time bins respectively. This illustrates that, while improvements were minimal, it is useful to make use of data from the previous day if the information is available. It is important to take note of this methods primary limitation which is a repeated multipath environment is required.

Multipath observable from the same day: The final method applied is the use of the multipath observable from within the same day. This method is possible by post-processing the dataset, generating the multipath observable which is fed into the PPP processor. This method has shown significant improvement in the rate of convergence, because the ambiguity term is accurately removed and the multipath observable is generated from the entire dataset, it would accurately represent the pseudorange

multipath and noise present. Also, unlike the running average, using the same day multipath observable provides corrections during the first epoch, thus improving the initial coordinate which is critical for reducing convergence period in PPP. Comparing the improvements between applying the multipath observable from the previous day to that generated within the dataset highlights that the noise on the pseudorange observable is one of the primary reasons for the current convergence period within the standard PPP solution. The benefits are seen within the first 30 minutes of PPP convergence. Improvements of 7.2, 14.3, 14.4 and 11.4% were seen in contrast to the standard PPP within the 0, 2, 4 and 6 minute time bins, respectively.

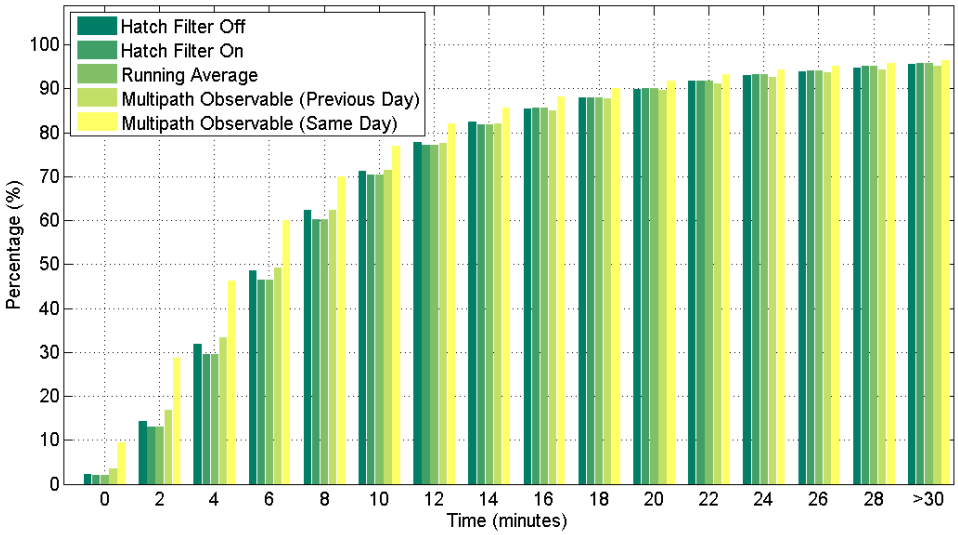

Figure 4.15: Different psuedorange multipath and noise mitigation techniques to the raw measurements

4.7.4 Reduction of convergence period using stochastic de-weighting

An alternative method which allows real-time processing is by applying an analytical de-weighting function based on the multipath observable (Bisnath and Langley, 2001). The

relationships between the observable and other weighting criteria such as the satellite elevation angle are also analyzed. Presented in equation 4.7 is sigma of unit weight (SUW) used to scale the pseudorange observable, which is simple a function of the sine of the elevation angle in radians.

$$SUWPR = sin(ELRAD) \tag{4.7}$$

The relationship between satellite elevation angle and ground bounced multipath can be seen in figure 4.7. The limitations of de-weighting observations based on the elevation angle are illustrated in Figure 4.8, when typical ground bounced multipath and noise are not present at the site.

Conceptually, in this mitigation approach, the multipath constituent in the pseudorange functional model is not treated as a deterministic quantity to be estimated, but rather it is coupled with the receiver thermal noise and tracking error terms and its variance is estimated with the linear combination presented in equation 4.4 and applied to the stochastic model. The strength of this model is it allows for real-time compensation of the effects of the pseudorange multipath and noise in the stochastic model, as long as realistic stochastic models are applied for each epoch in the position estimation process.

The multipath observable in position estimation was used in approximating the multipath variance of each satellite tracked for each epoch by continuously evaluating the observable for each satellite and applying these estimates in the positioning filter. For dual-frequency data, the ionosphere-free combination of the observables was used for

variance estimation. A simple fixed-interval, moving-variance algorithm was used, in which the rms is computed. The use of the variance would eliminate any bias over the computing interval and hence is not used. It has been found that the success of the technique is not overly sensitive to the window size selected; a few minute interval has worked well given a 30 second data sampling interval. Various weighting functions exist for GPS observables. If a stochastic model is used at all, it typically relies on the tracked satellite's elevation angle with respect to the receiver. The use of elevation angle-based weighting is very approximate and its use may produce reduced-accuracy positioning results.

Presented in Figure 4.16 is the data obtained from ALGO, DOY 249 for PRN 3. Figure 4.16a and Figure 4.16c illustrates the elevation angle and multipath observable with respect to the time of observation and the respective sigma of unit weight illustrated in Figure 4.16b and Figure 4.16d. As expected, the weight derived from the elevation angle of the satellite is a simple weighted function, while the weight derived from the multipath observable does reflects the measurement precision, which is a function of the multipath and noise.

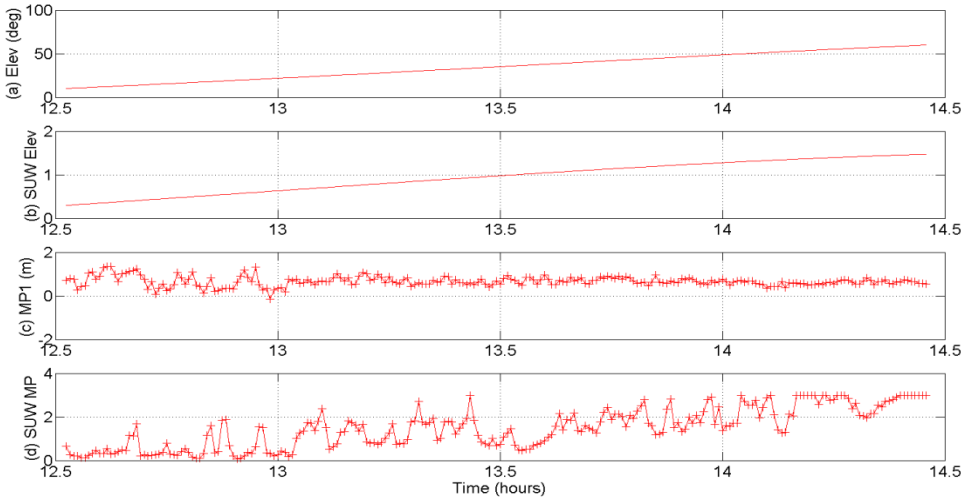

Figure 4.16: Weighting functions comparison using synthesized P-code observations collected from PRN 3 from ALGO DOY 249

Presented in Figure 4.17 is the stochastic de-weighting used for the pseudorange measurement for PRN 22, DOY 245 from the site BAIE (Baie-Comeau, Canada). One limitations of using the multipath observable is visible at the peak between hours 8-9. It is expected to have maximum weighting as pseudorange multipath and noise is at a minimum, but the satellites are momentarily de-weighted for some epochs.

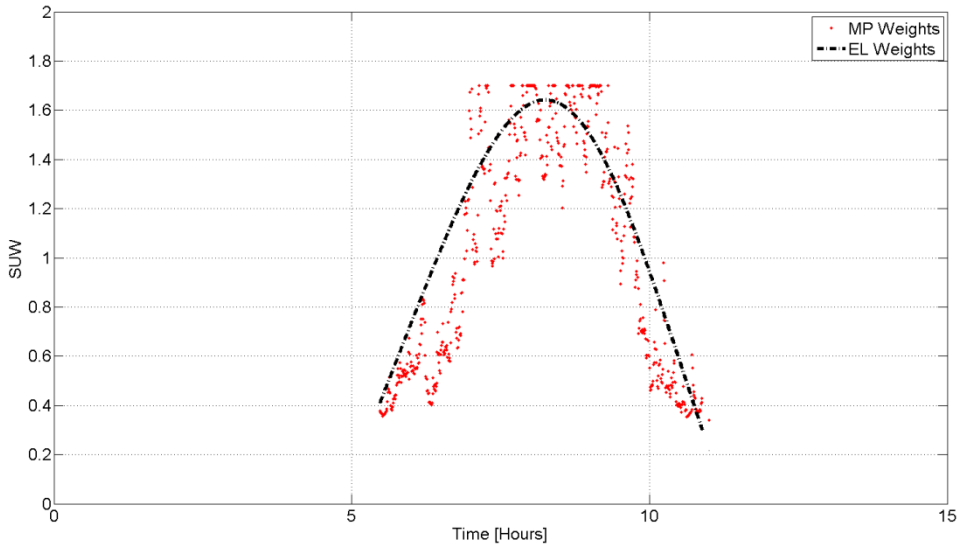

Figure 4.17: Stochastic de-weighting used for the pseudorange measurement for PRN 22, DOY 245 from the site BAIE

Presented in Figure 4.18 are varying convergence periods at the site BAIE on DOY 245 for scenarios with no weights, elevation weights, multipath weights and the same day filter coupled with elevation weights. A 3D accuracy level of 30 cm was set to examine the time the solution took to converge. As expected the largest convergence period occurred with no weights applied to the pseudorange measurements with a time of 13 minutes. At this site, when elevation weighting and same day filter coupled with elevation weighting had the same convergence period of 11 minutes. The solution converged the fastest using the multipath weights in a time of 7 minutes.

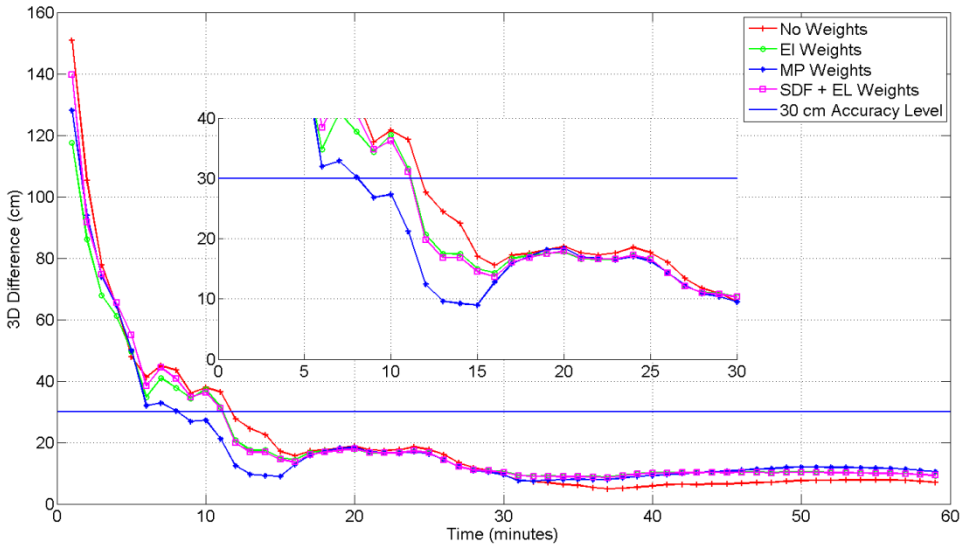

Figure 4.18: Site BAIE for DOY 245, illustrating varying convergence rates based on different pseudorange multipath and noise mitigation techniques

To examine the quality of the improvements on convergence, each stochastic de-weighting method was examined and compared to the standard PPP where the weights are the identity matrix for the pseudorange measurements. This is illustrated in Figure 4.19. Also, each stochastic de-weighting method was augmented with the same day

multipath observable, illustrated Figure 4.20. As previously stated, the most critical time period in PPP convergence is the first 30 minutes of data processing. The benefits of either de-weighting method can be easily noted when comparing the standard PPP solution to de-weighting the observations based on either elevation angle or multipath observable. The most influential time period is within the data sets that met the 30 cm 3D threshold within the first 10 minutes. Within the 0, 2, 4 and 6 minute time bin where improvements of 2.2, 11.4, 13.5 and 12%, respectively when elevation weights were used, and 2.3, 10.7, 12 and 11%, respectively, when the multipath observable weighting scheme was used. The performance of stochastically de-weighting the pseudorange observables using the elevation weights and multipath observable performed comparable.

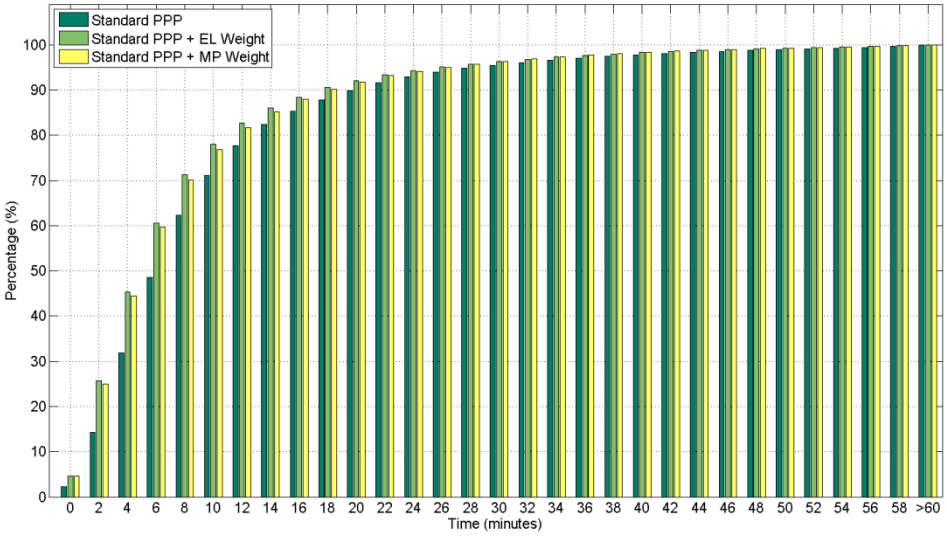

Figure 4.19: Standard PPP processing parameters with pseudorange observables de-weighted using elevation and multipath weights

This augmentation of the same day multipath observable and stochastic de-weighting was selected to observe the best possible results when examining pseudorange multipath and noise mitigation. Within the 0, 2, 4 and 6 minute time bins where improvements of 9.3,

20.7, 20.7 and 17%, respectively, when elevation weights were used and 8, 19, 19 and 15%, respectively, when the multipath observable weighting scheme was used.

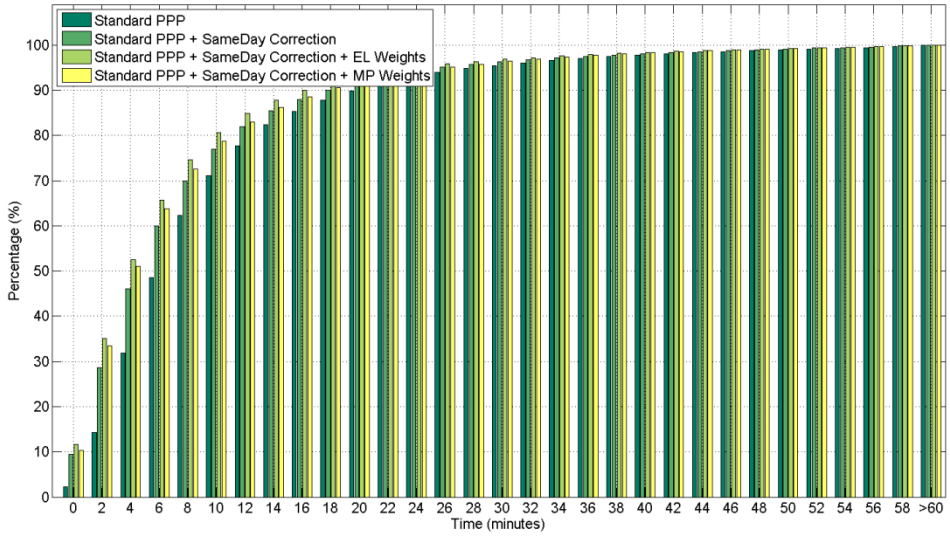

Figure 4.20: Standard PPP processing parameters with same day multipath correction as well as pseudorange observables de-weighted using elevation and multipath weights

4.8 Summary

The multipath linear combination was calculated to mitigate the raw pseudorange observable and stochastically de-weight pseudorange observables based on the magnitude of the pseudorange multipath and noise present. To correct the raw observables three different methods were applied; these included: 1) running average, 2) previous day multipath observable, and 3) the same day multipath observable. The least effective was the running average showing little to no improvements. This was due to the required convergence period of the running average. The same day filter showed a 47% improvement over the standard PPP. This method was most effective because it allowed the ambiguity term to be accurately removed and accurately removed the pseudorange

multipath and noise from the pseudorange measurements. The stochastic de-weighting method included the use of multipath observable and elevation angle of the satellite. Overall improvements at 39.1% and 36% were observed over standard PPP when using the elevation angle and the multipath observable, respectively. This indicates the importance of the de-weighting pseudorange measurements with multipath and noise as it decreased the convergence period of PPP.

5.0 Conclusions and Recommendations for Future Research

PPP requires a relatively long initialization period (few tens of minutes) for the carrier-phase ambiguities to converge to constant values and therefore allowing the solution to reach its optimal precision. This allows PPP to take full advantage of the precise, but ambiguous carrier-phase observables; however, the length of time it takes to reach the optimal solution is a major disadvantage for the broader use of this technique. This existing convergence period is due to the carrier-phase ambiguities being initialized by the pseudorange observables.

Given this problem, it was the objective of this study to manage the uncertainty of pseudorange observable, by reducing the convergence period. Before attempting to mitigate the pseudorange multipath and noise, a PPP software comparable to scientific

standards was developed. The PPP processor called, York-PPP was implemented in MATLAB and C++, capitalizing on the advantages that exist in both programming languages. MATLAB was used in the design of the graphical user interface (GUI) of the software as well as plotting of output data of the processor. The core of York-PPP consists of approximately 110 functions and over 32 000 lines of C++ code.

5.1 Conclusions

PPP Performance: The performance of the York-PPP software was examined using, one week of data from 80 globally distributed stations, providing an overall rms of 4, 5 and 27 mm in the north, east and up, respectively. The PPP processor was performing comparable to high scientific standard. The collected data were reprocessed with hourly reinitialization to increase the sample size to approximately 13 300 to analyze the rate of convergence. As part of the preliminary analysis, a 20 cm horizontal accuracy level was established and the time the solution took to achieve this level accuracy was analyzed. In static mode an exponential trend was observed in contrast to the quasi-linear trend in kinematic mode. The static solution took approximately 25 minutes for 96% of the data to converge to a horizontal accuracy level of 20 cm and 55 minutes in kinematic mode.

Convergence period: One of the challenges faced by PPP users is the required convergence period. Presented are the methods to define convergence, these include: 1) Required convergence period based on the application, 2) When the solution attains a steady state and 3) A modified version of horizontal protection level (HPL). In precision agriculture, hydrographic surveying and remote sensing the horizontal specifications

ranged from 10 to 100 cm. At an accuracy requirement of 10 cm or less, a minimum 50 minute convergence period is required. As the accuracy requirements decrease, the convergence period also exponentially decreases. To attain 15, 25 and a 100 cm requires 25, 20 and 7 minutes, respectively. The most stringent is geodetic control surveying with horizontal accuracy requirements of 0.5, 1 and 2 cm, with a convergence period of 24, 23 and 9 hours, respectively. The greatest rate of change was observed on average within the first 20 minutes followed by the solution achieving a steady state, with an average value of 10.3 cm and a standard deviation of 12 cm. The modified HPL was successfully examined using the same dataset with hourly reinitialization and is recommended as a real-time indicator of when a steady state has been attained.

Integrity monitoring and outlier detection: One proposed method to improve the integrity monitoring and outlier detection with PPP is the implementation of an Receiver Autonomous Integrity Monitoring (RAIM) algorithm. RAIM provides rigorous analysis of the post-fit residuals, assisting in detecting outliers within the residuals, which in some cases have been previously overlooked by standard PPP residual rejection. Unlike RAIM, the current standard method for rejecting residuals is based on analyzing the maximum pseudorange and carrier-phase post-fit residuals. If the carrier-phase residual is greater than 4.47 cm (an empirically set value) the measurement for the respective satellite is rejected and the epoch is reprocessed. Significant improvements were not seen over the standard PPP residual rejection. This was attributed to the fact that the data were collected from high quality geodetic receivers that are part of the IGS network. If data

were collected from lower quality receivers it would have a larger magnitude of pseudorange multipath and noise allowing the value of RAIM to be easily observed.

Pseudorange multipath and noise mitigation: If pseudoranges were more precise, there would be a reduction in the convergence period. Pseudorange multipath and noise together is the largest remaining unmanaged error source in PPP. By reducing the effects of the multipath and noise on the pseudorange observable, carrier-phase ambiguities will reach a steady state at an earlier time, thus reducing the initial convergence and re-convergence period of PPP. The multipath linear combination was calculated to mitigate the raw pseudorange observable and stochastically de-weight pseudorange observables based on the magnitude of the pseudorange multipath and noise present. To correct the raw observables three different methods were applied; these included: 1) running average, 2) previous day multipath observable, and 3) the same day multipath observable.

The running average filters the pseudorange multipath and noise in real-time. Its major limitation is the requirement of several epochs of data to successfully average the ambiguity term. By using a simple recursive algorithm to average estimate the ambiguity term and filter the pseudorange observables may introduce the uncertainty of the ambiguity term present in the running average. This why after 16 minutes of PPP processing with running average on and off presented equivalent results. Another possible reason why there was a lack of improvements may be attributed to some geodetic receivers that apply a smoothing correction for the pseudorange observables available in the raw data.

Another method analyzed was using the multipath observable from the previous day, where a 5% improvement was noted during the initial 6 minutes of convergence in contrast to the standard PPP solution. Significant improvements were not observed while using this observable, because of the pronounced effect of the pseudorange noise. While improvements were minimal, it is useful to make use of data from the previous day if the information is available, while it is important to take note of this methods primary limitation is a repeated multipath environment is required.

The final method applied is the use of the multipath observable from within the same day. This method is possible by post-processing the dataset, generating the multipath observable which is fed into the PPP processor. The same day filter showed a 47% improvement over the standard PPP. This method was most effective as it allowed the ambiguity term to be accurately removed and therefore accurately removed the pseudorange multipath and noise from the pseudorange measurements. Also, unlike the running average, using the same day multipath observable provides corrections during the first epoch, thus improving the initial coordinate which is critical for reducing convergence period in PPP.

Pseudorange multipath de-weighting: The benefits of either de-weighting using the elevation angle or the multipath observable were observed when compared to the standard PPP solution which used no weights on the pseudorange measurements. A 3D accuracy level of 30 cm was set to examine the improvements of both methods over the standard PPP solution. The most influential time period was observed within the 7

minutes. Overall improvements of 39.1% and 36% were observed over standard PPP when using the elevation angle and the multipath observable, respectively.

Of all the methods presented, the stochastic de-weighting using the pseudorange measurements is recommended to become a component of the standard PPP processor. The strength of this model is it allows for real-time compensation of the effects of the pseudorange multipath and noise in the stochastic model, as long as realistic stochastic models are applied for each epoch in the position estimation process. Its performance is comparable to elevation weighting, but with further tuning of the weighting strategy it is expected to show improved performance as was seen for individual sites.

5.2 Recommendations for Future Research

Although much ground has been covered in this research, there are many improvements in the software that can be made, as well as expanding the experiments.

Implement Ambiguity Resolution (AR) with multipath mitigation: Integer ambiguity resolution of undifferenced carrier-phase observables has been a difficult task in GPS processing and even more troublesome in PPP, where undifferenced carrier-phase is used. In PPP, the fractional-cycle biases in the GPS measurements are absorbed by the undifferenced ambiguity estimates and their integer properties are no longer present. By including the same day multipath linear combination, it is expected to allow the ambiguity to be resolved more efficiently, quickly and correctly. If the ambiguity term is

successfully resolved, there will improvements in the convergence period and solution accuracy.

Multi-GNSS PPP processing: Several advantages that could be gained from modernized GPS, GALILEO, COMPASS and GLONASS include more visible satellites, greater signal power level and more potential observable combinations, potentially resulting in improved positioning accuracy, availability and reliability. Some of the current issues existing with having a multi-GNSS PPP processor include the offset exists between GPS and GLONASS system times causing a bias between GPS and GLONASS measurements. Another limiting factor is the accuracy of the satellite orbits and clocks for GLONASS and improvements that are shown for GPS in this thesis can be applied to other GNSS.

Initialization of ambiguity terms using RTK corrections**:** For real-time applications using NRTK, observations from a reference station together with network-derived parameters to describe distance dependent errors or a virtual reference station are transmitted to GNSS users in the field using the RTCM standards. Essentially, "so-called PPP-RTK" is the augmentation of PPP estimation with precise un-differenced atmospheric corrections and satellite clock corrections from a reference network, allowing instantaneous ambiguity fixing for users within the network coverage. Three important benefits of PPP-RTK, which are, faster PPP convergence, improved static and kinematic solution and greater distance from the reference network. The expectation of PPP-RTK is almost instantaneous convergence within the first couple of epochs processed

Real-time PPP Processing: Expansion of the data processing options of York-PPP suitable for various real-time or near to-real-time applications. Real-time precise satellite orbits and clock corrections would be required and transmitted to the user-client along with atmospheric corrections via NTRIP. Applications would include real-time monitoring of co-seismic crustal motion combined with a multi-GNSS. Other applications would include positioning for vehicles such as navigation for agricultural vehicles. Some of the challenges of this would include reliability in the data stream, as well as the precision of real-time or prediction satellite orbits and clock corrections.

6.0 References

Agnew, D.C. and K.M. Larson (2007) Finding the repeat times of the GPS constellation, *GPS Solutions*, Vol. 11, No. 1, pp. 71-76.

Ashby, N. and J.J. Spilker (1996) Introduction to Relativistic Effects on the Global Positioning System, in Parkinson, B.W., J.J.S. Jr., and P.E. Penina Axelrad, *Global Positioning System, Theory and Application*, Volume 163, pp. 623-699

Axelrad, P., K. Larson, and B. Jones (2005) Use of the Correct Satellite Repeat Period to Characterize and Reduce Site-Specific Multipath Errors, *Proceedings of the 18th International Technical Meeting of the Satellite Division of The Institute of Navigation (ION GNSS 2005)*, pp. 2638 - 2648.

Beran, T., R.B. Langley, S.B. Bisnath, and L. Serrano (2007) High-Accuracy Point Positioning with Low-Cost GPS Receivers: How Good Can It Get?, Navigation: *Journal of The Institute of Navigation*, Vol. 54, No. 1, pp. 53-63.

Bisnath, S. and R. Langley (2001) Pseudorange Multipath Mitigation By Means of Multipath Monitoring and De-Weighting, IEEE 4th International Symposium on Kinematic Systems in Geodesy, *Geomatics and Navigation*, pp. 392–400

Bisnath, S. and Y. Gao (2009) Current state of precise point positioning and future prospects and limitations, *International Association of Geodesy Symposia*, Vol. 133, pp. 615-623.

Boehm, J., B. Werl, and H. Schuh, (2007) 'Troposphere mapping functions for GPS and very long baseline interferometry from European Centre for Medium-Range Weather Forecasts operational analysis data', Journal of Geodesy, vol. 81, no. 6. pp 246-257

Borre, K. (2009) GPS EASY Suite II: easy13 - RAIM, http://www.insidegnss.com/node /1610.

Broughton, R. (2003) Evaluation of a new satellite navigation integrity monitoring algorithm [*Msc Thesis*], Cranfield University.

Brown, R.G. (1992) A Baseline RAIM Scheme and a Note on the Equivalence of Three RAIM Methods, *Proceedings of the 1992 National Technical Meeting of The Institute of Navigation*, San Diego, CA, 127 - 137.

Cai, C. and Y. Gao (2007) Precise Point Positioning Using Combined GPS and GLONASS Observations, *Journal of Global Positioning Systems*, Vol. 6, No. 1, pp. 13-22.

Chen, K. and Y. Gao (2005) Real-Time Precise Point Positioning Using Single Frequency Data, *Proceedings of the 18th International Technical Meeting of the Satellite Division of The Institute of Navigation*, pp. 1514 - 1523.

Collins, J.P., F. Lahaye, P. Héroux, and S. Bisnath (2008) Precise Point Positioning with ambiguity resolution using the decoupled clock model, *Proceedings of the Institute of Navigation International Technical Meeting ION GNSS*, 16-19 September, pp. 1315-1322.

Collins, P. (2008) Isolating and Estimating Undifferenced GPS Integer Ambiguities, *Proceedings of the 2008 National Technical Meeting of The Institute of Navigation*, San Diego, CA, 720.

Collins, P., S. Bisnath, F. Lahaye, and P. Héroux (2010) Undifferenced GPS Ambiguity Resolution Using the Decoupled Clock Model and Ambiguity Datum Fixing, *ION GNSS*, Vol. 57, No. 2, pp. 123-135.

Collins, P., Y. Gao, F. Lahaye, P. Héroux, K. MacLeod, and K. Chen (2005) Accessing and Processing Real-Time GPS Corrections for Precise Point Positioning – Some User Considerations, *ION GNSS 18th International Technical Meeting of the Satellite Division*, 13-16 September.

Crustal Dynamics Data Information System (2012) ftp://cddis.gsfc.nasa.gov/pub/gps/ products/1651

Defraigne, P. and C. Bruyninx (2007) On the link between GPS pseudorange noise and day-boundary discontinuities in geodetic time transfer solutions, *GPS Solutions*, Vol. 11, pp. 239-249.

Dixon, T. H (1991) An introduction to the global positioning system and some

geological applications, *Reviews of Geophysics*, Vol. 29, pp. 249-276.

Du, S. and Y. Gao (2010) Integration of PPP GPS and low cost IMU, *Canadian Geomatics Conference 2010*.

Eckl, M.C., R. Snay, T. Soler, M.W. Cline, and G.L. Mader (2001) Accuracy of GPS derived relative positions as a function of interstation distance and observing session duration, *Journal of Geodesy*, Vol. 75, pp. 633-640.

El-Rabbany, A. (2006) *Introduction to GPS: The Global Positioning System*, 2nd edition, Boston: Artech House.

Elsobeiey, M. and A. El-Rabbany, (2009) 'Rigorous modelling of GPS residual errors for Precise Point Positioning', Proceedings of the 2010 Canadian Geomatics Conference, Calgary, pp. 80-194

Farmer, J. (2010) Jet Propulsion Laboratory, http://develop.larc.nasa.gov/Jet_Propulsion _Laboratory.html.

Federal Geographic Data Committee (1998a) Geospatial Positioning Accuracy Standards, PART 3: National Standard for Spatial Data Accuracy, Virgina.

Federal Geographic Data Committee (1998b) Geospatial Positioning Accuracy Standards - Part 2: Standards for Geodetic Networks, Virginia.

Federeal Aviation Administration (2011) Wide-area Augmentation System Performance Analysis Report, 35th edition, Atlantic City.

Fisheries and Oceans Canada (2012) Hydrographic Surveys, http://www.charts.gc.ca/data-gestion/hydrographic/hydrographic-eng.asp.

Gao, S., T. Brown, J.D. Xu, J.Z Li, (2012) Novel multipath mitigating ground planes for multiband global navigation satellite system antennas, Antennas and Propagation (EUCAP), *2012 6th European*, pp 1920 – 1924

Gao, Y. and K. Chen (2005) Performance Analysis of Precise Point Positioning Using Real-Time Orbit and Clock Products, *Journal of Global Positioning Systems*, Vol. 3, No. 1-2, pp. 95-100.

Ge, M., G. Gendt, M. Rothacher, C. Shi, and J. Liu (2008) Resolution of GPS carrier-phase ambiguities in precise point positioning (PPP) with daily observations, *Journal of Geodesy*, Vol. 82, No. 7. pp 65-78

Geng, J., F.N. Teferle, X. Meng, and A.H. Dodson (2011) Towards PPP-RTK: Ambiguity resolution in real-time precise point positioning, *Advances in Space*

Research, Vol. 47, No. 10, pp. 1664-1673.

Geng, J., X. Meng, A. Dodson, and F. Teferle (2010) Integer ambiguity resolution in precise point positioning: method comparison, *Journal of Geodesy*, Vol. 84, No. 9, pp. 569-581.

Geodetics Inc. (2010) Technologies - GPS Positioning, http://www.geodetics.com/products/technologies.php#gps_ins_integration.

Georgiadou, Y. and A. Kleusberg (1988) On carrier signal multipath effects in relative GPS positioning, *Manuscripta Geodaetica*, Vol. 13, pp. 172-179.

GMV (2010) About GMV, http://www.gmv.com/company/about_GMV/about_gmv.htm

Gurtner, W. (2000) [GPST] Re: Ashtech data + smoothing, http://www.bipm.org/static/gpst/mail/12Oct00.2.

Gurtner, W. (2002) Program ASRINEXO – Extract code and phase measurements from ASHTECH raw data files ftp://ftp.unibe.ch/aiub/pcrinex/asrinexo.f.

Hatch, R.R. (1982) The synergism of GPS code and carrier measurements, Proc. 3rd Int. Symposium. on "Satellite Doppler Positioning", New Mexico, Vol. 2 pp. 1213-1231.

Haustein, M. (2009) Effects of the Theory of Relativity in the GPS, http://osg.informatik.tu-chemnitz.de/lehre/old/ws0809/sem/online/GPS.pdf.

Héroux, P., Y. Gao, J. Kouba, F. Lahaye, Y. Mireault, P. Collins, K. Macleod, Tetreault, P., and K. Chen (2004) Products and Applications for Precise Point Positioning - Moving Towards Real-Time, *ION GNSS*, Long Beach, CA.

Hofmann-Wellenhof, B., H. Lichtenegger, and J. Collins (2001) *GPS Theory and Practice*, New York: Springer Wien.

ICD-GPS-200 (2000) GPS Interface Control Document (ICD), http://www.navcen.uscg.gov/pubs/gps/icd200/ICD200Cw1234.pdf.

IGS (2009) IGS Products, http://igscb.jpl.nasa.gov/components/prods.html.

International Hydrographic Organization (2005*) Chapter 6: Topographic Surveying, in Manual on Hydrography*, 1st edition, International Hydrographic Bureau.

Ipatov, V.P. and B.V. Shebshaveich (2010) GLONASS CDMA: Some Proposals on Signal Formats for Future GNSS Air Interface, *Inside GNSS*, http://www.insidegnss.com/node/2142.

Irsigler, M. (2008) Multipath Propagation, Mitigation and Monitoring in the Light of Galileo and the Modernized GPS, Muncheon: University of Bundeswehr Mucheon.

Irsigler, M. (2010) Characterization of multipath phase rates in different multipath environments, *GPS Solutions*, Vol. 14, No. 4, pp. 305.

Kalyanaraman, Sai K. (1999) A comparative study of advanced multipath mitigating global positioning system receiver architectures, [*Msc Thesis*] Ohio University.

Kaplan, E.D. (2006) *Understanding GPS: Principles and Applications*, Second Edition, 2nd edition, Boston : Artech House.

Kim, E., T. Walter, and J.D. Powell (2007) Adaptive Carrier Smoothing Using Code and Carrier Divergence, *Proceedings of the 2007 National Technical Meeting of The Institute of Navigation*, San Diego, pp. 141 - 152.

Kjørsvik, N., J.G. Gjevestad, E. Brøste, K. Gade, and O.-K. Hagen (2010) Tightly Coupled Precise Point Positioning And Inertial Navigation Systems, International Calibration and Orientation Workshop, EuroCOW 2010, Castelldefels, Spain.

Kouba, J. (2009a) A guide to using International GNSS Service (IGS) products, http://igscb.jpl.nasa.gov/components/usage.html.

Kouba, J. (2009b) A guide to using International GNSS Service (IGS) Products, http://igscb.jpl.nasa.gov/components/usage.html

Kouba, J. and Pierre Héroux (2001) Precise Point Positioning Using IGS Orbit and Clock Products, *GPS Solutions*, Vol. 5, No. 2, pp. 12-28.

Kumar J. (2006) GNSS Solutions: What receiver technologies exist for mitigating GNSS pseudorange and carrier phase multipath?, *Inside GNSS*, http://www.insidegnss.com/auto/Sept06GNSS_Solutions_secure.pdf.

Kunysz, Waldemar (1998) Effect of Antenna Performance on the GPS Signal Accuracy, *Proceedings of the 1998 National Technical Meeting of The Institute of Navigation*, Long Beach, CA, pp. 575-580.

Kuusniemi, H. (2007) GNSS Solutions: Is fault detection/RAIM useful in areas of severe signal degradation, in such as urban environments?, http://www.insidegnss.com/auto/JulyAug07-GNSS-Sol.pdf.

Landau, H., X. Chen, S. Klose, R. Leandro, and U. Vollath (2008) Trimble's RTK and DGPS Solutions in Comparison with Precise Point Positioning, *International Association of Geodesy Symposia*, Vol. 133, No. 4, pp. 709-718.

Langley, R.B. (1997) GPS Receiver System Noise, GPS World, Vol. 8, No. 6, pp. 40.

Laurichesse, D., F. Mercier, J.P. Berthias, P. Broca, and L. Cerri (2009) Integer Ambiguity Resolution on Undifferenced GPS Phase Measurements and Its Application to PPP and Satellite Precise Orbit Determination, *ION GNSSS*, Vol. 56, No. 2, pp. 135 - 149.

Leandro, R.F. (2009) Precise Point Positioning with GPS: A new approach for Positioning, atmospheric studies and signal analysis, [*Phd Thesis*] University of New Brunswick.

Leandro, R.F. and M.C. Santos (2006) Wide area based Precise Point Positioning, *ION GNSS 2006*, Fort Worth, Texas, pp. 2272-2278.

Leandro, R.F., M.C. Santos, and R.B. Langley (2007) GAPS: The GPS Analysis and Positioning Software – A Brief Overview, *ION GNSS 20th International Technical Meeting of the Satelite Division*, pp. 1807-1811.

Leandro, R.F., M.C. Santos, and R.B. Langley (2010) Analyzing GNSS data in precise point positioning software, *GPS Solutions*, Vol. 15, No. 1. pp 1-13

Leick, A. (2004) *GPS Satellite Surveying*, 3rd edition, New Jersey: John Wiley & Sons Inc.

Li, X., X. Zhang, and M. Ge (2011) Regional reference network augmented precise point positioning for instantaneous ambiguity resolution, *Journal of Geodesy*, Vol. 85, No. 3, pp. 151-158.

Li, X., X. Zhang, F. Guo (2009) Study on Precise Point Positioning Based on Combined GPS and GLONASS, *Proceedings of the 22nd International Technical Meeting of The Satellite Division of the Institute of Navigation*, Savannah, GA, pp. 2449-2459.

Mader, G.L. (1999) GPS Antenna Calibration at The National Geodetic Survey, *GPS Solutions*, Vol. 3, No. 1, pp. 50-58.

Mervart, L., Z. Lukes, C. Rocken, T. Iwabuchi (2008) 'Precise Point Positioning With Ambiguity Resolution In Real-Time',Proceedings of the 21st International Technical Meeting of the Satellite Division of The Institute of Navigation (ION GNSS 2008), pp. 397-405.

Microcom Systems Ltd (2012) Launch Schedule 2012, http://www.satelliteonthenet .co.uk/index.php/launch-schedule.

Mireault, Y., P. Tétreault, F. Lahaye, P. Héroux, and J. Kouba (2008) Innovation: Online

Precise Point Positioning, A New, Timely Service from Natural Resources Canada, http://www.gpsworld.com/gnss-system/innovation-online-precise-point-positioning-4252.

Mohamed, A., Y. Gao, and X. Shen (2002) Analyzing the Performance Characteristics of a Precise Point Positioning System, *15th International Technical Meeting of the Satellite Division of The Institute of Navigation*, Portland, OR.

Montenbruck, O., A. Hauschild, S. Erker, M. Meurer, R.B. Langley, and P. Steigenberger (2010) GPS Modernization, GPS L5: The Real Stuff, http://www.gpsworld.com/gnss-system/gps-modernization/news/gps-l5-the-real-stuff-10086.

Montenbruck, O. (2003) 'Kinematic GPS positioning of LEO satellites using ionosphere-free single frequency measurements', Aerospace Science and Technology, vol. 7, no. 5, pp. 365-405.

Moudrak, A., A. Konovaltsev, J. Furthner, J. Hammesfahr, P. Defraigne, A. Bauch, S. Bedrich, and A. Schroth (2005) Interoperability on Time, http://www.gpsworld.com/wireless/timing/interoperability-time-3748.

Nassar, S. and N. El-Sheimy (2005) Sensor Integration and Image Georeferencing in Support of Airborne Remote Sensing Applications, *Proceedings of the ISPRS International WG 1/2 Workshop 2005: 3D Mapping from InSAR and LiDAR*,June 7-10, Banff, Alberta.

National Coordination Office for Space-Based Positioning, Navigation, and Timing (2012), http://www.gps.gov/multimedia/presentations/2012/04/moscow/clore.pdf

National Space Science Data Center (2011) Transit 1B, http://nssdc.gsfc.nasa.gov/nmc/spacecraftDisplay.do?id=1960-003B.

NRCan (2010) About Us, http://www.nrcan-rncan.gc.ca/com/index-eng.php.

O'Keefe, K. (2000) Relativity and GPS Lead Discussion - Fall 2000, http://people.ucalgary.ca/~kpgokeef/pubs/ENGO625relativity.pdf.

Ovstedal, O. (2002) 'Absolute Positioning with Single Frequency GPS Receivers, GPS Solutions', GPS Solutions, vol. 5, no. 4, pp. 33-44.

Parkinson, B.W. and J.J. Spilker (1996) *Global Positioning System: Theory and Applications,Volume II*, AIAA, Progress in Astronautics and Aeronautics, ISBN 1-56347-107-8

Petrov, L. and J.-P. Boy (2004) Study of the atmospheric pressure loading signal in very

long baseline interferometry observations, *Journal of Geophysical Research*, Vol. 109, No. B03405.

Pierce, F.J. and P. Nowak (1999) Aspects of Precision Agriculture, *Advances in Agronomy*, Vol. 67, pp. 1-85.

Ray, J.K., M.E. Cannon, and P. Fenton, (1999) 'Code Range and Carrier Phase Multipath Mitigation Using SNR, Range and Phase Measurements in a Multi-Antenna System', Proceedings of the 12th International Technical Meeting of the Satellite Division of The Institute of Navigation, Nashville, Tennessee, pp. 1025-1034.

Reid, J.F., Q. Zhang, N. Noguchi, and M. Dickson (2000) Agricultural automatic guidance research in North America, *Computers and Electronics in Agriculture*, Vol. 25, pp. 155-167.

Schaer, S., W. Gurtner, and J. Feltens (1998) IONEX: The IONosphere Map EXchange Format Version 1, *IGS Analysis Centres Workshop*, Darmstadt, Germany.

Scherneck, H.-G. (2011) Ocean Tide Loading Provider , http://froste.oso.chalmers.se/loading//index.html.

Schowengerdt, R.A. (2006) Remote Sensing: Models and Methods for Image Processing, 3rd edition, Academic Press.

Shen, X. and Y. Gao (2006) Analyzing the impacts of Galileo and Modernized GPS on Precise Point Positioning, *Proceedings of ION NTM 2006*, Monterey, California, pp. 837-846.

Shi, J. and Y. Gao (2010) Analysis of the Integer Property of Ambiguity and Characteristics of Code and Phase Clocks in PPP using a Decoupled Clock Model, *Proceedings of the 23rd International Technical Meeting of The Satellite Division of the Institute of Navigation*, Portland, OR, pp. 2553-2564.

Sinha, A. (2007) *Linear Systems: Optimal and Robust Control*, 1st edition, CRC Press.

The Johns Hopkins University Gazette (2010) Satellites, rockets and more, http://gazette.jhu.edu/2010/03/01/satellites-rockets-and-more/.

Tolman, B.W., Kerkhoff, A., Rainwater, D., Munton, D., Bank, J. (2010) Absolute Precise Kinematic Positioning with GPS and GLONASS, Proceedings of the 23rd *International Technical Meeting of The Satellite Division of the Institute of Navigation*, Portland, OR, pp. 2565-2576.

Urquhart, L. (2009) 'Atmospheric Pressure Loading and its Effects on Precise Point Positioning', Proceedings of the 22nd International Technical Meeting of The Satellite

Division of the Institute of Navigation (ION GNSS 2009), Savannah, GA, pp. 658-667

Walter, T. and P. Enge (1995) Weighted RAIM for Precision Approach, http://waas.stanford.edu/~wwu/papers/gps/ABS/wraim_tfw95.html.

Wang, J. and Y. Feng (2009) Integrity determination of RTK solutions in precision farming applications, *Proceedings of the Surveying and Spatial Sciences Institute Biennial International Conference 2009*, 28 September - 2 October 2009, Adelaide, South Australia.

Weill, L. (1997) Conquering Multipath The GPS accuracy Battle, *GPS World*, Vol. 8, No. 4, p. 59.

Wells, D., N. Beck, D. Delikaraoglou, A. Kleusberg, E. Krakiwsky, G. Lachapelle, and R. Langley (1999) *Guide to GPS Positioning* , http://gge.unb.ca/Pubs/LN58.pdf.

Wubbena, G., M. Schmitz, and A. Bagg (2005) PPP-RTK: Precise Point Positioning using state-space representation in RTK networks, *Proceedings of ION GNSS 2005*, 13-16 September, Long Beach, California, 2584-2594.

Yunck, T.P. (1996) Orbit Determination, in American Institute of Aeronautics and Astronautics, *Global positioning systems: Theory and applications. Progress in Astronautics and Aeronautics*, Parkinson & Spilker, Jr.

Zhu, S.Y., F.-H. Massmann, Y. Yu, and C. Reigber (2002) Satellite antenna phase centre offsets and scale errors in GPS solutions, *Journal of Geodesy*, Vol. 76, pp. 668-672.

Zinoviev, A.E. (2005) Using GLONASS in Combined GNSS Receivers: Current Status, *ION GNSS 18th International Technical Meeting of the Satellite Division*, Long Beach, CA, pp. 1046-1057.

Zumberge, J.F., M.B. Heflin, D.C. Jefferson, and M.M. Watkins (1997) Precise point positioning for the efficient and robust analysis of GPS data from large networks.", *Journal of Geophysical Research*, Vol. 102, No. B3, pp. 5005-5018.

Zhang, B., P. Teunissen, O. Dennis (2011) A Novel Un-differenced PPP-RTK Concept, The Journal of Navigation, vol. 64, pp. 180-191